



This work is protected by copyright and other intellectual property rights and duplication or sale of all or part is not permitted, except that material may be duplicated by you for research, private study, criticism/review or educational purposes. Electronic or print copies are for your own personal, non-commercial use and shall not be passed to any other individual. No quotation may be published without proper acknowledgement. For any other use, or to quote extensively from the work, permission must be obtained from the copyright holder/s.

THE STRUCTURE OF POLYACRYLONITRILE BASED CARBON FIBRES
AS STUDIED BY ELECTRON SPIN RESONANCE
AND OTHER ELECTRONIC PROPERTIES

by

Fadel Y.I. Assabghy M.Sc.

Being a thesis
submitted to the University of Keele
for the Degree of Doctor of Philosophy

Department of Physics,
University of Keele,
Keele, Staffordshire.

August, 1970.

ABSTRACT

In view of their recently acquired technological importance, the structure and properties of carbon fibres are currently receiving considerable attention. Although the use of electron spin resonance (ESR) in the study of carbons and graphites has long been established, the application of this technique specifically to carbon fibres has not been previously reported. In this thesis the ESR characteristics of a number of high temperature fibres is investigated, in conjunction with other electronic properties such as the thermoelectric power (TEP), the magneto-resistance and the electrical resistivity.

The discovery of an anisotropy in the g-value of the ESR absorption of carbon fibres has made it possible to confirm that the graphitic crystallites, which make up the fibre structure, are preferentially aligned with their basal planes parallel to the fibre axis. This anisotropy is shown to be insensitive to slight crystallite misalignments, but on the other hand it clearly affords a good measure of the degree of graphitization in carbon fibres and indicates that crystallite development in these materials always remains inferior to perfect single crystal graphite. This is in line with their nominally non-graphitizing nature.

Comparing the ESR information with the results obtained from the other electronic properties investigated, reveals that the heat treatment temperature (HTT) of 1750°C is associated with a major electronic change in the structure of these materials. The processes

occurring at this HTT are discussed in terms of the available structural and band models in the carbon field. It is suggested that the appearance of the g-shift in this region is controlled by a critical interlayer or c-spacing in the graphitic crystallites. Furthermore it appears that the stresses formed in the material during the process of heat treatment are annealed in this region and this possibly plays a more significant role in the appearance of negative magneto-resistance than hitherto suspected.

It is found that hot stretching carbon fibres invariably produces a change in all the properties investigated, in the direction of increased graphitization.

Finally it is shown that correlation between the properties of different fibres can be satisfactorily achieved when these are expressed in terms of the g-anisotropy, which it is suggested, affords a good practical measure of graphitization or 'graphitic order' in these materials.

ACKNOWLEDGMENTS

The author would like to express his thanks and gratitude to the following:

Professor D.J.E. Ingram, for the provision of laboratory facilities and for his supervision of this thesis.

Dr. D. Robson, for advice and discussions throughout the course of this work.

Dr. E.F. Slade, for his cooperation and the use of his electromagnet.

Dr. G. Lancaster, for the use of his electromagnet.

Dr. B. Henderson, for the use of his Varian Q-band spectrometer and for supplying a sample of manganese doped magnesium oxide.

Mr. E.G. Cooper, Dr. R.D. Dowsing, Mr. P. Weightman and other members of the Physics Department for their cooperation.

Mr. W. Brearley, Mr. G. Dudley, Mr. M.G. Davies and the technical staff of the Physics Department for their assistance.

Miss K.B. Davies, for her care and patience in typing this thesis.

Mr. M. Cheney, for carrying out the photographic work.

The author also wishes to acknowledge the Research Establishment of Rolls-Royce Ltd. at Old Hall, Derby, for supplying the carbon fibres and pyrographite samples investigated in this thesis. Thanks are due to the following members of that establishment:

Dr. J. Johnson, Mr. P.G. Rose and Mr. J.R. Marjoram, for many useful discussions and their cooperation. The author is particularly indebted to Mr. J.R. Marjoram for supplying the X-ray data quoted in this thesis.

LIST OF FIGURES AND TABLES

<u>FIGURE</u>	<u>TITLE</u>	<u>Facing Page</u>
2.1	The Zeeman Splitting of a Free Electron	6
2.2	ESR Microwave Systems	14
3.1	Structure of the Hexagonal Form of Graphite (After Ubbelohde, A.R. and Lewis, F.A., Ref. 21)	20
3.2	Summary of Band Model and the Main Electronic Properties for Carbons due to Mrozowski's School	26
3.3	Classification of Carbonaceous Materials by their ESR Properties (After Singer, L.S., Ref. 40)	28
3.4	Fibrillar Structure of Carbon Fibres (After Fourdeux, A. et al., Ref. 61)	37
3.5	Crystallite Structure of Carbon Fibres (After Johnson, D.J. and Tyson, C.N., Ref. 66)	38
4.1	Block Diagram of X-band Spectrometer	40
4.2	Microwave Cavity and Accessories	41
4.3	Field Modulation of ESR Resonance Absorption (After Poole, C.P., Ref. 6)	43
4.4	Principle of AFC (After Poole, C.P., Ref. 6)	45
4.5	AFC Circuit Diagram	46
4.6	ESR of Phosphorous Doped Silicon	47
4.7	Mounting Carbon Fibres for ESR	48
4.8	Typical Fibre ESR with Mn ²⁺ Reference	49

<u>FIGURE</u>	<u>TITLE</u>	<u>Facing Page</u>
4.9	Gaussian and Lorentzian Shapes	50
4.10	Typical Line Shape Analysis	51
4.11	DPPH - Intensity Variation with Temperature	54
5.1	g-Anisotropy for Carbon Fibres compared to Graphite	56
	TABLE 5.1	57
5.2	Effect of A/B Asymmetry on g-value	58
5.3	Variation of g-value Anisotropy with Fibre HTT	59
5.4	Crystallites in Carbon Fibres	60
5.5	Effect of Crystallite Misalignment upon A_g (Private communication, E.G. Cooper, this department)	63
5.6	Reversal of g-Anisotropy with Temperature	64
5.7	Variation of Crystallite Anisotropy with HTT	65
5.8	Variation of ESR Intensity with HTT	66
	TABLE 5.2	68
5.9	X-Ray Parameters and the g-shift (X-ray data kindly provided by J.R. Marjoram)	72
5.10	Crystallite Anisotropy vs c-spacing	73
6.1(a)	Longitudinal Resistivity vs HTT	81
6.1(b,c)	Temperature Variation of Resistance	83
6.2	Fibres Mounted for TEP	86
6.3	Thermal E.M.F. vs Temperature	87
6.4	TEP vs HTT	88
6.5	Fibres Mounted for Magneto-resistance	91

<u>FIGURE</u>	<u>TITLE</u>	<u>Facing Page</u>
6.6	Angular Variation of Transverse Magneto-resistance	92
6.7	Field Dependence of Transverse Magneto-resistance	92
6.8	Field Dependence of Transverse Magneto-resistance (log-log)	93
6.9	Transverse Magneto-resistance vs HTT	93
6.10	Diffuse Scattering at Crystallite Boundaries (After Fujita, S., Ref. 39)	94
6.11	Band Overlap Model (After Mrozowski, S., Ref. 56)	97
7.1	Effect of Hot Stretching upon the g-Anisotropy	108
7.2	Reversal of g-Anisotropy with Temperature	109
7.3	g-Anisotropy for Fibre Crystallites and Single Crystal Graphite vs Temperature	110
	TABLE 7.1	110
7.4	Line Width Anisotropy	111
7.5	Effect of Hot Stretching upon the Electrical Resistance	112
7.6	Effect of Hot Stretching on TEP	113
7.7	Effect of Hot Stretching on Magneto-resistance	113
7.8	Angular Variation of Magneto-resistance	114
	TABLE 7.2	114
7.9	General Correlation of the Electronic Properties with g-Anisotropy	115
8.1	Mott's Band Model for Amorphous Materials (After Bahl, S.K. and Chopra, K.L., J. Appl. Phys., <u>41</u> , 2196, (1970).)	121

INDEX

	page
ABSTRACT	
CHAPTER 1 INTRODUCTION	1
CHAPTER 2 ESR : BASIC PRINCIPLES AND TECHNIQUES	5
2.1 The Phenomenon	5
2.1.1 The g-factor	6
2.1.2 Saturation	7
2.1.3 Relaxation	7
2.1.4 Spin-lattice relaxation	9
2.1.5 Dipolar and exchange interactions	10
2.1.6 Homogeneous and inhomogeneous broadening	11
2.2 Detection of the ESR Signal	13
2.2.1 Crystal video detection	13
2.2.2 Bridge systems	15
2.2.3 Bucking systems	15
2.2.4 Display systems	16
2.2.5 Automatic frequency control (AFC)	17
2.2.6 Spectrometers based on helices	18
CHAPTER 3 GRAPHITE AMORPHOUS CARBONS AND CARBON FIBRES	19
3.1 Graphite	19
3.1.1 Structure	19
3.1.2 Electronic properties	21
3.1.3 ESR	23
3.2 Amorphous Carbons	25
3.2.1 Electronic properties	25
3.2.2 ESR Properties	28
3.3 Carbon Fibres	32
3.3.1 Manufacture	34

CHAPTER 4	THE ESR SPECTROMETER AND EXPERIMENTAL TECHNIQUES	39
4.1	The ESR Spectrometer	39
4.1.1	The microwave bridge	39
4.1.2	The microwave cavity	40
4.1.3	The magnetic field assembly	41
4.1.4	Detection	42
4.1.5	AFC	44
4.1.6	Sensitivity	46
4.2	Mounting Carbon Fibres for ESR	48
4.3	Line Shapes	50
4.4	Spin Concentrations	51
4.5	The g-Value	53
CHAPTER 5	ESR STUDIES OF CARBON FIBRES	55
5.1	The Samples	55
5.2	The Resonance Line	55
5.3	The g-Value Anisotropy	56
5.4	Effect of Asymmetry on g-Value	58
5.5	Variation of Δg with HTT	59
5.6	Effect of Crystallite Misorientation on g-Anisotropy	60
5.7	Variation of Δg with Ambient Temperature	63
5.8	Variation of A with HTT	65
5.9	Variation of ESR Intensity with HTT	65
5.10	The Line Width	67
5.11	Discussion of ESR Results	69

CHAPTER 6	ELECTRONIC PROPERTIES OF CARBON FIBRES	77
6.1	Introduction	77
6.2	The Electrical Resistance	78
6.2.1	Measurement of longitudinal resistivity	79
6.2.2	Room temperature resistivity results	81
6.2.3	Variation of resistance with temperature	82
6.3	Thermoelectric Power (TEP)	84
6.3.1	Measurement of TEP	86
6.3.2	TEP results	87
6.4	The Magneto-Resistance	89
6.4.1	Measurement of magneto-resistance	91
6.4.2	Results	92
6.5	General Discussion	95
6.5.1	Band overlap model	96
6.5.2	The ESR intensity	97
6.5.3	The TEP	98
6.5.4	The magneto-resistance	99
6.5.5	Origin of stresses	101
6.5.6	The g-anisotropy	102
CHAPTER 7	EFFECT OF HOT STRETCHING	106
7.1	Introduction	106
7.2	The g-Anisotropy	108
7.3	Line Width Anisotropy	110
7.4	The Electrical Resistivity	112
7.5	The TEP	112
7.6	The Magneto-Resistance	113
7.7	Conclusion	115

CHAPTER 8	CONCLUSIONS AND SUGGESTIONS FOR FUTURE WORK	117
8.1	Electrons in Amorphous Materials	121
REFERENCES		124

CHAPTER 1

INTRODUCTION

The importance of carbon fibres lies in the fact that they can be made stronger and stiffer than any other synthetic or natural material of the same weight except for single crystal 'whiskers', which can only be produced on a microscopic scale. These fine filaments of carbon can then be used to reinforce a resin matrix producing a composite material which can be as stiff as steel but only one fifth as heavy. The resulting technological implications have led to very considerable interest being devoted to these fibres in recent years. Although it would probably be fair to say that the ways in which these new materials can now be manufactured have been brought to a satisfactory level of reproducibility, there is still considerable lack of knowledge on their internal composition and structure, particularly at the atomic level.

It has been known for some time that unpaired electrons are associated with various types of carbonaceous materials, but although ESR techniques have been widely used to investigate the structure of a variety of these materials, they have not previously been specifically applied to carbon fibres. In this work the ESR parameters of carbon fibres are examined in conjunction with other electronic properties, such as the electrical resistivity, the thermo-electric power (TEP) and magneto-resistance.

The fibres investigated were all high temperature fibres having been heat treated above approximately 1000°C . Two sets of fibres were considered. The first consisted of a number of fibres subjected to a heat treatment temperature (HTT) ranging between 1000°C and 2800°C . The second set of fibres had in addition been heat treated under stress (hot stretched) at various HTT between 1800°C and 3000°C . The study was undertaken in cooperation with the research establishment of Rolls-Royce Ltd. at Old Hall, Derby, who kindly supplied the author with all the carbon fibres investigated in this thesis.

Because the properties of carbon fibres are so intimately related to the graphitic crystallites making up the structure, attention has been given at various stages to the properties of single crystal graphite. Some measurements on stress recrystallized pyrographite, which behaved as single crystal graphite, are presented whenever relevant to the discussion of the carbon fibre results.

Since an important part of the study is concerned with investigating the ESR parameters of carbon fibres, a whole chapter (Chapter 2) is devoted to a summary of the basic phenomena and techniques of ESR. The emphasis is placed on those aspects of the techniques relevant to the ESR of carbons and the treatment is necessarily far from exhaustive. Since its advent immediately after World War II, ESR spectroscopy has become a well established discipline and a wealth of excellent books and review articles are available on the subject ⁽¹⁾⁻⁽⁸⁾.

At the outset of this work, the available ESR spectrometer was of the type employing a helix instead of a microwave cavity. This arrangement was found to be unsuitable for examining carbon fibres and consequently it was reconstructed into a bridge system, using a microwave reflection cavity. The changeover did not require major modifications in the detecting circuitry, but the building of an automatic frequency control (AFC) system was a necessity. The spectrometer set up is described in detail in Chapter 4, together with the various experimental techniques relating to ESR of carbon fibres.

The background literature for the carbon field is introduced in Chapter 3, together with a discussion on the structure and electronic properties of graphite. Amorphous carbons are then considered in detail. Three dominant aspects of these materials which are subsequently of considerable importance to this work are developed. These are:

- (i) The ESR line results from the separable contributions of two spin species, namely localized and conduction electrons.
- (ii) The g-value for the conduction part will, as a result of motional averaging, represent the spatial average of the g-values of the individual graphitic crystallites.
- (iii) The band theory proposed some years ago to explain the properties of carbons is examined in detail.

In view of the importance of the manufacturing procedures on the properties of carbon fibres, the latter part of this chapter is devoted to describing how these were developed.

The ESR and electronic data collected for the first series of fibres (i.e. not hot stretched) are presented and briefly discussed in Chapters 5 and 6 respectively. Chapter 6 is divided into four parts. The first three deal respectively with the electrical resistivity, thermo-electric power and magneto-resistance. The remaining fourth section is devoted to a detailed general discussion encompassing both the ESR and electronic information presented in Chapters 5 and 6.

The effect of hot stretching upon all of these properties, are examined in Chapter 7. The second set of fibres was used for this purpose and the results obtained are combined with the results of the first set and an overall picture is discussed.

The final conclusions are drawn in Chapter 8, which includes wherever possible suggestions for future work.

CHAPTER 2

ESR : BASIC PRINCIPLES AND TECHNIQUES

2.1 The Phenomenon

The phenomenon of paramagnetic resonance can be approached classically^(1,2) by considering the magnetic moment $\underline{\mu}$ associated with a free spin. The application of a static magnetic field H will cause μ to precess about H at the Larmour precession frequency. Resonance occurs when the frequency of an applied oscillating field is the same as the precession frequency.

Paramagnetic resonance can also be viewed quantum mechanically⁽³⁾ as the Zeeman splitting of the degenerate zero field level by the application of the external magnetic field H . The magnetic moment $\underline{\mu}$ of an electron is given by

$$\underline{\mu} = -g\beta\underline{S} \quad (2.1)$$

where \underline{S} is the spin angular momentum vector of the electron, g is a dimensionless constant called the 'g-factor' and β is the Bohr magneton.

The interaction between the electronic magnetic moment and an applied magnetic field H is represented by the Hamiltonian

$$\mathcal{H} = -\underline{\mu} \cdot \underline{H} \quad (2.2)$$

If the applied field is in the z direction this becomes

$$\mathcal{H} = g\beta H S_z \quad (2.3)$$

THE ZEEMAN SPLITTING FOR A FREE ELECTRON

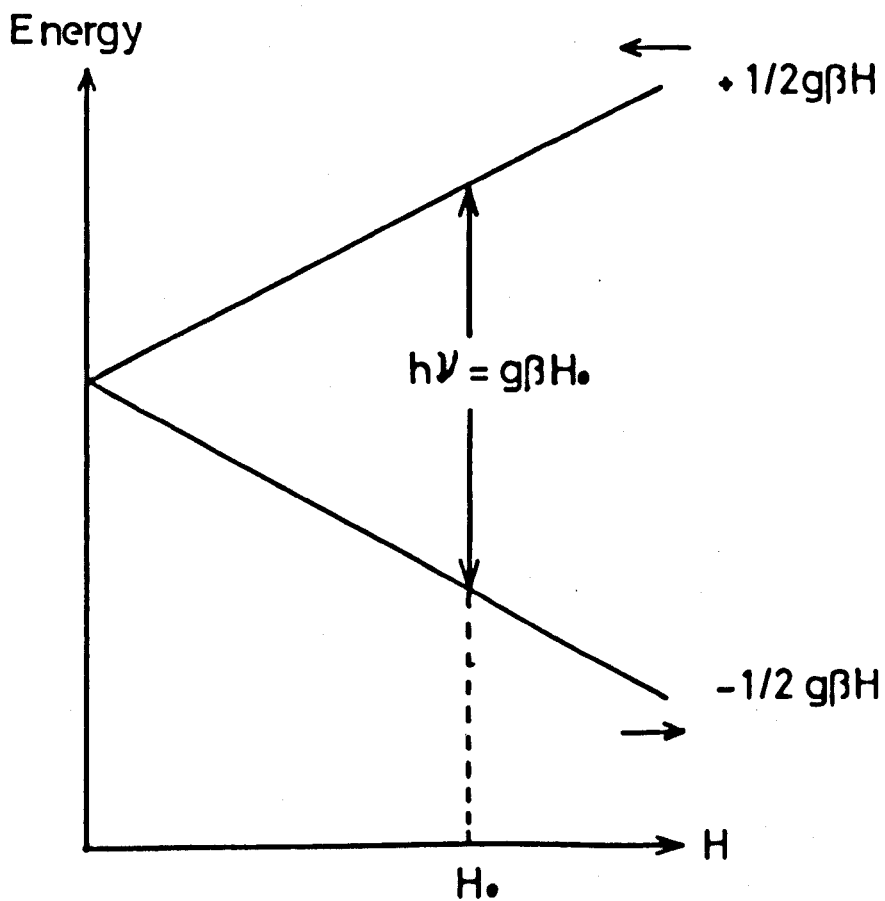


FIGURE 2.1.

For an isolated free electron in a magnetic field there are two allowed orientations of the spins, parallel or antiparallel to H_z . The former being the low energy state and the latter the high energy state. Transitions between the levels, or 'spin flips' can be induced by the application of an oscillating magnetic field perpendicular to H ; provided the oscillation frequency ν is such that it satisfies the resonance condition (see fig. 2.1)

$$h\nu = g\beta H \quad (2.4)$$

Generally for a spin system with spin number S , there will be $(2S+1)$ sub-levels or Zeeman levels, each characterized by the magnetic quantum number M_S which can have $(2S+1)$ values.

By computing the transition probabilities using first order time dependent perturbation theory it can be shown that only transitions with $\Delta M_S = \pm 1$ are allowed. Higher order calculations however, allow otherwise forbidden transitions to occur under certain circumstances.

2.1.1 The g-factor

The 'g-factor' or 'spectroscopic splitting factor' is a measure of the admixture of the orbital motion of an electron with its spin momentum. An electron in a typical paramagnetic ion is affected not only by the applied magnetic field, but is also under the influence of its own orbital motion and thus 'spin-orbit coupling' occurs and can cause the g-value to deviate appreciably from the value of 2.0023 observed for a completely free electron. As a result of distortion of the orbits

of a paramagnetic ion in a crystal lattice by the crystal field, the g-value may show anisotropy with respect to the crystal axis.

In aromatic free radicals, however, as a consequence of the delocalized nature of the unpaired electrons, there is very little coupling between spins and their orbital motion and hence the g-value falls very close to the free spin value of 2.0023.

2.1.2 Saturation

When a spin system is in thermal equilibrium with its surroundings there exists, according to Boltzmann's statistics, a slight population excess in the lower energy state. The application of a resonant oscillating magnetic field to the spin system will cause transitions to occur. Time dependent perturbation theory shows that the probabilities for upward and downward transitions are equal.

Furthermore it can be shown that the application of the resonant r.f. field results in the exponential decay of the population difference and eventually the levels will be equally populated⁽³⁾. This state of affairs is described as 'saturation' and will cause the ESR signal to decrease in intensity and ultimately to disappear, unless some non-radiative process is available which allows the spins to 'relax' and transfer their energy to other degrees of freedom, and hence return to the ground state.

2.1.3 Relaxation

This process of non-radiative transitions, is called spin-lattice relaxation; the term 'lattice' being used in a broad sense to

refer generally to other degrees of freedom not directly related to the spin system. Spin-lattice relaxation is possible because the spin system is coupled to the lattice via the spin-orbit coupling⁽⁹⁾.

The energy of the spin system is in equilibrium with the thermal energy of the 'lattice', which means that the probabilities of spontaneous spin transitions up and down are no longer equal as they were for r.f. induced transitions. Application of the resonant r.f. field disturbs this equilibrium by increasing the energy of the spin system, which then 'relaxes' exponentially, transferring its excess energy to the lattice, with a characteristic time constant T_1 known as the spin-lattice relaxation time, or longitudinal relaxation time.

Taking a macroscopic view and considering the bulk magnetic moment of a large assembly of spins to be M at a certain temperature, then the z component, M_z , of the magnetic moment decays to zero with a characteristic time T_1 .

In the absence of a magnetic field H_0 , there is no physical distinction between the z -direction and any other direction and in the absence of field M_x and M_y also decay to zero.

The introduction of a steady field H_0 along the z axis alters the situation; M_z no longer vanishes but tends to approach a steady state value M_0 proportional to the static magnetic field susceptibility χ_0 .

Furthermore, although the transverse components M_x and M_y still decay to zero, they do so with a time constant which is generally different from T_1 and it is necessary to introduce another relaxation time, the 'transverse relaxation time', T_2 .

The longitudinal and transverse relaxation times T_1 and T_2 are different because they depend on different processes. Changes in M_x and M_y do not alter the total Zeeman energy of the spins, whereas changes of M_z need an exchange of Zeeman energy with the lattice. T_1 is therefore identifiable with the spin-lattice relaxation time and is expected to be temperature dependent. It is found that T_1 increases with decreasing temperature agreeing with the theoretical predictions of Van Vleck⁽¹⁰⁾.

The transverse-or spin-spin relaxation time T_2 is related to the effect of dipole-dipole interaction and can be considered as a measure of the rate at which the spin system comes to equilibrium within itself rather than with the lattice.

If the above macroscopic views are combined with the effect of Larmour precession, a set of equations known as Bloch's phenomenological equations⁽¹¹⁾ can be arrived at, which describe the spin as performing 'a damped precession in which the rotating transverse components of M decay to zero with a characteristic time T_2 , while M_z relaxes towards its equilibrium value M_0 with a decay time T_1 '.

Bloch's equations show that the two relaxation times play quite distinct roles. The spin-lattice relaxation time determines the degree of saturation and the spin-spin relaxation time determines the unsaturated line width.

2.1.4 Spin-lattice relaxation

A useful concept to describe spin-lattice relaxation is that of a spin temperature distinct from the lattice temperature. The energy

dissipated inside the spin system by the r.f. field raises the spin temperature above the lattice temperature and this excess energy is transferred to the lattice by a spin-lattice relaxation mechanism. A complete treatment of the concept of spin temperature can be found in Abragam's book⁽¹²⁾. However it can be noted that the assumptions of a spin temperature correctly describe the behaviour of Zeeman systems with one or more spin species.

Bloembergen and Wang⁽¹³⁾ pointed out that energy of spin orientation may first make its way to an intermediate thermal reservoir which is the so-called exchange system. This intermediate reservoir can in turn transfer energy to the lattice vibrations. They showed that in this two step process the transference of energy from the magnetic to the exchange system can be the slowest and therefore the rate controlling step, which determines the overall relaxation time T_1 . This would make T_1 independent of temperature.

The first part of this two step relaxation process was calculated by Kubo and Tomita^(14,15); the second part was treated by Griffith⁽¹⁶⁾ and a complete discussion on the two step spin-relaxation process via the intermediate exchange reservoir has been presented by Van Vleck⁽¹⁷⁾.

2.1.5 Dipolar and exchange interactions

The dipole moment of an unpaired electron will produce a static field in the region of its neighbours which will depend on the spatial orientation of the dipoles. This local variation produces slight changes in the resonance condition for each spin centre and a broadening of the line will result.

It was soon noted however that magnetic resonance lines were usually sharper than one would suppose on the basis of the effect of dipolar broadening⁽¹⁸⁾. This problem was solved in 1948 by Van Vleck⁽¹⁹⁾, who not only provided a quantitative measure of dipolar broadening but also explained the anomalously narrow lines, which he showed to be caused by the exchange interactions between neighbouring paramagnetic ions.

If the ions are similar the effect of exchange is to narrow the lines at the centre and broaden them in the wings, leaving the second moment unchanged but reducing the width at the half power points. On the other hand if the exchange is taking place between dissimilar ions, the interaction will tend to bring the two different transitions together and hence produce one wider line. The changes in line shape from Gaussian to Lorentzian can be taken as good evidence that exchange narrowing has taken place. Gaussian and Lorentzian lines are defined and discussed in section 4.3.

Dipolar interactions can also exist between electronic moments and nuclear spins. This gives rise to further splitting of the Zeeman levels. In non-crystalline phases this splitting is smeared out due to the random orientation of the nuclear dipoles and leads to a further broadening resulting from the unresolved nuclear hyperfine interactions.

2.1.6 Homogeneous and inhomogeneous broadening

The experimental effects of the different dipolar interactions which cause broadening of the ESR line can now be analysed. When the interactions of the spins with themselves and their surroundings are so fast that the absorption of energy involves the spin system as a whole

the resulting broadening is often referred to as homogeneous broadening. Dipolar broadening, exchange narrowing and motional averaging (section 3.2.2.) are included in this type of broadening. If one or more of the homogeneous interactions control the line width, the relaxation time T_2 can be related to the line width.

On the other hand, when the interactions vary slowly with respect to the time required for a spin transition then energy will only be transferred to those spins whose local fields satisfy the resonance condition and the resulting broadening is referred to as inhomogeneous broadening. The overall response of the spin system will be a superposition of the individual responses, and here the resultant absorption line is a superposition of the individual absorption lines. When inhomogeneous broadening controls the line width, T_2 cannot strictly be related to the width. Types of inhomogeneous broadening are: unresolved hyperfine interactions, g anisotropy broadening and broadening resulting from inhomogeneity of samples or magnetic field.

Homogeneously and inhomogeneously broadened lines behave differently when under saturation conditions. For homogeneously broadened lines saturation will decrease the apparent absorption; but this decrease occurs first in the centre of the lines where the greatest power is absorbed before it affects the wings. This will alter the line shape, increasing the apparent line width. In the case of inhomogeneous broadening saturation takes place for individual lines or components separately; and hence the overall line shape does not change.

This difference in behaviour between homogeneously and inhomogeneously broadened absorption lines under saturation conditions can be used to differentiate between them.

2.2 Detection of the ESR Signal

Basically an ESR spectrometer must be capable of detecting small changes in the magnetic susceptibility of the sample as it is taken through the resonant condition described by equation (2.4). From this equation one finds that for a field of 10,000 gauss, the resonance frequency of a free electron (with $g = 2.00232$) is 28,026 MHz. ESR spectrometers are therefore normally designed to operate in the microwave range of frequencies. Two commonly used wavelengths are 3.2 cm (X-band or Marine Radar Band) and 8 mm (Q-band or Airport Control Radar Band).

2.2.1 Crystal video detection

In the simplest type of spectrometer the sample under investigation is placed in a microwave cavity inserted between the poles of an electromagnet. Such a cavity has the advantage that standing wave patterns, or cavity modes, are set up within it leading to very large values of the oscillating r.f. magnetic field. Generally the power concentrated, and thus the signal observed is increased by a Quality factor, or Q-factor, of the cavity defined as

$$Q = \frac{\text{Energy stored at resonance}}{\text{Energy dissipated per cycle}} \times w$$

where w is the resonant frequency.

ESR MICROWAVE SYSTEMS

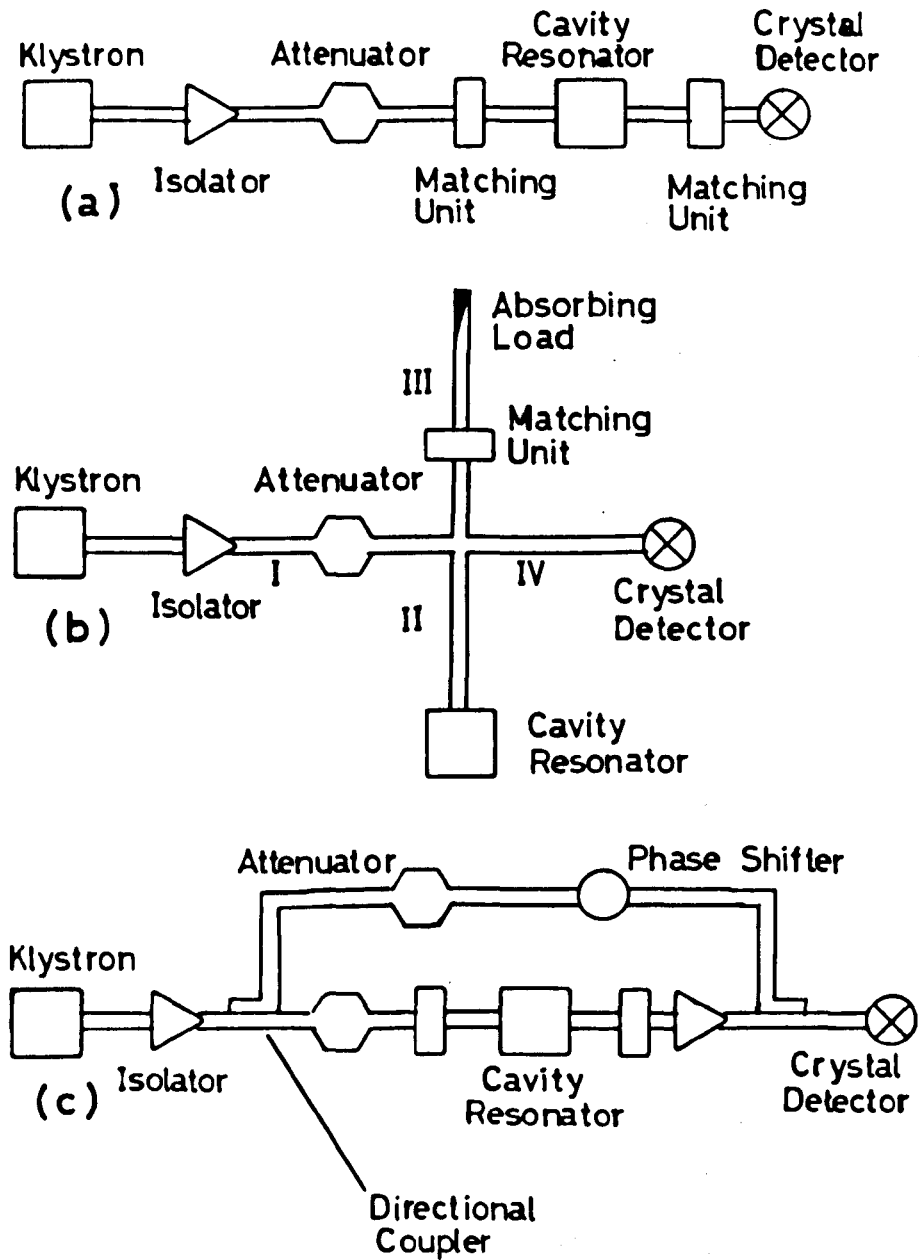


FIGURE 2.2.

Most microwave components have a fairly narrow band performance, and it is usually easier to sweep through the resonance condition by varying the magnetic field and keeping the r.f. frequency constant rather than the reverse.

The level of power in the case of a transmission cavity is monitored by feeding a fraction out to a crystal detector (see Fig. 2.2a). Absorption of power at resonance by the sample will cause a drop in the level of power detected by the crystal rectifier. If the magnetic field is a.c. modulated, the resonance absorption can be displayed directly on an oscilloscope.

Besides the fact that a transmission cavity is, by theoretical considerations, shown to be only half as sensitive as a reflection cavity, the crystal video system of detection suffers from technical drawbacks associated with the properties of the detecting crystal. In order to obtain a reasonable absorption signal from the specimen, the microwave power of the cavity should be as large as possible. But increase of power on the detecting crystal will increase the excess noise produced by the crystal. The conversion loss, on the other hand, decreases with increasing power, so that there exists an optimum operating point (or crystal bias or leakage current) for maximum sensitivity of detection.

There are, in fact, two ways in which independent adjustment of the microwave power in the cavity and the microwave level at the detecting crystal can be made. These are now briefly examined.

2.2.2 Bridge systems

The microwave cavity in these systems is placed in the arm of a microwave bridge, so that, when the bridge is balanced, the power from the klystron is fed to the microwave cavity and the third arm of the bridge, containing a matched load, and no power passes on to the detecting crystal in the fourth arm (see Fig. 2.2b). Resonance absorption changes the reflection coefficient of the cavity and the bridge then becomes unbalanced. A signal is then passed into the fourth arm which is detected by the crystal. The crystal can be adjusted to operate at its optimum conditions by slightly unbalancing the bridge at the onset.

The principle disadvantage with this bridge system is that it does not permit the spectrometer to be operated at low microwave powers since there would not then be enough power available to bias the detector crystal. This can be overcome by the use of microwave bucking techniques.

2.2.3 Bucking systems

This consists basically of a simple transmission system, but with a by-pass arm which takes some of the microwave power from the waveguide before it enters the cavity, and then returns this power to the output waveguide, after the cavity and before the detecting crystal (see Fig. 2.2c). This by-pass, or bucking arm, contains both an attenuator and a phase-shifter, so that the amount of power feedback can be varied in both magnitude and phase to give the desired crystal bias.

A basic microwave component in the design of both microwave bridges and bucking systems is the directional coupler, or magic-T, which however suffers from the disadvantage that half the microwave power is lost each time it is employed. The advent of microwave circulators has overcome this drawback, and greatly simplified the design of complex spectrometer systems. Microwave circulators are non reciprocal devices based on the rotation of the plane of polarization of the microwaves by suitably magnetized ferrite inserts. The device allows microwaves to pass only in one direction around the linking circle of wave guides.

2.2.4 Display systems

It has been shown that the employment of a balanced bridge, or bucking system, can ensure that the detecting crystal is operated at the optimum level of mean detectable current. The excess flicker noise produced by the detecting crystal varies inversely with frequency. It follows that video systems where detection involves low frequency modulation of the magnetic field, will be inherently very noisy.

The fact that crystal noise decreases with higher frequency of detection, taken by itself, suggests that increasing sensitivities can be obtained by working at higher and higher modulating frequencies. This, however, is not the case since above 50 MHz amplifier noise becomes appreciable.

It is found in practice that modulation of 100 KHz reduces crystal noise to very low values and spectrometers employing 100 KHz field

modulation are widely used. Usually the depth of modulation is kept small compared to the line width and the d.c. magnetic field is slowly swept through the resonance condition. The high frequency modulation scans the profile of the absorption line and in this way samples the gradient of the line. The 100 KHz signal detected by the crystal will then be proportional to the first derivative of the absorption line. This signal is fed via a narrow band amplifier into a phase sensitive detector, the output of which can be displayed on the screen of an oscilloscope or traced out on a pen recorder. This system has all the advantages of phase sensitive detection which eliminates the noise of previous amplifier stages. (See Chapter 4 for more detailed discussion.)

2.2.5 Automatic frequency control (AFC)

It is usually necessary to prevent the frequency of the klystron from drifting away from the resonance frequency of the cavity. There are two methods of ensuring this. One can either lock the klystron frequency to an absolute standard of frequency (harmonics of a quartz crystal or high Q-cavity) or one can lock the klystron frequency to the actual sample cavity. If the cavity frequency shifts slightly (as is the case in variable temperature experiments) the klystron frequency will adjust itself to remain at the cavity resonance frequency. In accurate g-value determinations, allowances must be made for this shift in frequency.

The most common way of locking the klystron frequency to the cavity is by frequency modulation of the klystron output. The frequency

modulation is then converted into amplitude modulation, by the cavity resonance curve and this can be used to produce a d.c. correcting voltage to be fed to the klystron reflector. (See Chapter 4 for more detailed discussion.)

2.2.6 Spectrometers based on helices

A helix is a broad band microwave device that can be used in place of cavity resonators in microwave bridges or bucking systems. Helices are relatively frequency insensitive devices and thus critical matching conditions associated with microwave cavities and frequency modulating noise can be avoided. Furthermore their open structure enables various double resonance techniques to be used. Such devices have been shown theoretically⁽²⁰⁾ not to diminish a spectrometer's sensitivity.

CHAPTER 3

GRAPHITE AMORPHOUS CARBONS AND CARBON FIBRES

3.1 Graphite

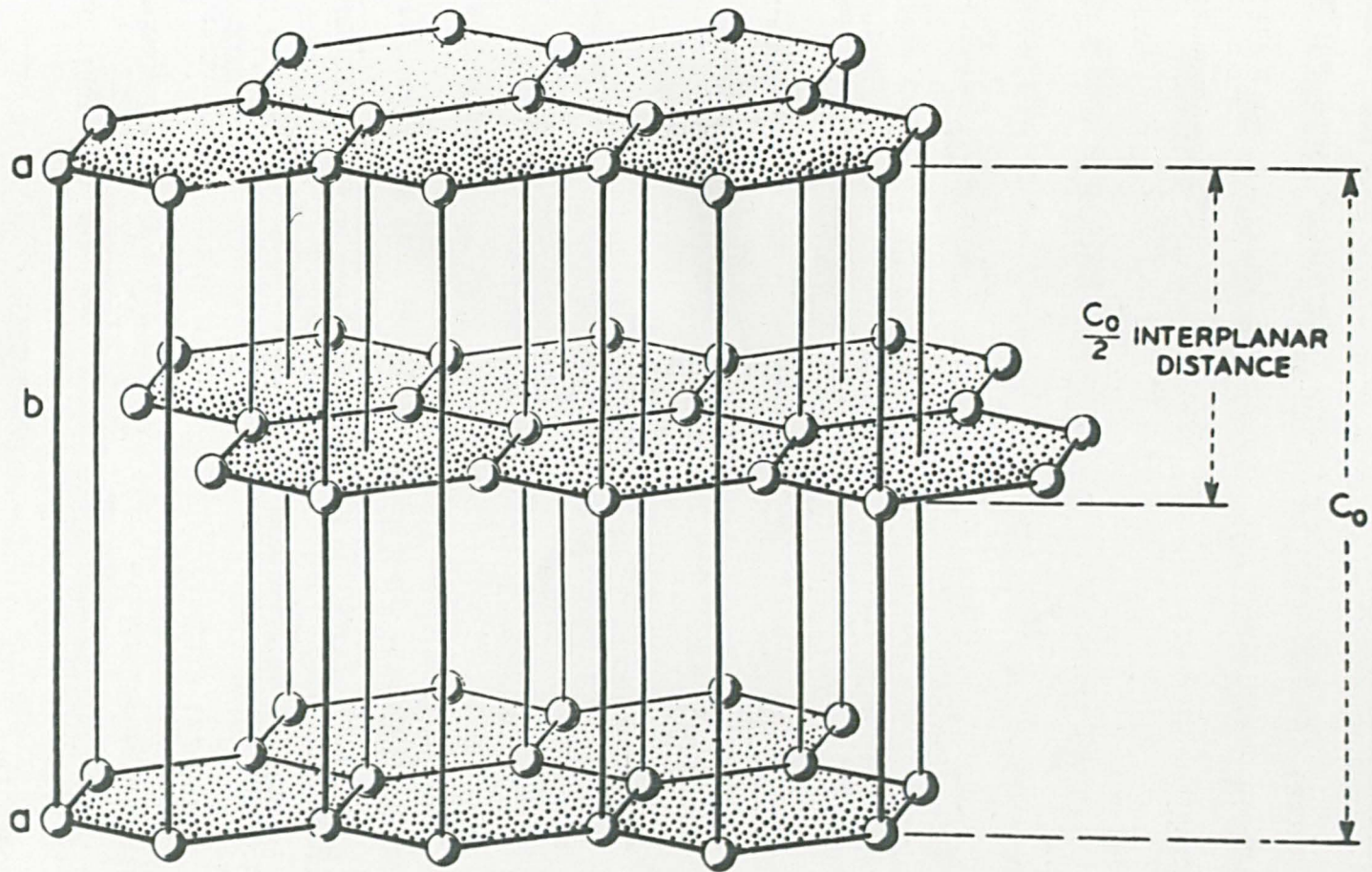
A discussion of carbonaceous materials in general is best introduced by considering the properties and crystal structure of graphite. These in fact have been extensively reviewed⁽²¹⁾ and only a brief description will be given here.

Graphite can occur naturally, in various parts of the world, in deposits from which fragments can be selected that behave as fairly perfect single crystals. Another source of graphite is Kish graphite which crystallizes out in the course of smelting iron.

Graphite can also be synthesized by various processes of progressive dehydrogenation and polymerization of solid organic materials. Pyrolytic graphites are synthesized by heating a rod or plate of graphite in a chamber containing a hydrocarbon usually carried in an inert gas. The deposit of carbon formed on the substrate, is usually obtained with a high degree of preferred orientation of the layer planes.

3.1.1 Structure

The carbon atoms in graphite form a network of regular hexagons arranged in parallel layers or basal planes. In the hexagonal structure, the predominant form in which graphite is found, the layer planes are arranged in an abab.... packing sequence, the carbon atoms in any one layer lying over the mid points of the regular hexagons in the layer immediately below (see Fig. 3.1).



Structure of the hexagonal form of graphite.

FIGURE 3.1

Each atom has four valence electrons; three σ -electrons which establish tight covalent bonds with nearest neighbours in the planes, and a loosely bound π -electron. This state of affairs results in a lattice that is characterized by the close proximity (1.42Å) of the atoms in a layer compared to the spacing (3.35Å) between the layers. The anisotropy of graphite is a direct consequence of this structural feature.

Graphite normally has the hexagonal structure, but a small amount of the rhombohedral modification can co-exist with it. In the rhombohedral lattice, the same layers of flat hexagon networks are formed, but the packing sequence with respect to the c-axis is abcabc. The fact that rhombohedral packing is almost absent in synthetic graphite and that on heating to 2000°C - 3000°C any rhombohedral modification is transformed to the hexagonal form indicates the latter is more stable.

Graphites, the hexagonal networks of which may be substantially perfect but in which the layers though parallel show no ordered packing sequence, are termed "turbostratic".

Ideal graphite has a unique π -electron band structure, which on a two-dimensional band model, i.e. ignoring the interlayer interaction, is characterized by touching π -bands at the corner of the hexagon which forms the first Brillouin zone^{*(22)}. On current three dimensional band models the π -bands actually overlap along the zone edge⁽²³⁾.

* As there are two atoms per unit cell, there are eight bands in all arranged in order of increasing energy $\sigma\sigma\sigma\pi\pi\sigma\sigma\sigma$. The lower 3 σ - and a single π -band are filled, while the upper four bands are unoccupied.

Furthermore, it has been shown that turbostraticity greatly affects the band structure⁽²⁴⁾.

The positive and negative carriers in these band structures are balanced fairly closely in concentration and mobility⁽²⁵⁾.

Moreover the number of free carriers is only a fraction of the number of atoms which leads to typical semimetallic characteristics.

A shift in the Fermi level, which in perfect single crystal graphite is located in the band overlap region, can be induced by relatively small amounts of defects or impurities and causes pronounced changes in the electronic properties.

Graphitic materials exhibit a great variety of structural configurations. The most highly organized structures are those with crystallites of considerable size, well aligned with respect to each other, and consisting of well-ordered carbon layers. All the c-axes point in the same direction, and within each crystallite the structure is essentially that of 'ideal' graphite. The most disorganized structures are found in the so-called 'amorphous' carbons. Their crystallites are small, turbostratic and randomly oriented with respect to each other. Intermediate between these two extremes there exists a whole range of 'transitional' structures.

3.1.2 Electronic properties

The layered structure of graphite is reflected in the marked anisotropy exhibited by all the electronic properties of graphite.

The electrical resistance parallel to the c-axis (ρ_{\parallel}) for example is

several orders of magnitude larger than the resistance along the graphitic planes (ρ_{\perp}). Crystallite imperfections, such as screw dislocations make the measurement of ρ_{\parallel} difficult by short circuiting the high resistance path, consequently the values of $\rho_{\perp}/\rho_{\parallel}$ quoted in the literature vary somewhat, the highest value quoted being $\rho_{\perp}/\rho_{\parallel} \sim 10^4$ ⁽²⁶⁾.

There seems to be agreement in indicating a positive temperature coefficient of resistance, in the direction parallel to the layer planes⁽²⁵⁾, while both a positive⁽²⁷⁾ and a negative⁽²⁶⁾ coefficient have been reported in the c-direction.

The resistance along the c-axis varies with the application of a magnetic field, a property known as the magneto-resistance effect (see section 6.4). This effect rises to very high positive values as the temperature is lowered and exhibits de Haas - Van Alphen periodicities at liquid helium temperatures from which the effective masses of carriers can be obtained⁽²⁵⁾. Similar periodicities are observed at these low temperatures in the Hall effect yielding values of the effective masses which compare well with those obtained from the magneto-resistance, and cyclotron resonance studies⁽²⁸⁾. The results of these studies and others such as the thermo-electric power, show that both electron and holes are 'majority carriers' in approximately equal numbers as is expected for touching or overlapping bands.

3.1.3 ESR

The first reported observation of ESR in graphite was that by Castle⁽²⁹⁾. He attributed the resonance to charge carriers and although doubt was later cast on this interpretation⁽³⁰⁾, the detailed work of Wagoner⁽³¹⁾ on single crystal graphite firmly confirmed that the resonance arises from mobile charge carriers.

Single crystals with dimensions greater than the skin depth result in an ESR line of the peculiar shape characteristic of the resonance of mobile charge carriers. Dyson⁽³²⁾ has treated this case theoretically for metals and has shown that the precise form of the resonance depends on the rate of diffusion of the charge carriers. Feher and Kipp⁽³³⁾ have verified experimentally Dyson's predictions by their work on the resonance of conduction electrons in sodium, potassium, lithium and beryllium.

The conclusion from the Dysonian line shape that the spin resonance in graphite is due to charge carriers is strengthened by the fact that the intensity of the resonance agrees, both in absolute magnitude and in temperature dependence with the values calculated from the band model of graphite by McClure⁽³⁴⁾. The intensity is found to increase approximately linearly with temperature in distinct contrast to the Curie behaviour expected for impurity atoms or lattice imperfections possessing localized spin centres.

The most remarkable feature of the spin resonance in graphite is the large g-value anisotropy. McClure and Yafet⁽³⁵⁾ have shown theoretically that the g-shift arises from interlayer interactions and

depends quite sensitively on the various band parameters. The g-value of graphite may be closely fitted by a \cos^2 function of the form

$$g = g_1 + A \cos^2\theta$$

where θ is the angle between the static magnetic field and the c-axis and A is the g-value anisotropy in pure graphite.

$$A = g_3 - g_1 = 0.047 \text{ at room temperature}$$

The g-value perpendicular to the c-axis (g_1) is independent of temperature and is approximately equal to the free electron g-value ($g = 2.0026$), whereas the g-value along the c-axis (g_3) is strongly temperature dependent and increases with decreasing temperature ($g_3 = 2.0495$ at 300°K and 2.1270 at 77°K).

The astonishing dependence of the anisotropy A on small changes of the Fermi level is clearly demonstrated by drastic reduction of the anisotropy on addition of small amounts of electrically active impurity.

The line width decreases with increasing temperature, the values being roughly five gauss at 77°K , four gauss at RT, and one gauss at 600°C . This dependence strongly suggests spin-lattice relaxation through interaction with spin-orbit coupling of impurity atoms. The line width of the resonance is extremely narrow in comparison with the field shifts caused by the anisotropy and remains so even for polycrystalline samples, suggesting that a type of averaging similar to that which occurs in motion and exchange narrowing may be present (see section 3.2.2).

3.2 Amorphous Carbons

When an organic compound is heated to about 200°C in a reducing or inert atmosphere, regardless of whether the original organic is aliphatic or aromatic in nature, polymerization with the creation of large condensed ring molecules occurs during the process of charring. At temperatures above $700 - 800^{\circ}\text{C}$ these substances, having lost most of the atoms or groups, attached at the periphery of the molecules, form a class of materials collectively known as amorphous carbons. The structure of these materials, which is complex, can be regarded as containing small graphitic regions or crystallites bonded together by what can only be described as amorphous carbon. These crystallites consist of turbostratic graphite (or packs of parallel graphitic planes about $20 - 30\text{A}$ in diameter) having no directional relationship to each other.

Providing the carbon is graphitizing (see section 3.3), increasing the HTT above $\sim 1000^{\circ}\text{C}$ will cause the growth, ordering and perfection of the crystallites to improve, so that the structure and properties of the carbon gradually approach those of graphite. At HTT of $2500 - 3000^{\circ}\text{C}$ synthetic graphite can be obtained.

3.2.1 Electronic properties

A considerable number of studies have been carried out on the electrical, thermo-electric and galvano-magnetic properties of various carbons, mainly by Mrozowski's group^(36,37,38). With the exception of the magneto-resistive behaviour, these properties were qualitatively explained in terms of an energy band model. On the basis of results

SUMMARY OF BAND MODEL AND THE MAIN ELECTRONIC PROPERTIES FOR CARBONS DUE TO MROZOWSKI'S SCHOOL

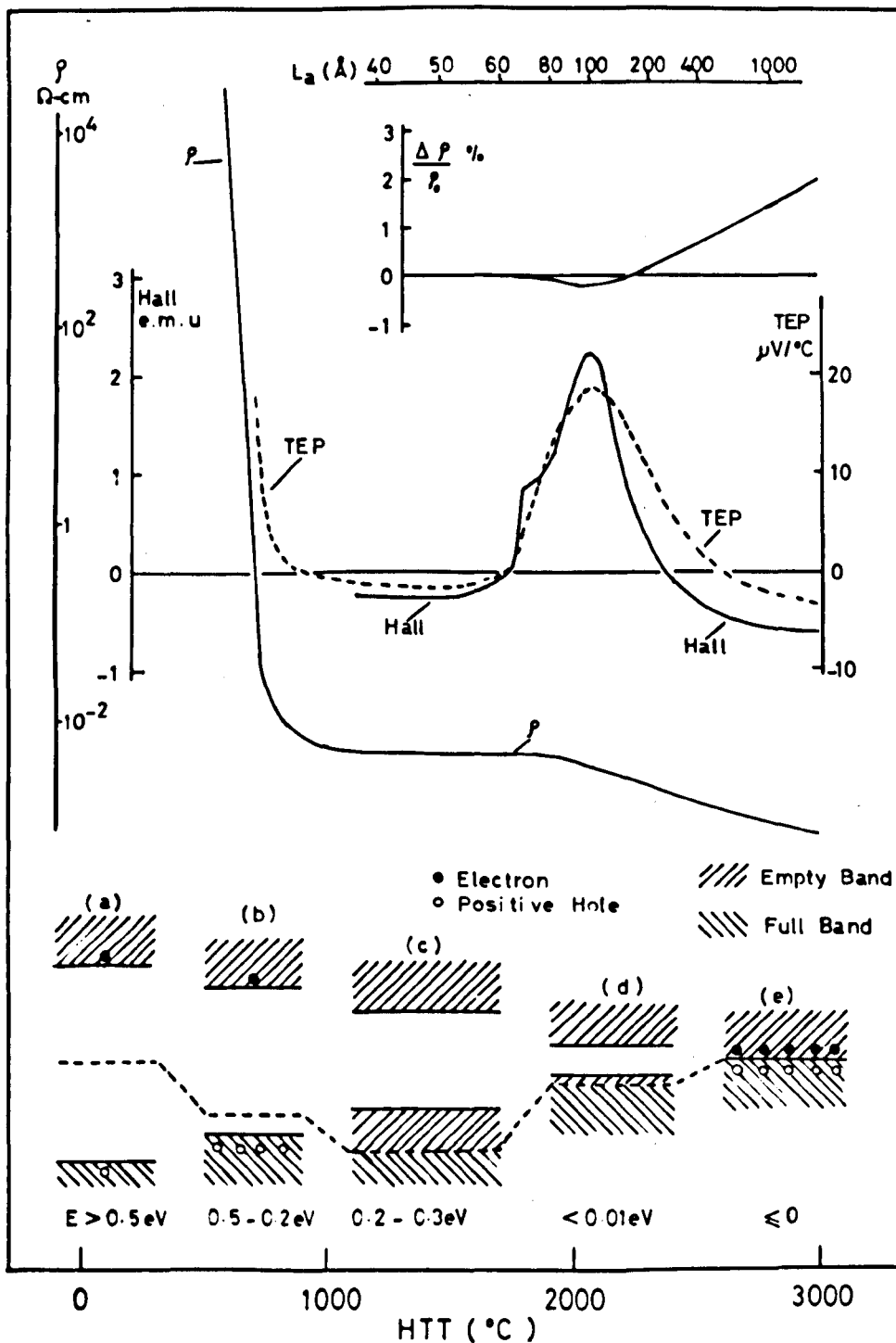


FIGURE 3.2.

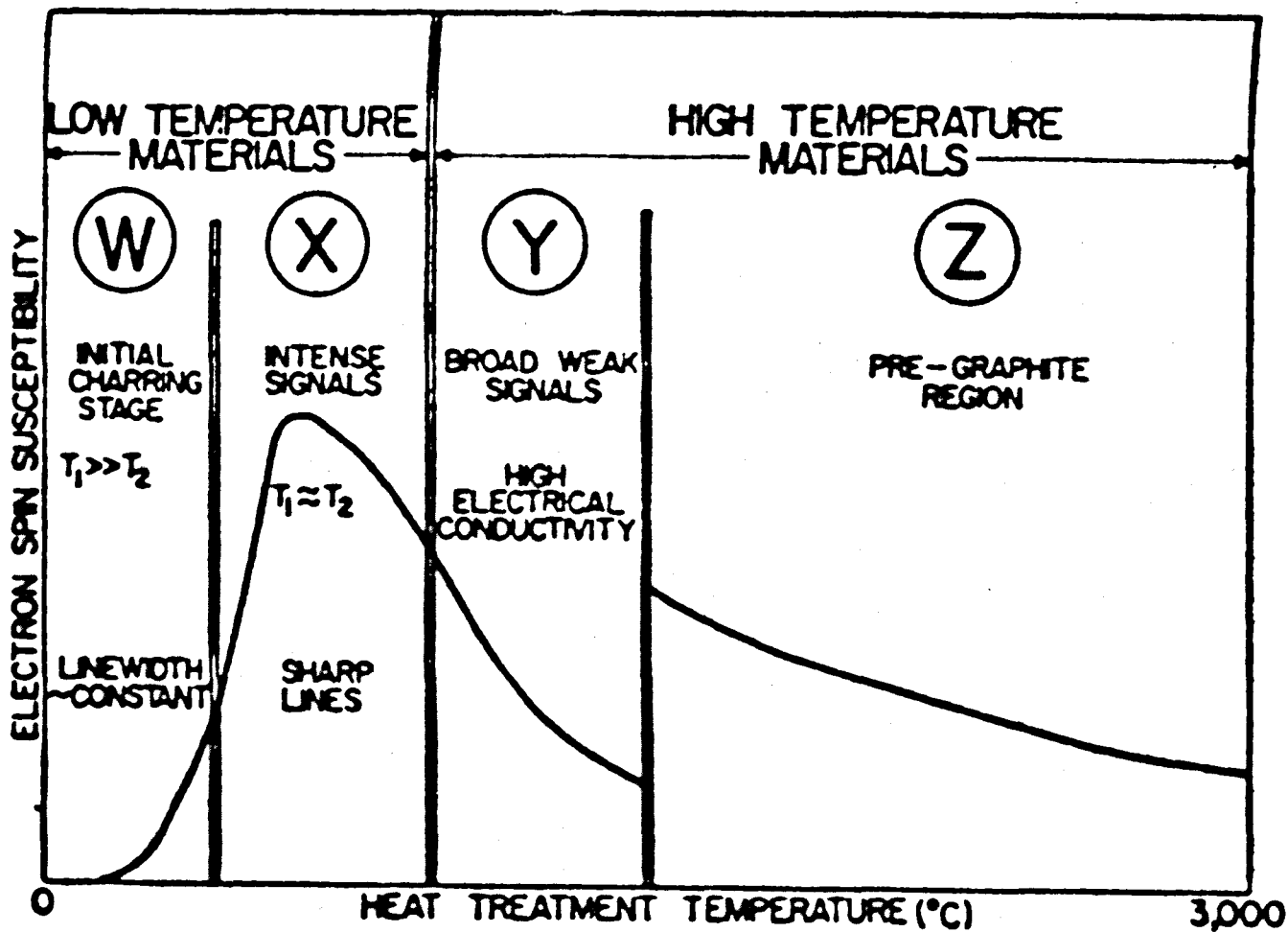
obtained from studies of the temperature coefficient of resistance and HTT it was shown that amorphous carbon behaved as a semiconductor with the energy gap between the conduction band and valence band gradually decreasing with increasing HTT and crystallite size, finally disappearing or even overlapping for large graphite crystals.

A summary of the results and band model of Mrozowski's school is illustrated in Fig. 3.2. Below HTT of 600°C the resistivity is very high ($>10^7$ ohm-cm) because of the low concentration and mobility of the carriers. The large drop in resistivity between HTT $600 - 1000^{\circ}\text{C}$ is mainly ascribed to the increase in the number of carriers. This is believed to occur during the evolution of gases (hydrogen etc.) in the carbonization process which leaves free valence σ -electrons in the periphery of crystallites and these trap π -electrons leaving a large excess of holes in the valence band. In line with these ideas the thermo-electric power rapidly decreases in this range since its magnitude is inversely proportional to the hole concentration. The fact that the TEP and Hall coefficient actually becomes negative in the range $1000 - 1750^{\circ}\text{C}$ is taken to indicate that the Fermi level is depressed so low as to become located below the E vs K inflection surface of the valence band. From 1400°C onwards the Fermi level is believed to be rising as the number of electron traps are reduced by coalescence of crystallites. The Hall coefficient and TEP become positive again and increase in magnitude as the number of hole carriers is reduced. Throughout this region (HTT $1000^{\circ}\text{C} - 2000^{\circ}\text{C}$) the resistivity remains approximately constant due to the increasing mobility of the carriers (reduced scattering at crystallite boundaries), being offset by their decreasing number.

Above HTT $\sim 2000^{\circ}\text{C}$ the number of carriers is believed to increase again as a result of thermal excitation of electrons into the conduction band which has gradually approached the valence band until it is separated from it by only a very small energy gap ($\sim 0.01\text{eV}$). The increase in carriers explains the decrease in Hall coefficient and TEP and also the knee in the resistivity curve. The change of the Hall coefficient from positive to negative values for well graphitized materials is believed to be due to the increasing contribution of more mobile negative carriers in the upper band. The TEP in this region is complicated by the phonon drag effect.

On this model the position of the positive maximum in the Hall constant and TEP in the region of HTT 2000°C is determined by a balance between the decreasing number of holes and increasing number of electrons created by thermal excitation into the conduction band. The experimental observation of a shift in the maximum to higher HTT with decrease in ambient temperature is consistent with this idea.

No explanation of the magneto-resistive behaviour was given; however its close correlation with the Hall coefficient suggested an association between the sign of the magneto-resistance and the sign of the current carriers. In particular the origin of the negative magneto-resistance in poorly graphitized carbons has not been conclusively clarified. It has been suggested that diffuse scattering at the crystallite boundaries is influenced by the magnetic field to such an extent it could cause a negative magneto-resistance of the observed magnitude⁽³⁹⁾. It seems however that negative magneto-resistance is a fairly good measure of the degree of graphitization.



Classification of carbonaceous materials by their ESR properties.

FIGURE 3.3

3.2.2 ESR properties

The subject of ESR in carbonaceous materials has been critically and comprehensively reviewed by Singer⁽⁴⁰⁾ and only a brief outline will be given here. For the purpose of his review, Singer divided carbonaceous materials, primarily on the basis of their ESR properties, into four classes as shown in Fig. 3.3. The electron spin susceptibility curve is followed quite generally for most chars.

In the initial charring region W, very little is known about the rate of appearance of spin paramagnetism. This is due mainly to the $T_1 \gg T_2$ property which requires superheterodyne detection for adequate sensitivity at low microwave powers. Some light has been shed, however, on the paramagnetism in this region by Singer and Lewis^(41,42,43) who carried out carbonizations in inert liquids. Here the tumbling motion in the liquid averages out the nuclear hyperfine interactions and the resulting hyperfine spectra allows the identification of the free radicals produced in the early stages of carbonization. Interestingly, a tentative correlation between the planarity of the free radical intermediate and the degree of order of the final graphite seems to have been established⁽⁴³⁾.

The spin concentration rapidly increases and reaches a maximum in region X, where the line width becomes very narrow and T_1 decreases and becomes independent of temperature, an indication that exchange effects are probably occurring.

The origin of paramagnetism in low temperature chars has been ascribed to σ -electrons localized at carbon atoms⁽⁴⁴⁾. However, the

grinding experiments on which this conclusion was based⁽⁴⁵⁾ are now subject to question because of skin depth complications. Another view on the origin of paramagnetism, in this region, is that hydrogen or edge groups are removed by homolytic bond scission during carbonization and unpaired spins become stabilized in the aromatic skeleton as π -electrons⁽⁴⁶⁾. Evidence in favour of this view comes from several sources: firstly it was observed that the presence of aromatic rings appear to be necessary for the stability of the spin centres⁽⁴⁷⁾. Secondly, exchange narrowing can apparently occur, even at comparatively low spin concentrations, and thirdly well resolved hyperfine spectra were observed in the charring experiments of Lewis and Singer^(41,42,43) suggesting a considerable degree of delocalization of the electrons. The delocalization of electrons over the molecules gains further support from observations of their general stability and from double resonance studies on carbons⁽⁴⁸⁾.

The suggestion that an odd carbon molecule resulting in an odd number of π -electrons might be responsible for part of the ESR⁽⁴⁹⁾ has gained some support when such radicals were identified⁽⁴¹⁾.

The decrease in the spin susceptibility after the peak (HTT - 500°C) can then be ascribed to the gradual formation of large aromatic sheets resulting in the saturation of most of the broken edge bonds.

The high temperature carbons of regions Y and Z (HTT > 600°C) are characterized by their good electrical conductance. The ESR of materials having resistivities less than -10 ohm.cm can be dominated

by their electrical rather than their magnetic properties and usually exhibit skin depths of the order of one millimeter or so at X-band. For samples large compared to the skin depth the line will be Dysonian and can be analysed by the method of Feher and Kipp⁽³³⁾. For powders, particles of a size less than the skin depth can be dispersed in an insulating matrix to avoid skin depth complications.

Another feature of amorphous carbons is the coexistence of two carbon phases, one consisting of turbostratic crystallites of graphite and the other consisting of the amorphous carbon matrix cementing the crystallites with each other. The observed ESR signal is still found to be one narrow line. This is ascribed to the remarkable phenomenon of "crystallite averaging"⁽⁵⁰⁾ which occurs in partly graphitizing carbons and polycrystalline graphite. Essentially this averaging is similar to motional averaging, the mobility of the charge carriers enabling them to 'sample' several crystallites before they relax. The result is that the g-value of the resonance due to the conduction electrons will correspond to the spatial average of the crystallites distributed through the carbon.

Some years ago Mrozowski⁽⁵¹⁾ showed that the temperature behaviour of lightly irradiated polycrystalline graphite was intermediate between that characteristic of charge carriers in pure graphite and that of localized spin centres. On the basis of a detailed study of the temperature dependence as a function of neutron irradiation and doping, he concluded that the experimental results could be readily explained by assuming that the single absorption line is due to

both charge carriers and localized spin centres, the single g-value of the line being the result of the presence of an exchange mixing mechanism (named mixing or M-effect). Essentially the same conclusions were independently arrived at by Marchand and Delhaes⁽⁵²⁾. It is assumed that both types of centres contribute to the ESR intensity independently and that the individual contributions can be obtained by splitting the intensity (I) vs temperature (T) curves into two parts, a purely curve part with $I \propto 1/T$, characteristic of the localized centres and a part which is to a first approximation temperature independent due to conduction carriers.

If X is the fraction of the total intensity due to charge carriers at a temperature T, then the ratio R of the intensities between T and another temperature T', can be written as

$$R_{(TT')} = \frac{I(T')}{I(T)} = \frac{a + bT'}{a + bT} X_{(T)} + \frac{T}{T'}(1 - X_{(T)}) \quad (3.1)$$

The resonance intensity I is usually measured between room and liquid nitrogen temperatures so that $T = 300^{\circ}\text{K}$ and $T' = 77^{\circ}\text{K}$. The coefficient of $X_{(T)}$ represents the temperature variation of the intensity of conduction electrons⁽⁵⁰⁾. The variation is in fact small so that this term is nearly equal to one. (Mrozowski⁽⁵¹⁾ takes the value to be between 0.88 and 1 between 77 and 300°K). The coefficient of $(1 - X_T)$ is of course the Curie term responsible for the intensity variation of localized centres. The coefficient R between room and liquid nitrogen temperatures can then be written as

$$R = I_{77}/I_{300} = X_{300} + 3.89 (1 - X_{300}) \quad (3.2)$$

From a knowledge of R, obtained experimentally, it is then an easy matter, using equation (3.2) to compute X, the fraction of the total intensity due to charge carriers.

The exchange mixing mechanism (M-effect) also governs the g-value of the resonance line, whose g-value will be intermediate between that for localized spin centres g_L (which is isotropic and has a value $g_L = 2.0023$) and that for conduction carriers g_c . It is then possible to write

$$g_{\text{expt}} = Xg_c + (1 - X)g_L \quad (3.3)$$

It should be noted that g_{expt} is the spatial average over all crystallites in the material.

Mrozowski's school^(53,54,55,56) has subsequently shown that the basis for the mixed character of the ESR line was firmly supported by a mass of experimental evidence.

3.3 Carbon Fibres

Because of the high melting point of carbon and its insolubility in solvents carbon fibres cannot be manufactured by spinning and are obtained by carbonization and pyrolysis of organic materials.

The initial organic, the precursor, is usually an organic polymer textile fibre consisting of a highly oriented array of huge molecules each comprising a backbone of carbon bearing branches of nitrogen and hydrogen. The structure of the carbon produced depends

critically on the choice of the precursor. For example, taking two very similar vinyl polymers, Polyvinyl chloride (PVC) and Polyvinylidene chloride (PVDC) and pyrolyzing them, PVC yields a carbon which graphitizes easily while PVDC yields a carbon which does not graphitize and forms an amorphous carbon devoid of any crystal structure so as to be almost glassy.

Franklin⁽⁵⁷⁾ appears to have been the first to discuss the nature of graphitizing and non-graphitizing carbons (Mrozowski⁽³⁶⁾ prefers the terms soft and hard carbons respectively) in any detail. In non-graphitizing carbons, extensive crystallite development is thought to be hindered by rigid cross-linking between neighbouring crystallites. This system of cross-linking is believed to be formed during the early stages of carbonization and is preserved upon heating to higher temperatures. The cross-links hold neighbouring crystallites apart and in a random orientation with respect to each other and effectively hinders coalescence which is a necessary preliminary of complete graphitization. For a carbon to graphitize it appears that the crystallites must be in close proximity (few pores) and furthermore, they must be approximately parallel to each other. By carrying out detailed studies Franklin also showed that those materials which had an excess of hydrogen, or were poorer in oxygen or possessed a reasonable degree of parallelism in the starting molecular units, could usually produce graphitizing carbons. Those with the opposite characteristics lead to non-graphitizing carbons. In addition graphitizing carbons lose considerable weight during heat treatment so that the yield of carbon is poor. PVC for example loses 90% of its carbon content, PVDC retains nearly all its carbon content⁽⁵⁸⁾.

The advantageous mechanical properties associated with carbon fibres appear to be linked with the graphitization within the fibre. Consequently the choice of the precursor becomes of primary importance. Precursors leading to graphitizing carbons coalesce or flow at low temperature causing the disruption of the ordered molecular array and the loss of the advantages of working with fine fibres. On the other hand fibres of the non-graphitizing type do not have this drawback but neither do they attain the desired degree of graphitization.

3.3.1 Manufacture

In his classical paper Shindo⁽⁵⁹⁾ examined the possibility of producing high modulus carbon fibres from a polyacrylonitrile (PAN) precursor fibre. He recognized the beneficial effect of oxidizing the fibre in the early stages of pyrolysis on the yield of carbon and on the mechanical properties of the fibre. The production technique developed by Shindo consisted in pre-oxidizing the PAN fibre at $\sim 300^{\circ}\text{C}$, then carbonizing it at $\sim 1000^{\circ}\text{C}$ and graphitizing it at $\sim 3000^{\circ}\text{C}$. The term graphitization appears to be widely used in carbon fibre literature to refer to the high HTT process where considerable crystallite growth occurs ($1000 - 3000^{\circ}\text{C}$). It should be emphasized, however, that these fibres are strictly non-graphitic carbons, whose crystallites do not attain the size nor achieve the perfection of typical graphitizing materials.

Graphitization leads to an increase in crystallite size from $\sim 10\text{\AA}$ at 1000°C to $\sim 100\text{\AA}$ at 3000°C . The fibres produced by Shindo however

did not possess the outstanding mechanical properties which distinguish carbon fibres now available.

Three British scientists, Johnson, Phillips and Watt⁽⁶⁰⁾ produced a PAN based carbon fibre by carrying out essentially the same steps, namely pre-oxidation, carbonization and graphitization developed by Shindo but they discovered a way of improving the crystallite orientation. This they achieved by simply restraining the natural shrinkage of the PAN fibre during the initial pre-oxidation at quite low temperatures. The molecular chains are now less free to relax during the heat treatment and the final layers of graphitic hexagons become highly oriented parallel to the fibre axis. This step in the production process leads to the high modulus fibres now being used in several important industrial applications.

The American process of production of carbon fibres involves the pyrolysis of a cellulose precursor. The viscous thread is heated to about 2000°C, and then stretched up to 52% while at this temperature. This pulls the graphite crystallites into orientation with substantial gains in modulus.

The properties of ordinary carbons either increase or decrease continuously with HTT. The tensile strengths of carbon fibres, however, go through a maximum at about a HTT of 1500°C and then decrease, whereas their moduli continue to increase with HTT. This behaviour has given rise to two types of carbon fibres, one with high strength and low modulus and the other with high modulus and somewhat lower strength.

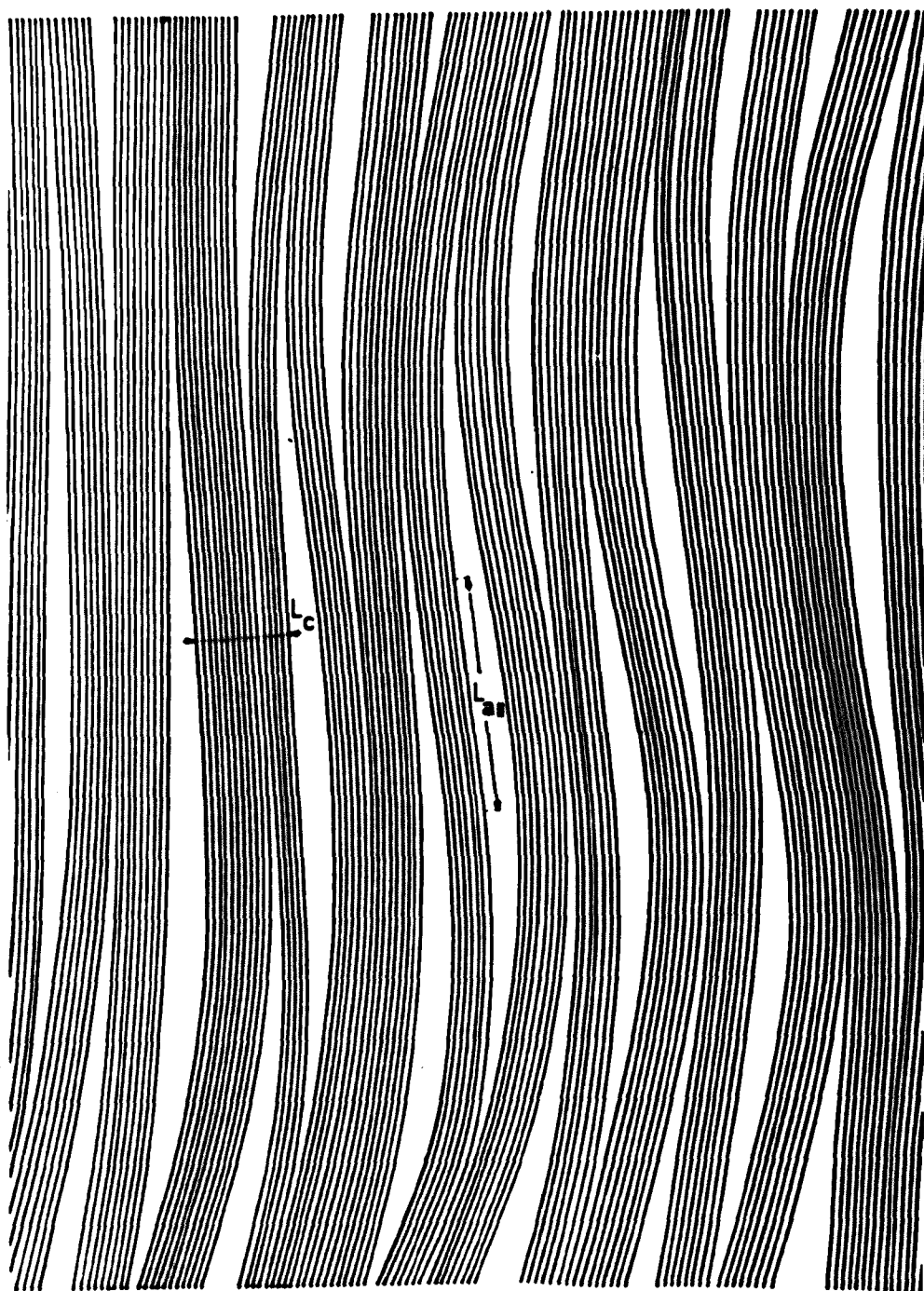
3.3.2 Structure

Much of the literature concerning carbon fibres has been collected together by Fourdeux et al.⁽⁶¹⁾ in a paper summarizing the present knowledge on the structure of carbon fibres. The majority of papers have dealt with the structure of PAN based or rayon based fibre. The basic structural features however being similar for both types, the observation on either one can be considered as valid for both.

Shindo's original findings that the carbon atoms form two dimensional hexagonal layers packed in small stacks or crystallites of varying sizes with the layer planes parallel to the fibre axis, has been generally substantiated by X-ray and electron diffraction studies^(62,63). The absence of three dimensional reflections (hkl) in the X-ray diffraction patterns, even at the higher HTT, indicates that these fibres are essentially non-graphitizing. The main difference between the structure of carbon fibres and that of bulk non-graphitic (glassy) carbons is the preferred orientation of the carbon layers which is responsible for the anisotropy of various physical properties of carbon fibres. In general, the orientation of the carbon layers becomes more perfect with increasing heat treatment and stretching. The average deviation from the perfect orientation is of the order of $\pm 10^\circ$ ⁽⁶³⁾ but can be of the order of $\pm 4^\circ$ ⁽⁶⁴⁾ for good quality fibres.

X-ray diffraction has shown that the crystallites are turbostratic (c spacing $\sim 3.39\text{\AA}$ compared to 3.35\AA for graphite) with L_c at least twelve layer planes (50\AA) and L_a in the range of $60 - 120\text{\AA}$ ⁽⁶²⁾. These crystallites are stacked end to end to form chains along the fibre axis.

FIBRILAR STRUCTURE OF CARBON FIBRES



200 Å

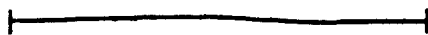


FIGURE 3.4

Sharp edged needle-like pores with cross-sections in the 10 - 20A range and length above 300A separate these crystallites and account for 5% to 30% of the total volume⁽⁶⁵⁾. The pore axes are preferentially oriented parallel to the fibre axis and sharpness of the density transitions at the pore boundary suggests that the pore walls are predominantly formed by carbon planes.

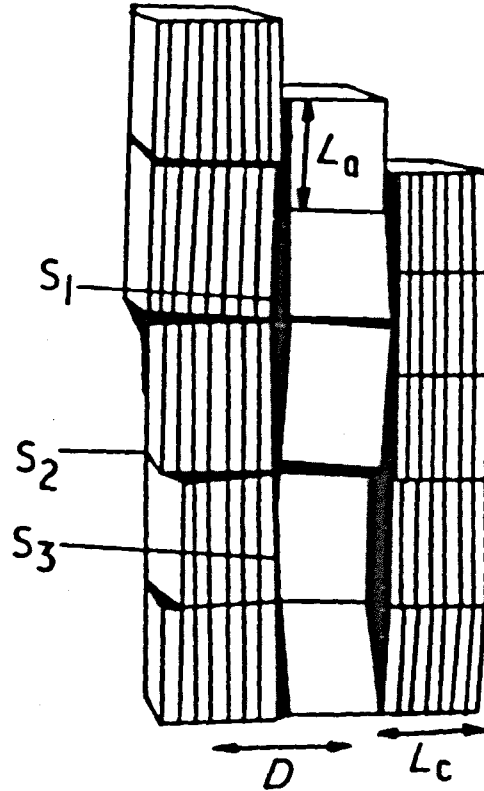
Electron diffraction studies confirm the X-ray estimate of crystallite size and show that the crystallites form long chains lying parallel to the fibre axis. These chains are bonded together to form a network of branched fibrils that appear to run through the full length of fibre.

Bacon and Tang⁽⁶⁶⁾ have shown that a direct correspondence exists between the cellulose molecular orientation and preferred orientation of the carbon fibre and suggest that the "carbon chains" are formed along the paths of the original cellulose chains preserving a "replica" of the original fibre structure. This "memory" carbon fibres retain of the original precursor structure seems to be generally substantiated by other workers, the size and degree of branching of the fibrils being derived from the fibril structure of the parent fibre.

The modulus of the carbon fibre is determined by the orientation of the graphite crystallites within the carbon fibrils while the strength is a function of the inter-fibrillar bonding by cross-linking.

Franklin⁽⁵⁷⁾ proposed that the cross-linking was composed of strong covalent tetrahedral (sp^3) bonds which were also responsible for the non-graphitizing characteristics of these solids. The presence of this

CRYSTALLITE STRUCTURE OF CARBON FIBRES



Schematic, idealized diagram summarizing x-ray diffraction evidence. S_1 , void; S_2 , subgrain twist boundary; S_3 , intercrystallite boundary.

FIGURE 3.5

cross-linking would preclude the formation of lamellar compounds in such materials. But it was shown clearly that potassium and caesium can be intercalated easily and in stoichiometric quantities, without disturbing the preferred orientation of the carbon layers⁽⁶⁵⁾. These results indicate that there are essentially no cross-links perpendicular to the carbon layers. The favourable mechanical strength of carbon fibres must then be accounted for by a form of fibrillar branching or by some other form of cross-linking.

A schematic presentation of this fibrillar structure of carbon fibres is presented in Fig. 3.4. The thickness of these fibrils which is equivalent to the c-axis dimension of a graphitic crystallite L_c , is of the order of 50A. They are believed, however, to have a length of up to several thousand angström units, the low X-ray value for this dimension ($L_a \sim 50A$) being a measure not so much of the fibrillar length but rather of the distance between successive discontinuities in it.

An arrangement for the crystallites within a fibre has been described by Johnson and Tyson⁽⁶⁷⁾ and their model is shown in Fig. 3.5. These authors also report the existence of a perfectly stacked three-dimensional graphite phase which although is only present in small amounts in normal conditions becomes the predominant phase when the fibres are recrystallized in the presence of nickel.

CHAPTER 4

THE ESR SPECTROMETER AND EXPERIMENTAL TECHNIQUES

4.1 The ESR Spectrometer

At the outset, the ESR spectrometer available was of the type employing a helix (see section 2.2.6) instead of a microwave cavity. In addition to complications due to electrical conductivity, frequent exchange and positioning of samples in the confined space enclosed in the helix, proved to be somewhat difficult. Furthermore, although operation at liquid nitrogen temperatures was possible, variable temperature facilities were not available. It was therefore found necessary to convert the helix based spectrometer into a bridge system employing a microwave reflection cavity. This entailed the construction of an AFC unit, which of course the helix, as a broad band device, did not necessitate.

The X-band ESR spectrometer eventually assembled featured a microwave bridge system employing a bucking arm, and a microwave circulator. Phase sensitive detection at 100 KHz magnetic field modulation was employed and a 10 KHz AFC system used to lock the klystron frequency to that of the resonance cavity. The block diagram for this ESR spectrometer is shown in Fig. 4.1.

4.1.1 The microwave bridge

The 3 cm wavelength microwave radiation is provided by an E.M.I. klystron valve (E.M.I. R9696) inserted in an E.M.I. cavity (E.M.I. 25157),

BLOCK DIAGRAM OF X-BAND ESR SPECTROMETER.

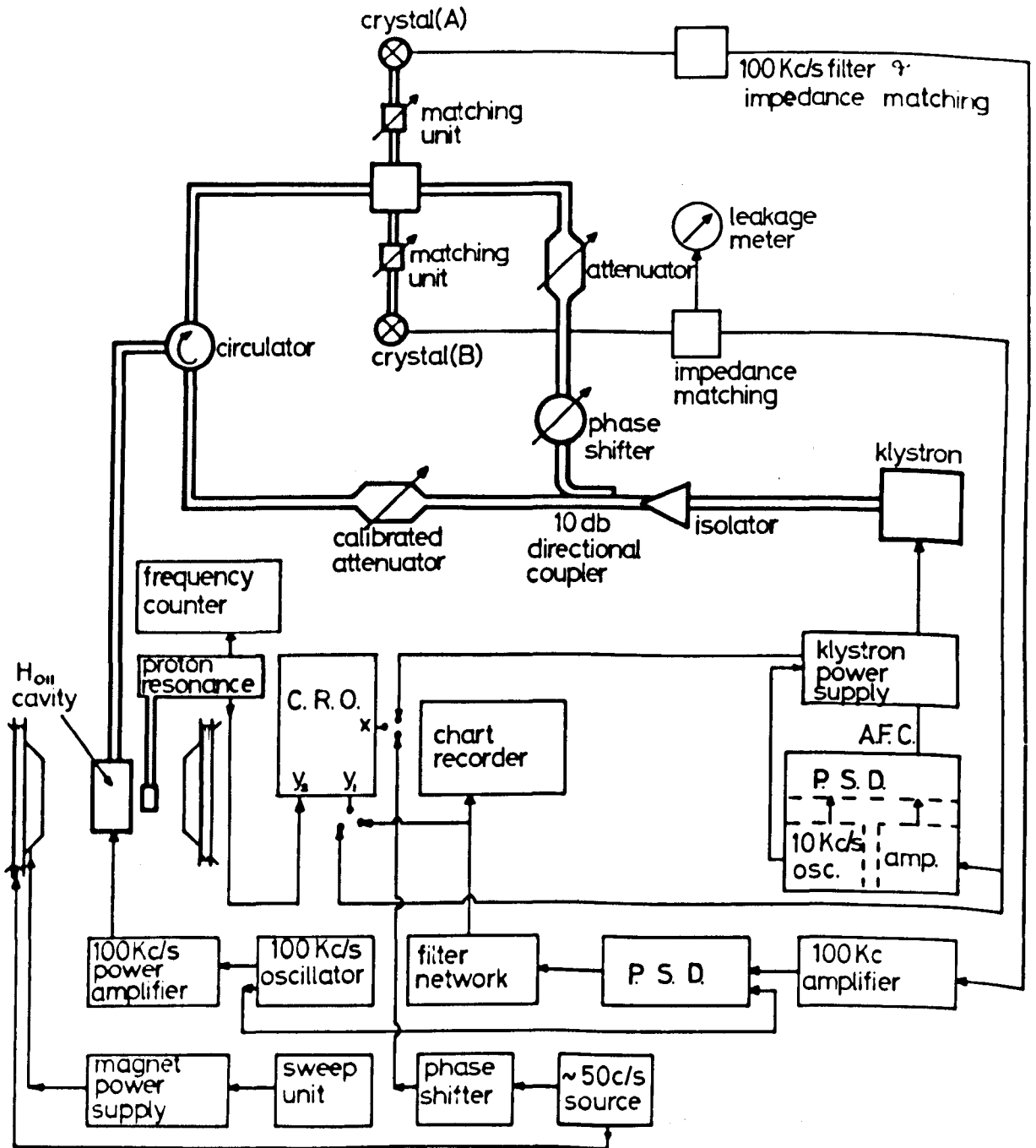


FIGURE 4.1.

powered by a Hewlett Packard klystron power supply (HP7163). The klystron valve had a nominal output power of 100 mW and a tunable range of about 30%. The microwave power feeds into a standard X-band wave guide run of internal dimensions 0.4×0.9 inches.

The isolator is placed immediately after the klystron with the purpose of allowing oncoming power from the klystron to pass unattenuated while absorbing any power reflected in the opposite direction, which if allowed to reach the klystron might affect its frequency stability. Some of the power is then extracted by means of a 10 db directional coupler and is suitably phased and attenuated to provide the operating bias for the crystal detectors, the remainder being fed to the microwave cavity via a calibrated attenuator. A circulator (Marconi F1046-32) is used to direct the incident power into the cavity and the reflected power to the crystal detectors A and B via a magic-T, the fourth arm of which is attached to the bucking arm supplying the crystal bias.

4.1.2 The microwave cavity

The resonance cavity employed throughout this study was a cylindrical (Microspin type W932) cavity, operating in the H_{011} mode. The cavity and its various accessories are shown in Fig. 4.2. The microwave power is transmitted to and from the cavity via a coaxial line (central column) which emerged on the inside of the upper cavity wall in a small bent 'hook' whose orientation could be varied, to critically couple the cavity to the coaxial line. The 100 KHz field modulation is fed (via two side columns) to two pairs of rods parallel

MICROWAVE CAVITY AND
ACCESSORIES

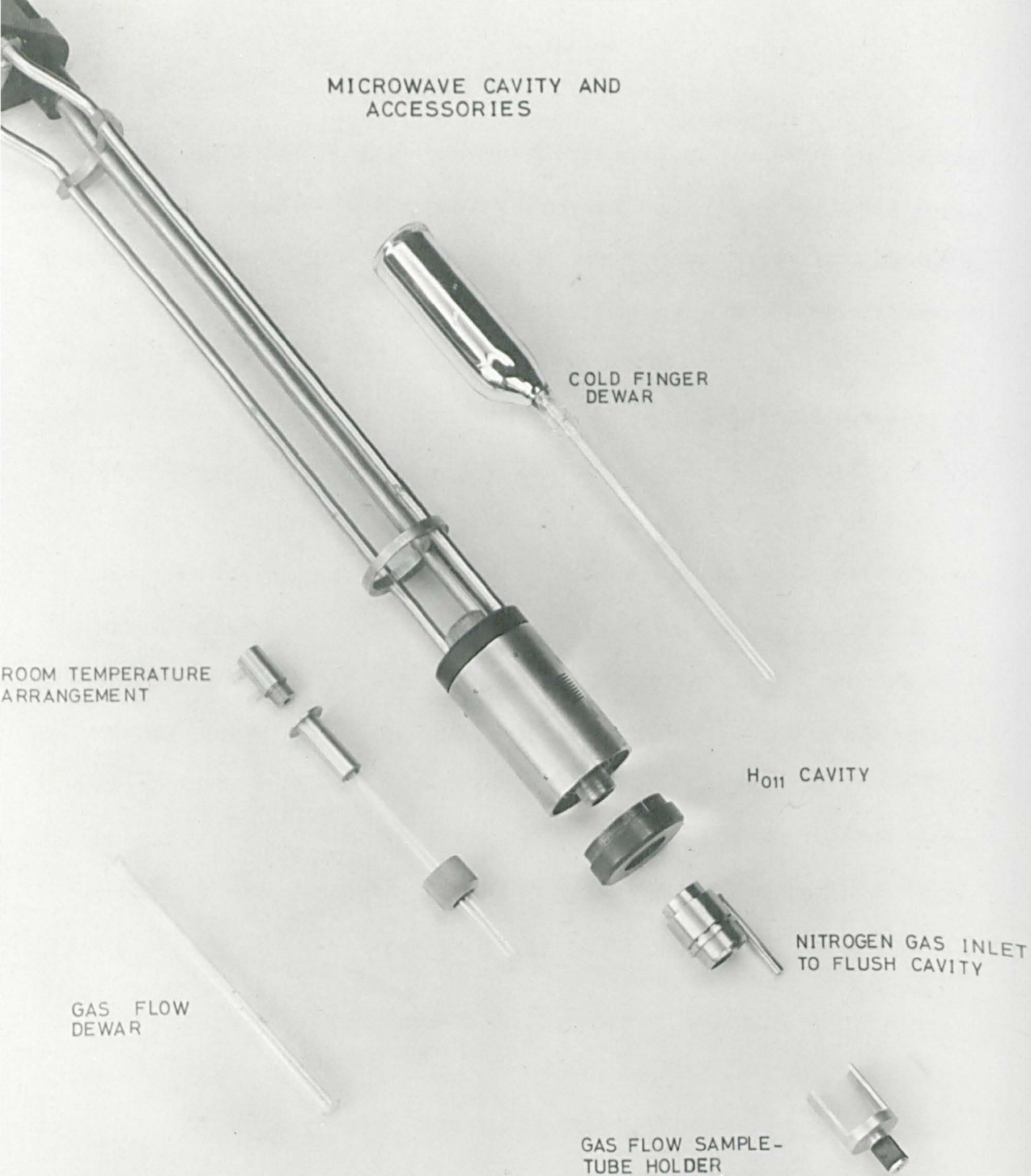


FIGURE 4.2.

to the cavity axis and positioned so as not to interfere with the E-fields set up within the cavity. The direction of the modulating field could be shifted by 90° by switching from one pair of rods to the other, thus ensuring a modulation component along the static magnetic field for any position of the rotating magnet.

For studies at 77°K , the sample was immersed in liquid nitrogen and positioned inside the cavity by means of the quartz finger dewar (Fig. 4.2).

For variable temperature studies a gas flow system was used. Cold nitrogen gas, emerging from a heat exchanger immersed in liquid nitrogen cools the sample placed inside the cylindrical quartz dewar inserted inside the cavity. The temperature, monitored by a copper-constantan thermo-couple, could be varied by altering the rate of flow of the nitrogen gas.

At temperatures below 0°C it is necessary to ensure against the condensation of water vapour inside the cavity, which would result in damping of the cavity Q. This is achieved by flushing the cavity with dry nitrogen gas.

4.1.3 The magnetic field assembly

The magnetic field was supplied by a Newport type E, 7 inch, air cooled electromagnet powered by a Newport D104 supply. Shims on the magnet pole pieces enabled improvement of the magnetic field homogeneity. A sweep unit (Newport SSU) allowed the resonances to be slowly swept through. The main d.c. magnetic field could also be modulated by a small

50 Hz field through subsidiary Helmholtz coils surrounding the poles of the magnet. The magnet as a whole is placed on a rotating mount which enables the magnetic field to be rotated about the cylindrical axis of the cavity.

A proton resonance unit (Newport PMK II) was used to measure the magnetic field. This consists of a coil containing some hydrogenous materials (waxes, oils or aqueous solutions) being placed in the magnetic field. The r.f. frequency in the coil can be varied by means of a variable air condenser to satisfy the N.M.R. resonance condition for protons. The resonance can be displayed on the C.R.O. The resonance frequency ν_p is then measured by means of an electronic counter (Marconi Instruments frequency converter TM5951 - counter 1417/2).

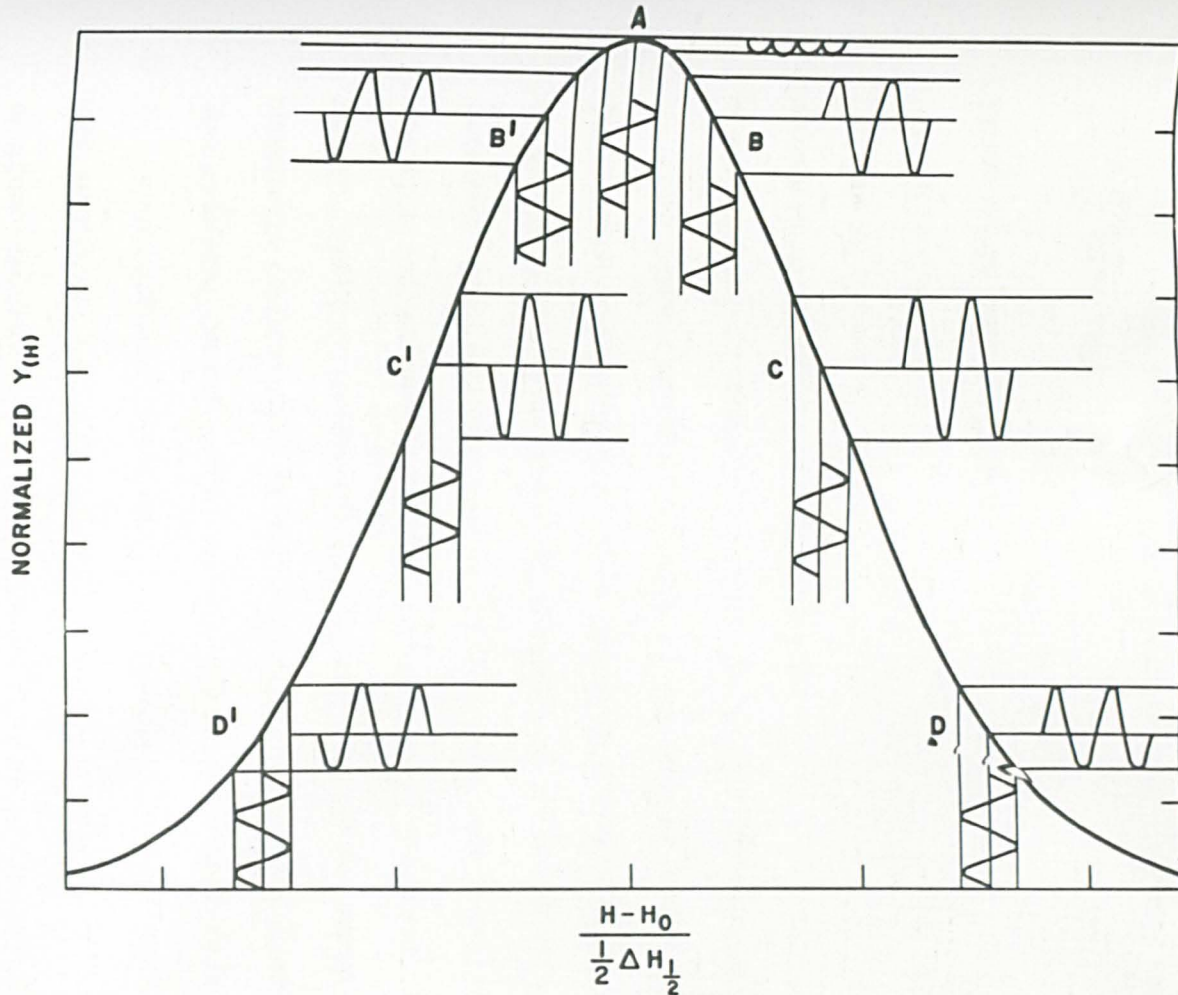
The gyromagnetic ratio of the proton having been determined to a high degree of accuracy (1 part in 10^5 at least) the value of the magnetic field can be calculated from

$$H = 2.3487 \times 10^{-4} \nu_p \text{ gauss}$$

where ν_p is measured in Hz.

4.1.4 Detection

Phase sensitive detection can be obtained by modulating the magnetic field with an a.c. (preferably 100 KHz, see section 2.2.4) field whose amplitude is small compared to the width of the resonance line one wishes to observe. An alternating magnetic field is thus superimposed on the constant magnetic field. The "constant" magnetic field is then



The ESR signal produced at various points on the resonant line in a magnetic field modulated spectrometer. The vertical magnetic field modulation interacts with the bell-shaped absorption curve [χ' or $Y(H)$] to produce the horizontal ESR signal.

FIGURE 4.3

slowly and linearly swept through the resonances. The magnetic field modulation is transformed, by the shape of the resonance absorption curve, to microwave power modulation, according to the mechanism illustrated in Fig. 4.3. The amplitude of the resultant microwave modulation will correspond to the gradient of the absorption curve, its phase being reversed upon passage through the absorption maximum. Amplification and phase sensitive detection of the 100 KHz modulated microwave signal yields the first derivative of the absorption line which can then be readily traced out on a pen recorder.

The first derivative of the absorption line can also be displayed on the screen of a C.R.O. by imposing a 50 Hz sweep on the magnetic field and feeding onto the Y-plates the output of the P.S.D. which takes as its reference signal a voltage from the original oscillator via a suitable phase shifter. Scope presentation however is inherently less sensitive, as the band width of the amplifier is necessarily made large enough to include the lower frequency 50 Hz sweep, and tracing out the first derivative of the absorption curve on a pen recorder is the normal way of presentation.

A 100 KHz home-made oscillator was available, the output of which was amplified by a power amplifier (Microspin FA211) to provide the modulating rods in the cavity with 100 KHz a.c. voltage. A separate output from this oscillator supplies the P.S.D. with the reference signal. The modulated 100 KHz microwave power is rectified and detected at the detecting crystals A and B. (A;AEI cs9-B 5G - B;AEI cs10-B) together with the 10 KHz AFC signal (see section 4.1.5). The 100 KHz frequency

containing the ESR information is extracted from the output of crystal A by means of a 100 KHz tuned filter circuit. This is then amplified by a low noise amplifier (Brookdeal LA350 - Max. gain 100 db) and fed to the input of the P.S.D. (Brookdeal PP313A), the reference signal of which is taken directly from the 100 KHz oscillation via a phase shifter. The d.c. output of the P.S.D. is filtered by an R.C. circuit and traced out on a pen recorder (TOA EPR-2TB).

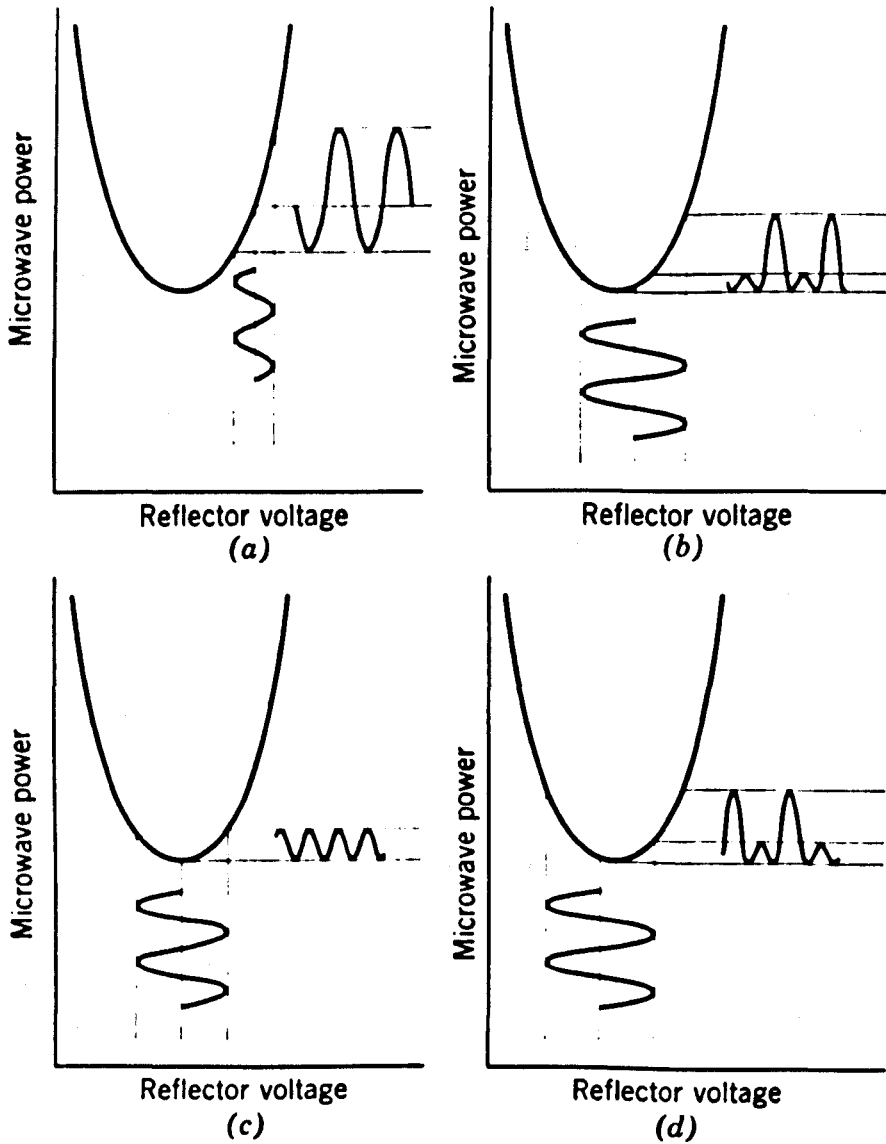
The 10 KHz AFC frequency is picked up from crystal detector B and fed to the input of the AFC unit.

4.1.5 A.F.C.

Basically the function of an AFC system is to respond to any change in klystron frequency by supplying an error voltage, the polarity of which depends on whether the frequency has drifted above or below that of a standard frequency. This error voltage may then be applied to the klystron reflector in such a way as to lock the klystron frequency to that of the standard. If the standard frequency is taken to be that of the resonant cavity, as in our case, then the AFC system will have the added advantage of adjusting the klystron to compensate for any changes which might occur in the cavity resonance arising, for example, in variable temperature experiments. Caution must then be observed when accurate g-value determinations are required, since such shifts in frequency may result in erroneous determinations.

The most common way of locking the klystron to the cavity is by frequency modulating the klystron output by voltage modulating the

PRINCIPLE OF AFC



Error signal klystron stabilizer in the neighborhood of resonance:
 (a) far off resonance ($f \gg f_0$); (b) close to resonance ($f > f_0$); (c) on resonance ($f = f_0$); (d) close to resonance ($f < f_0$)

FIGURE 4.4

reflector of the klystron valve. The frequency modulation is converted to an amplitude modulated error signal by the cavity resonance as illustrated in Fig. 4.4. When the klystron frequency f is equal to the resonant frequency of the cavity, f_0 , the error signal produced is twice the frequency of the modulating signal. Drift in frequencies from f_0 will give rise to an error signal, the amplitude of which increases with the extent of drift, and the phase will depend on whether $f \gtrless f_0$. Amplification and phase sensitive detection will produce a d.c. voltage whose polarity will depend on f being greater or smaller than f_0 and whose amplitude will be zero at $f = f_0$ and increase with increasing difference between f and f_0 . This voltage can then be applied to the klystron reflector to correct for any frequency drift.

The 10 KHz AFC system constructed for this work (Fig. 4.5) is a modified and somewhat simplified version of the fully transistorized system described by Jung⁽⁶⁸⁾ which operated at 50 KHz. The main features of the circuit consist of a 10 KHz tuned collector oscillator, an amplifier and a PSD. The oscillator provides two independent outputs with two emitter followers. The first emitter follower (point X, Fig. 4.5) supplies the klystron reflector with a 10 KHz modulating voltage. The second emitter follower provides a reference signal which triggers the PSD via a phase shifter. The resulting error signal is amplified and fed through the PSD to provide the correcting voltage which is applied to the klystron reflector via a $1\text{ M}\Omega$ series resistance in the klystron power supply.

AFC CIRCUIT DIAGRAM

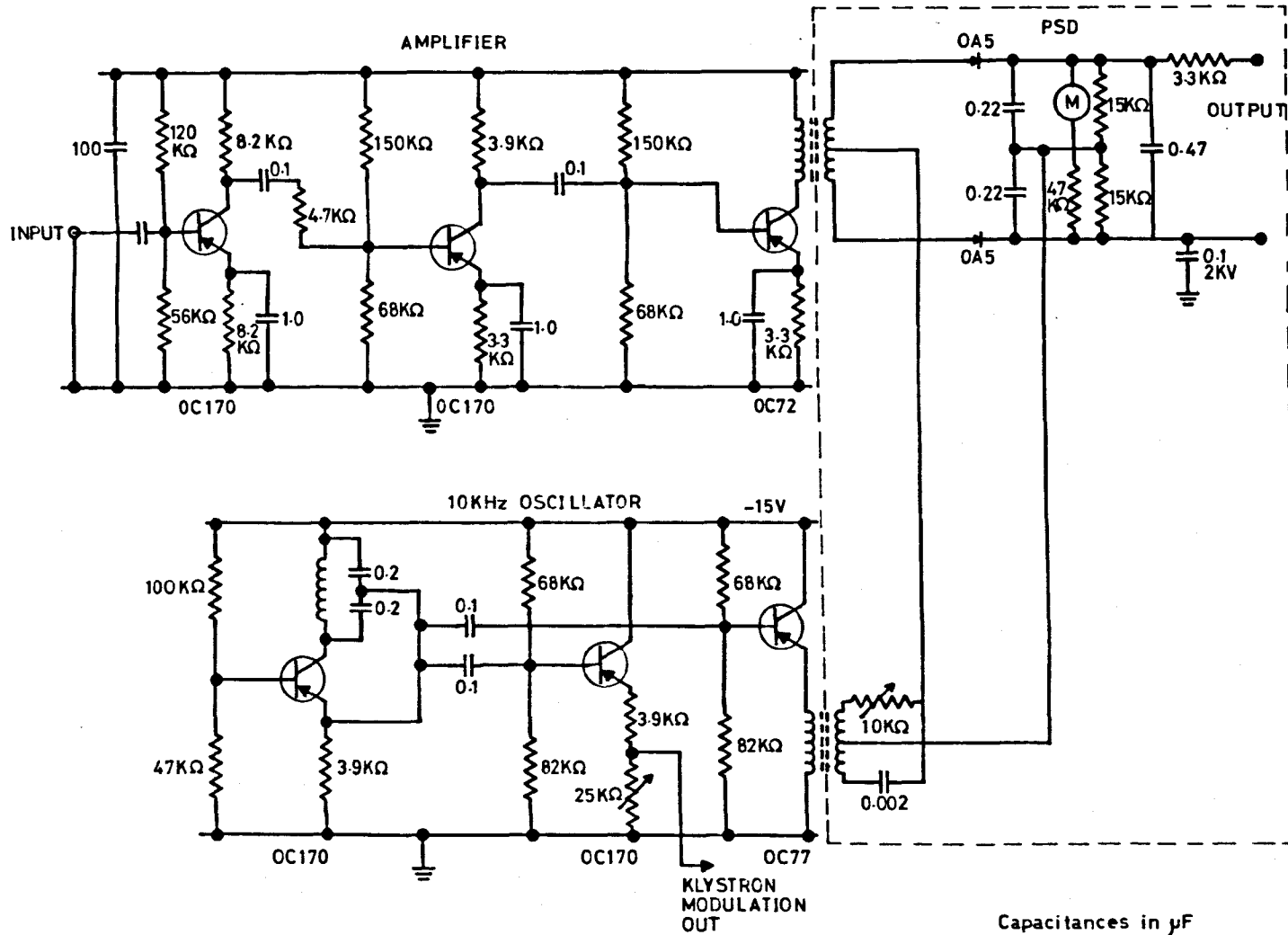


FIGURE 4.5.

This simple transistorized AFC system was found to operate satisfactorily for our purpose and could lock the klystron frequency to that of the cavity over some 7 or 8 reflector volts. This in fact was sufficient to operate the spectrometer with a finger dewar containing liquid nitrogen inserted in the cavity, the system being able to lock to bubbling liquid nitrogen.

The use of 10 KHz reflector modulation precludes observations on line widths narrower than about 200 milligauss, which were not encountered during the course of this study.

4.1.6 Sensitivity

The sensitivity of an ESR spectrometer is generally expressed in terms of a minimum number of detectable spins, N_{\min} . For the classical analysis of ESR spectrometer sensitivities the reader is referred to Feher⁽⁶⁹⁾ and Ingram⁽⁷⁰⁾.

Experimentally an estimate of the sensitivity of a spectrometer can easily be made by recording the trace of a sample containing a known number of spins N_s and extrapolating to a signal just distinguishable from the noise, i.e. extrapolating usually to a signal-to-noise ratio of unity (some workers prefer to use a signal-to-noise ratio of 2:1). Since the number of spins present is equal to the area under the absorption curve, then clearly a narrow line will have a greater height than a broad line. The line width of the absorption curve, or the square of the line width of the first derivative curve, ΔH^2 , must therefore be divided into the spin concentration N_s to give the sensitivity.

ESR OF PHOSPHOROUS DOPED SILICON

2.5×10^{14} Spins

$\Delta H = 19.6$ Gauss

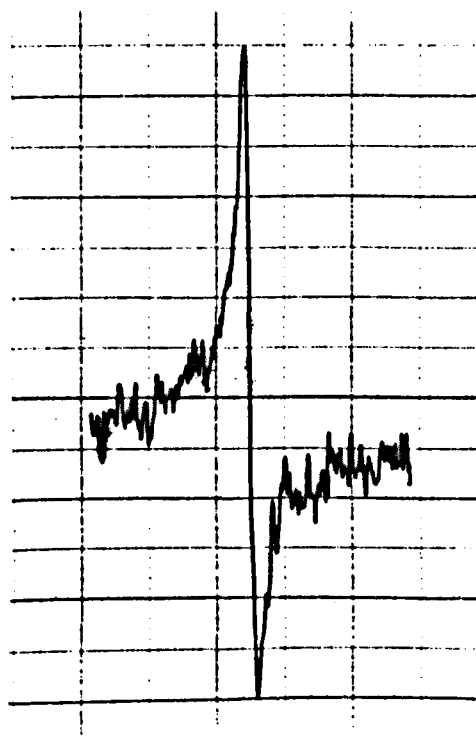


FIGURE 4.6.

Furthermore the height of the line depends on the modulation amplitude, H_{mod} and also increases as the square root of the microwave power P (as long as it is not modulation broadened or power saturated).

The sensitivity is therefore usually expressed for a modulation of 1 gauss and 1 mW power in the microwave cavity.

A suitable equation for calculating sensitivities will then be ^{*}

$$N_{\text{min}} = \frac{N_s H_{\text{mod}} \sqrt{P}}{\Delta H^2 Y'_m} \quad (4.1)$$

where Y'_m is the signal-to-noise ratio of the test sample.

To estimate the sensitivity of the spectrometer used in this work the signal from a standard sample of phosphorous doped silicon containing 2.5×10^{14} spins was traced out on the recorder chart and is shown in Fig. 4.6. The line had a width $\Delta H = 19.6$ gauss and a signal-to-noise ratio $Y'_m \sim 10:1$ and was recorded at a microwave power level $P \sim 100$ mW and a value of modulation amplitude $H_{\text{mod}} = 2.5$ gauss.

The sensitivity obtained, by substituting these values in equation 4.1, gives a minimum number of detectable spins $N_{\text{min}} \sim 10^{12}$ ΔH spins at R.T.

* This equation can be derived from equation 4.5 by obtaining the number of spins $N^A = N_{\text{min}}$ of line width $\Delta H^A = 1$ gauss which is just detectable from the noise $Y'_m{}^A = 1:1$ for an amplitude of modulation $H_{\text{mod}}^A = 1$ gauss detected at a microwave power level $P = 1$ mW at the cavity.

MOUNTING CARBON FIBRES FOR ESR

CARBON FIBRE
BUNDLE

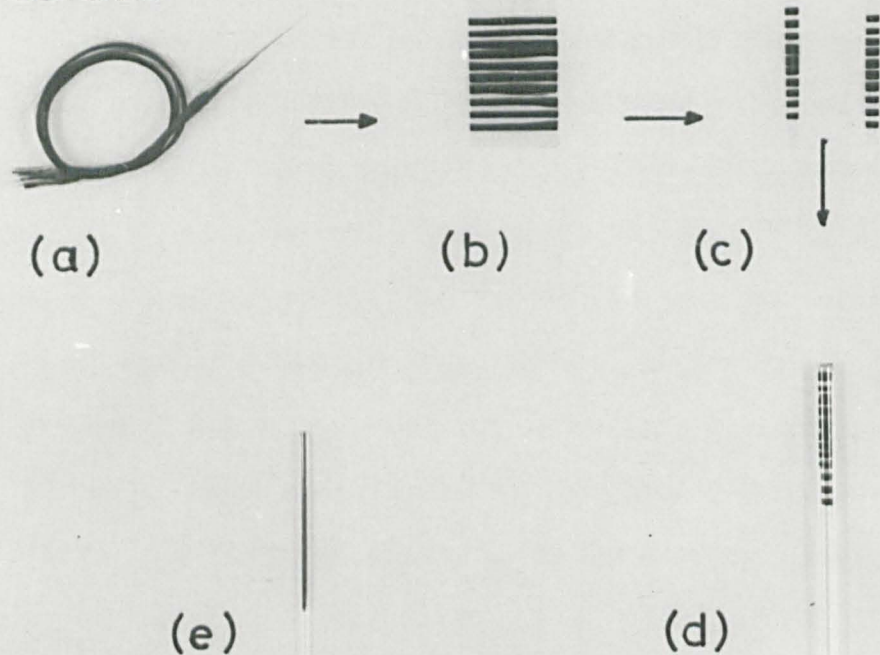


FIG. 4.7.

4.2 Mounting Carbon Fibres for ESR

The detection of any g-shift which might arise from the preferential alignment of graphitic crystallites along the fibre axis, necessitates the mounting of parallel bundles of fibres with their axes perpendicular to the axis of the cavity. The external magnetic field can then be rotated in a plane containing the fibre axis and the angular dependence of the g-shift can be obtained.

The carbon fibres studied in this work are good conductors of electricity ($\sim 10^{-3}$ ohm.cm) and exhibit a skin depth at X-band of $\sim 20\mu$. It is therefore necessary if the cavity Q is to be preserved to contain the sample within a small cylinder of diameter not greater than 2 or 3 mm along the axis of the cavity. Since the fibres must be mounted with their axes perpendicular to that of the cavity their length must not exceed ~ 3 mm. Furthermore a sufficient quantity of parallel fibres must be introduced into the cavity to enable an ESR signal to be observed.

These requirements were achieved as follows. Small bundles of fibres (Fig. 4.7a) wetted with acetone to bring individual fibres within a bundle into alignment, were gently stretched parallel to each other between two strips of ordinary cello tape (which was previously checked for the absence of an ESR signal) as shown in Fig. 4.7b. These were then cut up perpendicularly to the bundles into small strips 2 to 3 mm in breadth (Fig. 4.7c). The thin strips were then stacked on top of each other in a thin quartz tube (Fig. 4.7d) which could then be inserted in the cavity.

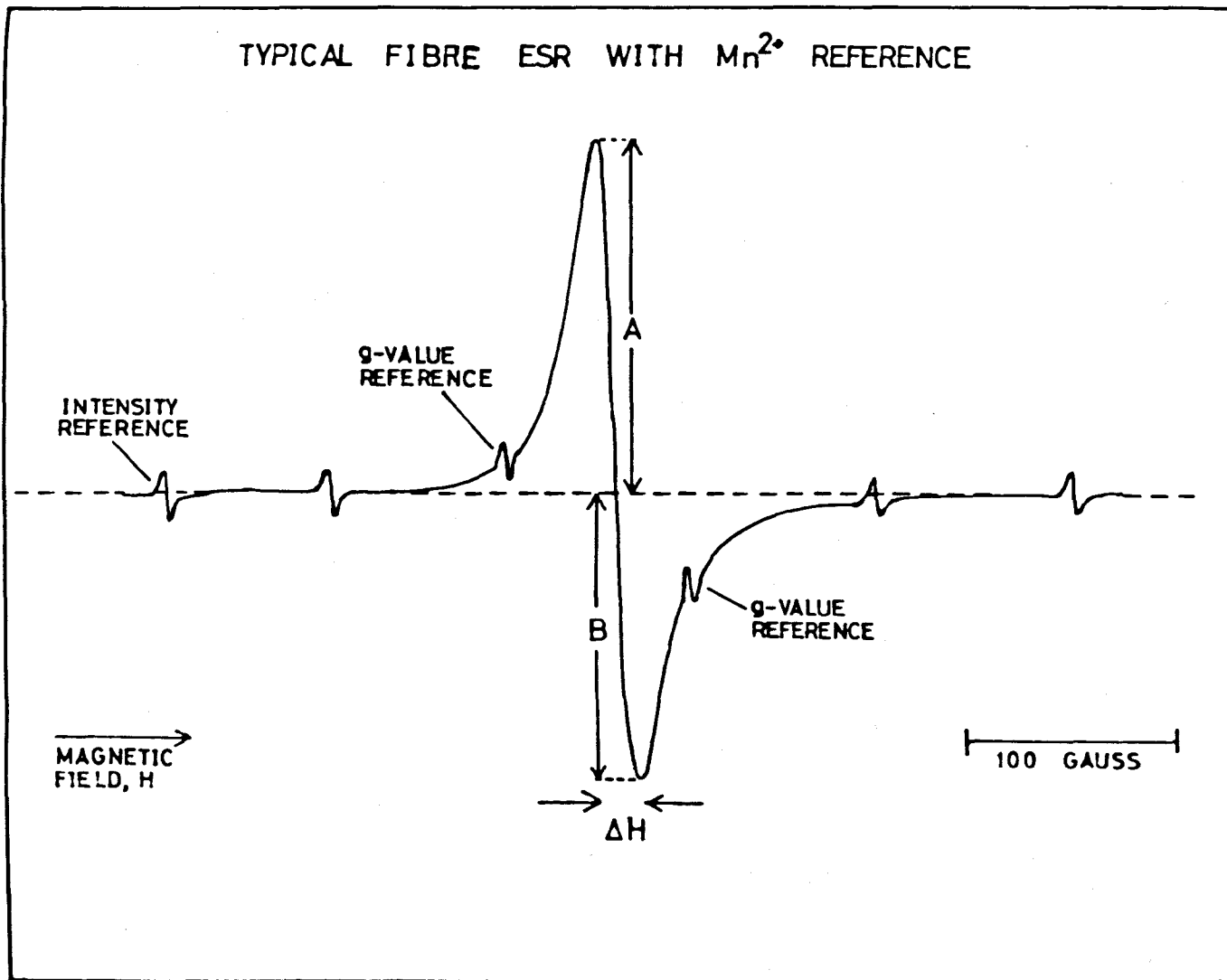


FIGURE 4.8.

This method of mounting and aligning the fibres has the advantage of simplicity and although depending on orientation by eye, is sufficiently accurate for present purposes. This is especially true for the two orientations where H_0 is parallel or perpendicular to the fibre axis where because of the \cos^2 angular variation of the g-shift (see section 3.1.3) a misorientation of $\pm 5^\circ$ would make a negligible change in the measured g-value and would not affect the conclusions. For a carefully prepared sample it was estimated that the degree of misorientation was well within $\pm 5^\circ$.

The number of fibres within a bundle was kept as low as possible to minimize inter fibre electrical contacts and hence reduce microwave skin effect complications to a minimum. It will be seen later that a small asymmetry was often present in the resonance line and was attributed to this skin effect.

When the g-anisotropy was not being investigated, for example during intensity measurements, a bundle of fibres was simply slotted through a thin capillary quartz tube of internal diameter 1mm, which was then inserted into the cavity (Fig. 4.7e).

The ESR line consisted of a single fairly broad resonance line with a width of about 10 - 100 gauss, compared with the somewhat narrower width 2 - 20 gauss, encountered with carbon blacks. A typical carbon fibre resonance line, together with the six lines of a Manganese doped Magnesium oxide standard used as a reference, is shown in Fig. 4.8. In order to extract the maximum amount of reliable information from this line considerable attention was devoted to the detailed structure of the resonance.

GAUSSIAN AND LORENTZIAN SHAPES

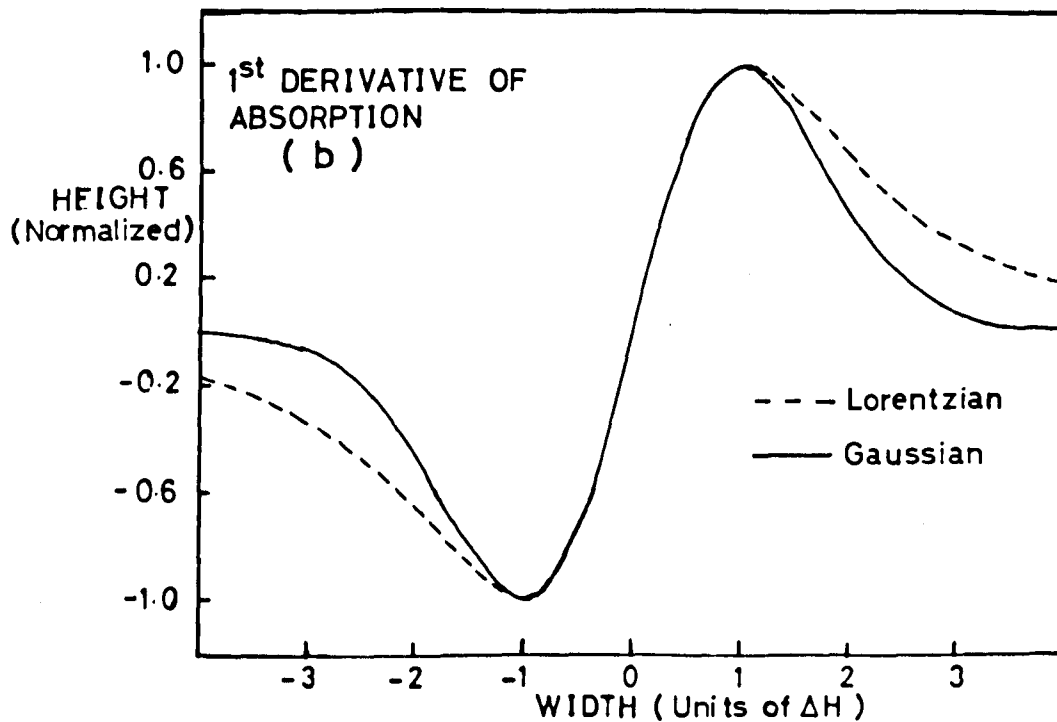
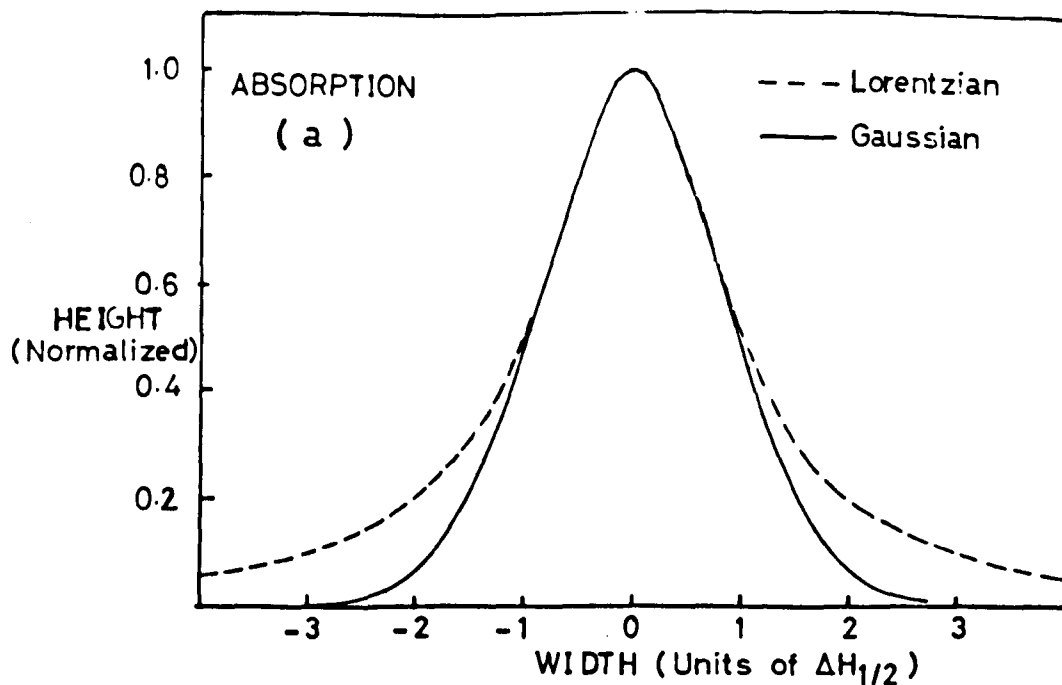


FIGURE 4.9.

$$L_{Y(H)} = \frac{16 Y'_m \frac{H - H_0}{\frac{1}{2}\Delta H}}{\left[3 + \left(\frac{H - H_0}{\frac{1}{2}\Delta H} \right)^2 \right]^2} \quad (4.3b)$$

where $Y'_m = \frac{4}{3}(\Delta H)Y'_m$, $\Delta H_{\frac{1}{2}}/\Delta H = 3^{\frac{1}{2}}$, for a Lorentzian shape.

The first derivative curves obtained from these equations are shown in Fig. 4.9b for a Gaussian and a Lorentzian shape. From these curves it is possible to obtain the widths at various fractional heights for both functions. A plot of these theoretical widths against the widths of an experimental curve measured for the same fractional height will yield a straight line with the function with which the experimental derivative curve conforms. Furthermore the slope of the resulting straight line will yield a very reliable value of $\frac{1}{2}\Delta H$. A typical line shape analysis is shown in Fig. 4.10.

4.4 Spin Concentrations

The number of spins in a paramagnetic sample is proportional to the area under the absorption curve (i.e. the second integral of the first derivative curve) and is usually determined by comparison with a standard sample with the same spin number. If the two line shapes under consideration are the same then the following equation can be used for comparing spins⁽⁶⁾

$$\frac{N^A \text{ spin}}{N^B \text{ spin}} = \left(\frac{\Delta H^A}{\Delta H^B} \right)^2 \cdot \frac{H^B_{\text{mod}}}{H^A_{\text{mod}}} \cdot \frac{Y'_m{}^A}{Y'_m{}^B} \cdot \left(\frac{P^B}{P^A} \right)^{\frac{1}{2}} \\ \frac{Q_L^B}{Q_L^A} \cdot \frac{\eta^B}{\eta^A} \cdot \frac{V_S^A}{V_S^B} \quad (4.4)$$

4.3 Line Shapes

The shape of an ESR absorption curve can often be closely approximated to one of two mathematical functions, the Gaussian or Lorentzian function, depending on the interaction which is the principal source of broadening. The Gaussian and Lorentzian functions for an absorption curve can be written in the form⁽⁶⁾

$$G_{Y(H)} = Y_m \exp \left[-0.693 \left(\frac{H - H_0}{\frac{1}{2}\Delta H_{\frac{1}{2}}} \right)^2 \right] \quad (4.2a)$$

for a Gaussian shape and

$$L_{Y(H)} = \frac{Y_m}{1 + \left(\frac{H - H_0}{\frac{1}{2}\Delta H_{\frac{1}{2}}} \right)^2} \quad (4.2b)$$

for a Lorentzian shape.

Where $\Delta H_{\frac{1}{2}}$ is the width at half maximum of the absorption curve, H_0 is the field at resonance and Y_m is the maximum height of the absorption curve. The Gaussian and Lorentzian absorption curves normalized for a maximum absorption Y_m of unit are shown in Fig. 4.9a, the abscissa being given in units of $\frac{1}{2}\Delta H_{\frac{1}{2}}$.

In ESR however one is dealing with the first derivative of the absorption curve and it is therefore necessary to differentiate equations 4.2a and 4.2b. The absorption functions then become:

$$G_{Y'(H)} = 1.649 Y'_m \frac{H - H_0}{\frac{1}{2}\Delta H} \exp \left[-\frac{1}{2} \left(\frac{H - H_0}{\Delta H} \right)^2 \right] \quad (4.3a)$$

where $Y'_m = e^{\frac{1}{2}}(Y'_m \Delta H)$ and $\Delta H_{\frac{1}{2}}/\Delta H = (2\ln 2)^{\frac{1}{2}}$, for a Gaussian shape and

TYPICAL LINE SHAPE ANALYSIS

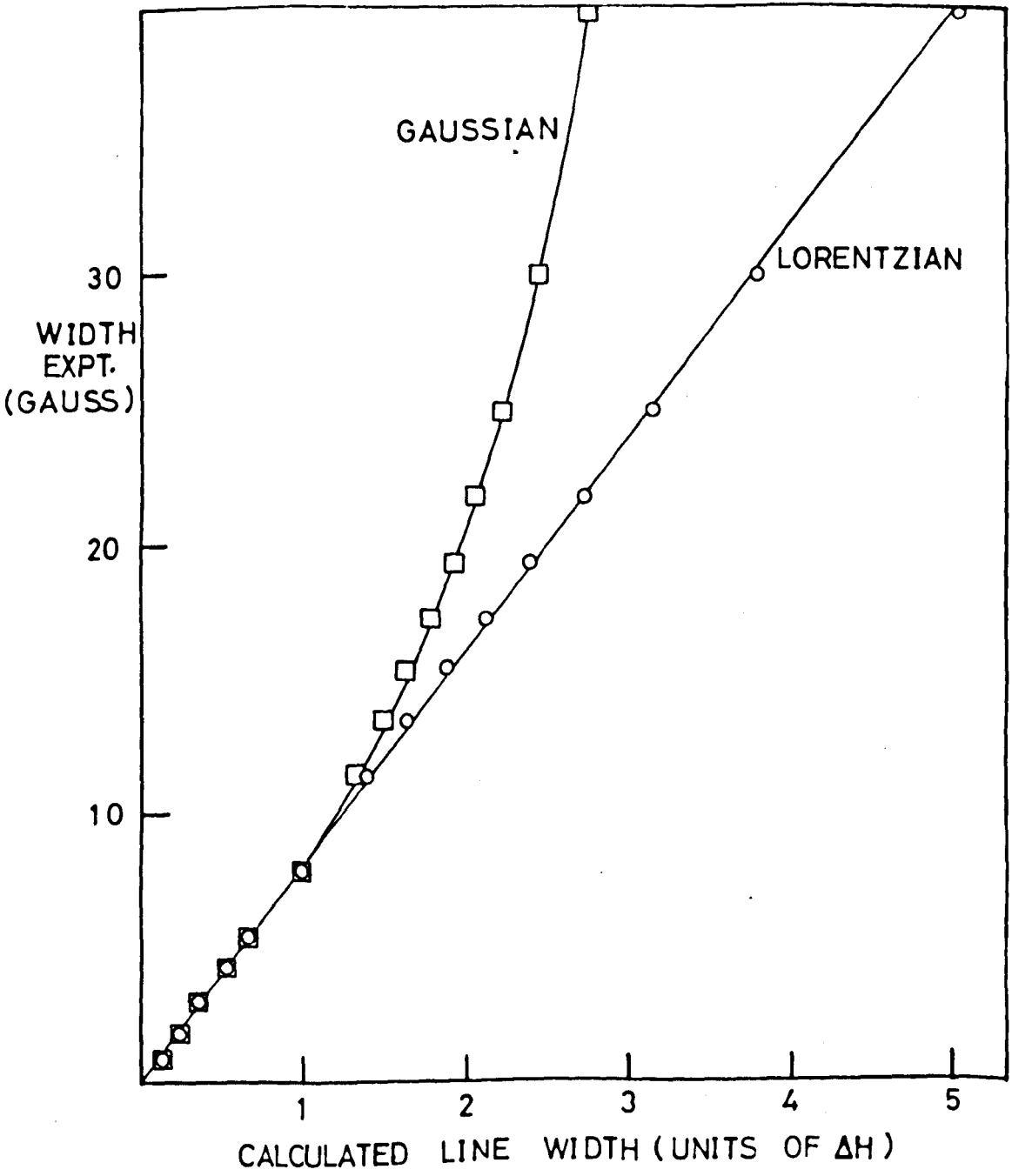


FIGURE 4.10.

where Y'_m can be considered as the amplification, Q_L the loaded Q, η the filling factor and V_s the sample volume.

To eliminate changes in Q_L which might occur on insertion of different carbon fibre samples into the cavity, the intensity of the ESR line was always referred to the lowest field line of the manganese reference (due care being taken not to saturate this line) mounted inside the cavity. To obtain similar filling factors η and sample volumes V_s , the same length of weighed carbon fibre bundles was always slotted into the capillary tubes, and these were positioned in identical axial locations in the cavity. Equation 4.4 now reduces to:

$$\frac{N^A_{\text{spin}}}{N^B_{\text{spin}}} = \left(\frac{\Delta H^A}{\Delta H^B} \right)^2 \cdot \frac{H^B_{\text{mod}}}{H^A_{\text{mod}}} \cdot \frac{Y'_m{}^A}{Y'_m{}^B} \cdot \left(\frac{P^B_w}{P^A_w} \right)^{\frac{1}{2}} \quad (4.5)$$

In practice the comparison was usually carried out with the same power p in the cavity and the same modulation amplitude H_{mod} , so that this equation is further reduced to

$$\frac{N^A_{\text{spin}}}{N^B_{\text{spin}}} = \left(\frac{\Delta H^A}{\Delta H^B} \right)^2 \cdot \frac{Y'_m{}^A}{Y'_m{}^B} \quad (4.6)$$

This equation, which in fact requires that the intensities of the resonance lines be proportional to $(\Delta H)^2 Y'_m$, is valid only for identical line shapes and was used extensively in this work to compare the intensities of carbon fibres with each other; the ESR line shapes of these fibres being always Lorentzian to at least four line widths. Checks of the validity of this proportionality were carried out using numerical integrations such as that of Wyard⁽⁷¹⁾.

To obtain an absolute value for the spin concentration use was made of a secondary standard consisting of powdered carbon dispersed in chalk. This secondary standard was calibrated against DPPH and also against a single $\text{CuSO}_4 \cdot 5\text{H}_2\text{O}$ crystal. The integrated area under the absorption curve was used here for comparing intensities. The ESR intensity of the calibrated Carbon standard was then referred to the first Mn^{2+} line and compared to the fibre ESR intensity (care being taken as before to obtain a similar η and V_s).

4.5 g-value

The g-value was taken as the mid-point of the derivative line. It was evaluated by reference to the central two lines of the Mn^{++} standard. The two Mn^{++} lines were calibrated against powdered polycrystalline DPPH which was taken to have a g-value of 2.0036. The calibration against DPPH was performed at the same microwave frequency as that used to observe the fibre resonance to eliminate possible small errors due to second order effects.

4.6 Temperature Variation of Intensity

The determination of the ratio $R (I_{77^\circ\text{K}}/I_{300^\circ\text{K}})$ involves the measurement of the resonance intensity both at room temperature and at liquid nitrogen temperatures. The measurement at 77°K was carried out using the cold finger arrangement (see section 4.1.2). Again, to eliminate the effect of possible changes in cavity Q, the intensity was always referred to the first line of the Mn^{++} standard, which was

DPPH - INTENSITY VARIATION
WITH TEMPERATURE

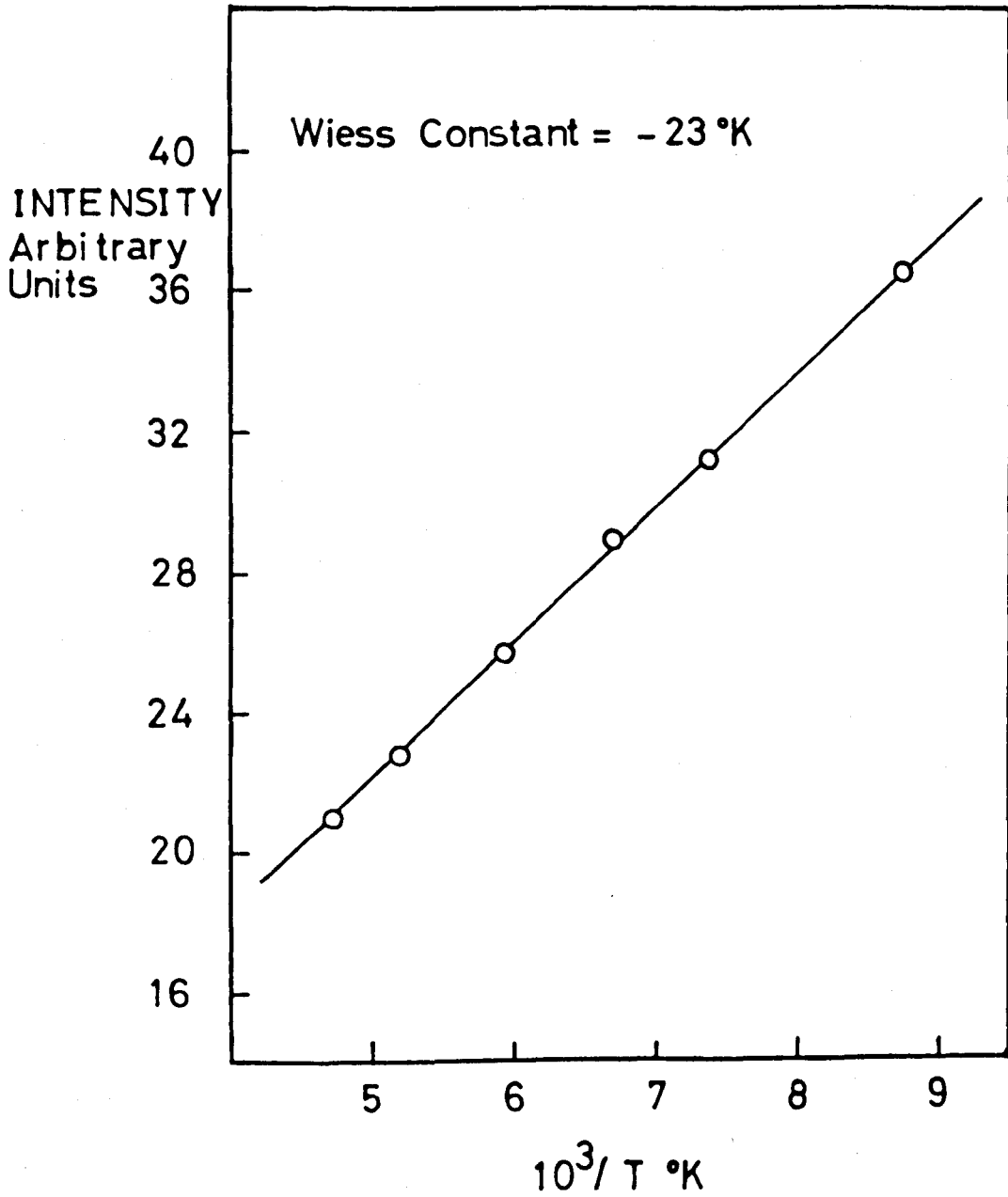


FIGURE 4.11

positioned in the immediate vicinity of the sample. The temperature dependence of the Mn^{++} standard was required in order to calculate R. This was taken to follow a Curie law and because of the importance of this assumption with regards to the accuracy with which R could be determined, it was felt necessary to check its validity.

On the assumption of a Curie type behaviour for the Mn^{++} standard, a low temperature carbon (HTT - $400^{\circ}C$) was found to follow a Curie Law temperature dependence, as indeed one would expect from such a material with completely localized centres. Furthermore, DPPH was found to follow a Curie Weiss Law $[I \propto 1/(T-\phi)]$ with a Weiss constant $\phi = -20^{\circ}K$, which agrees well with the value of $\phi = -23^{\circ}K$ which was obtained by a plot of I vs $1/T$ (see Fig. 4.11) for DPPH over a small range of temperatures (so that Q changes could be neglected) and with the values quoted by other authors, viz. $-28^{\circ}K$ ⁽⁷²⁾, $-25^{\circ}K$ ⁽⁷³⁾.

CHAPTER 5

ESR STUDIES OF CARBON FIBRES

The X-ray and electron microscopy studies^(62,63) on the structure of carbon fibres, generally substantiate Shindo's⁽⁵⁹⁾ initial findings that the polynuclear aromatic planar fragments become strongly oriented with their planes parallel to the fibre axis. Because of the high g-value anisotropy associated with graphite, such an alignment might be expected to confer anisotropic properties to the ESR of carbon fibres. Primarily with this in mind the ESR spectra of these materials were investigated.

5.1 The Samples

The PAN fibres examined in this chapter had been pre-oxidized at 300°C in air under restraint before being 'carbonized' by controlled pyrolysis up to 1000°C in an inert atmosphere. They had then been 'graphitized' by further heat treatments at varying temperatures up to 2500°C in an inert atmosphere. The fibres were then mounted for ESR as described in section 4.2.

5.2 The Resonance Line

The ESR signals consisted of a single broad line (see Fig. 4.8), which on analysis (see section 4.3) was invariably Lorentzian in shape out to at least five line widths. The shape did not change with either temperature or orientation in the magnetic field. Although great care

g-ANISOTROPY FOR CARBON FIBRES COMPARED TO GRAPHITE

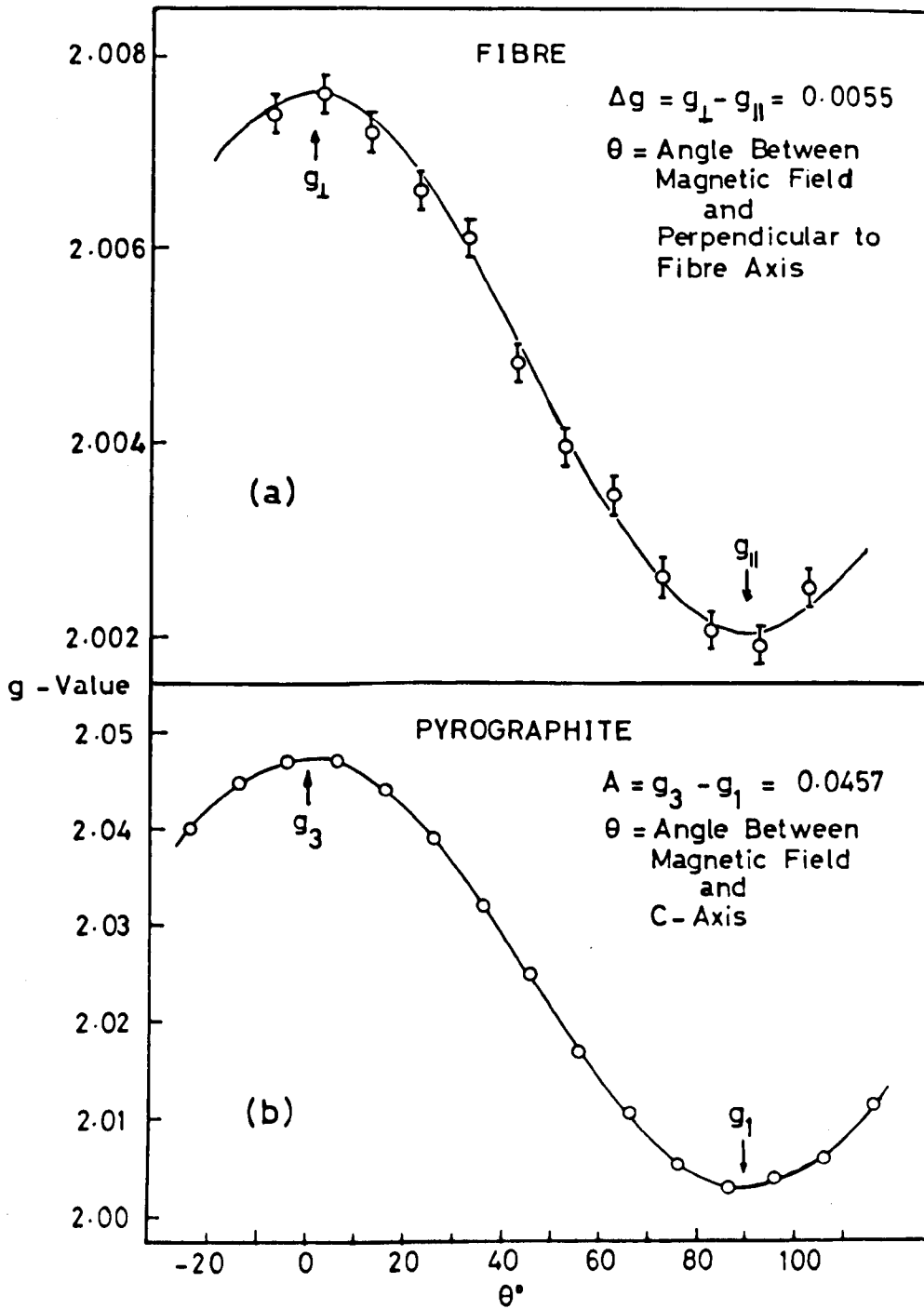


FIGURE 5.1.

was taken to minimize skin effects while mounting the fibres for ESR work, there often remained a slight asymmetry in the line which was ascribed to these effects. The deviation from symmetry about the centre represented by the ratio A/B (see Fig. 4.8) varied between 1.0 and 1.5 (see Table 5.1), and the effect of this on the ESR parameters will be discussed in section 5.4.

5.3 g-Value Anisotropy

The measurement of the g-value of the resonance line was carried out as outlined in section 4.5 for different orientations of the fibre's axis relative to the static magnetic field. This was achieved by rotating the magnetic field about an axis perpendicular to the fibre axis. A systematic variation of the g-value with orientation in the magnetic field was observed for a number of fibres. There occurs a maximum in the g-value when the static field is perpendicular to the fibre axis (defined as g_{\perp}) and a minimum when the magnetic field is parallel to the fibre axis (defined as g_{\parallel}).

A typical curve for a fibre treated to 2,700°C is illustrated in Fig. 5.1a. The g-value angular variation for a stress recrystallized pyrographite (PG) is plotted out in Fig. 4.1b for comparison. The close agreement for the value of the anisotropy $A = 0.046$ with Wagoner's⁽³¹⁾ value of 0.047 indicates that the pyrographite sample behaved in effect as a single crystal of graphite. The experimental points, for both the fibre and pyrographite are closely fitted by a \cos^2 function (continuous line Fig. 5.1). Although at times the line

Table 5.1

HTT (°C)	Temp (°K)	ΔH (Gauss)	Expt.	A/B	Correction (Gauss)	Correction g	g Corrected
1000	300	40	2.0019	1.11±02	1.24	0.0007	2.0026
1000	77	50	2.0013	1.15±02	1.55	0.0009	2.0022
1750	300	18	2.0027	1.23±02	0.79	0.0005	2.0032
1750	77	26	2.0021	1.23±02	1.14	0.0007	2.0028
2300(1)	300	23	2.0020	1.16±02	0.71	0.0004	2.0024
2300(1)	77	28	2.0022	1.19±02	1.04	0.0006	2.0028
2300(2)	300	23	2.0021	1.38±02	1.52	0.0009	2.0030
2300(2)	77	28	2.0017	1.34±04	1.69	0.0010	2.0027
2400	300	19	2.0021	1.18±02	0.67	0.0004	2.0025
2400	77	16	2.0025	1.18±02	0.56	0.0003	2.0028
2500	300	80	1.9996	1.33±02	4.72	0.0028	2.0024
2500	77	68	2.0001	1.33±04	4.01	0.0024	2.0025
2700	300	36	2.0018	1.16±02	1.12	0.0007	2.0025
2700	77	28	2.0022	1.23±02	1.23	0.0007	2.0029
2800	300	63	2.0005	1.24±02	2.83	0.0017	2.0022
2800	77	48	2.0015	1.24±02	2.16	0.0013	2.0028

widths of the fibre resonances can be quite large the g-value variations are believed to be real and correct within an overall uncertainty of ± 0.0005 .

The significance of this result can be appraised by considering the nature of the ESR absorption observed in carbons and what is known of the structure of carbon fibres.

Previously reported information (see sections 3.2.2 and 3.3.2) indicates that the solid can be considered, from some points of view, to be a two phase material, i.e. to consist of small 'crystallites' held together by a material exhibiting a much lower degree of order. Since one observes only a single line of characteristic Lorentzian shape, it is assumed that the line is completely motionally averaged⁽⁵⁰⁾, that is to say, the crystallites are in good electrical contact and the charge carriers responsible for the resonance move through a large number of crystallites before flipping their spins. The observed g-value is then an average value for all crystallite orientations.

Other evidence in support of motional averaging comes from several sources. Firstly there exists no correlation between the line width and the magnitude of the g-anisotropy (see section 5.9). Secondly, on the basis of some Q-band (35 GHz) measurements, the line width appears to a first approximation to be frequency independent. Thirdly a simple calculation of the mean free path of the charge carriers from conductivity data, leads to the result that the carriers travel a distance of $\sim 10^4 \text{ \AA}$ between spin flips and thus should sample a wide variety of crystallites in its relaxation time.

EFFECT OF A/B ASYMMETRY ON
OBSERVED g -VALUE

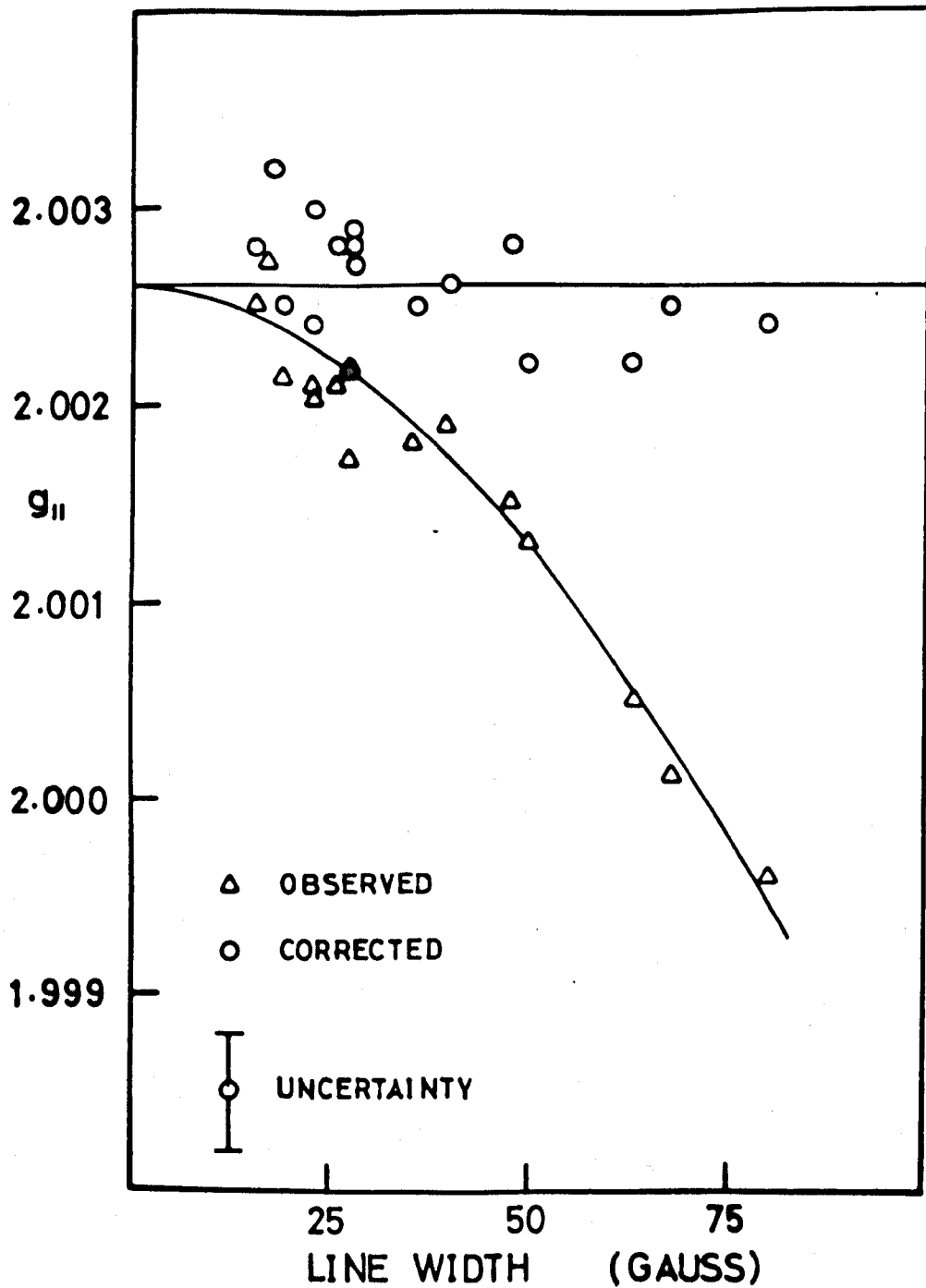


FIGURE 5.2.

Bearing in mind therefore, that as a result of complete motional averaging, the g -value for carbon fibres is an average value for all crystallite orientations, the g -anisotropy in carbon fibres and the PG can be compared. For the PG (Fig. 5.1b) the maximum in g -value occurs when the field is parallel to the crystallographic c -axis. Thus the occurrence of a maximum in the g -value when the static magnetic field is perpendicular to the fibre axis (Fig. 4.1a) leads to the conclusion that the crystallites are preferentially aligned with their basal planes lying parallel to the fibre axis.

5.4 Effect of Asymmetry on g -value

It was noticed that the value of $g_{||}$ decreased in a fairly uniform manner with increase in line width, suggesting some inter-relationship. This can be seen from Fig. 5.2, where the values of $g_{||}$ for various fibres are plotted against the line width of the resonance. However at the same time it was noticed that the line, although Lorentzian in shape, exhibited a small asymmetry about the centre, expressed by the ratio of A/B (see Fig. 4.8) and which was ascribed to skin effects.

Now Delhaes and Marchand⁽⁷⁴⁾ have examined the case of specimens which have dimensions of the same order as the skin depth, and which therefore applies to the present situation. They have assumed that in this case the resonance curve can be expressed by a mixture of the absorption curve χ'' and dispersion curve χ' , of the complex paramagnetic susceptibility. The correction factor to be applied to the experimentally observed resonance is determined by the line width as well

VARIATION OF g-VALUE ANISOTROPY WITH FIBRE HTT

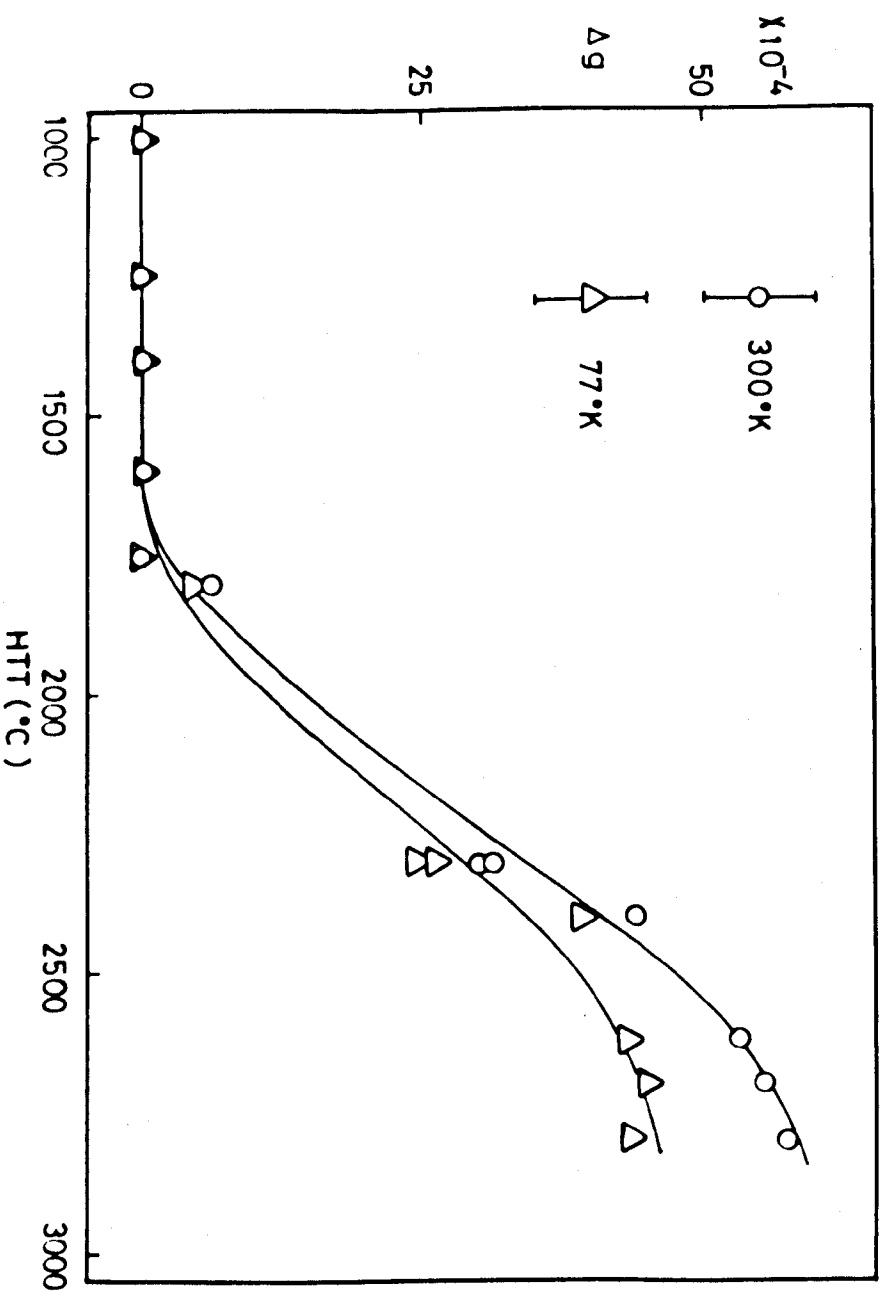


FIGURE 5.3.

as the asymmetry ratio A/B. This factor was duly calculated with the aid of Figure 2 of the cited reference⁽⁷⁴⁾. Upon applying this correction all the $g_{||}$ -values were raised to around the value 2.0026 expected for g_{\perp} for graphitic crystallites and showed little or no systematic variation with line width.

The details of the calculation of these correction factors for a number of fibres are given in Table 5.1. The ratio A/B varies approximately between 1.1 and 1.4 but shows little change with HTT. The two entries given for HTT 2300°C represent two separate mountings of fibres with different degrees of packing. It was found that this asymmetry has only an effect upon the apparent g-value and in no way influences the validity of other measured parameters. It should be noted that the g-anisotropy Δg also remains unaffected by the line asymmetry. This is because, to a first approximation, the line shape and line width do not vary, at the two orientations, so that the correction, which in any case is small, will be the same for both $g_{||}$ and g_{\perp} and will disappear on subtraction.

5.5 Variation of Δg with HTT

The variation of Δg with HTT is shown in Fig. 5.3 for two temperatures, 300°K and 77°K. The anisotropy Δg at 77°K is observed to be lower than that at 300°K. The reason for this becomes apparent in section 5.6. No anisotropy is observed up to a HTT of 1750°C at which a value for Δg first begins to make its appearance and above which then proceeds to increase with increasing HTT. It appears that the g-anisotropy,

CRYSTALLITES IN CARBON FIBRES

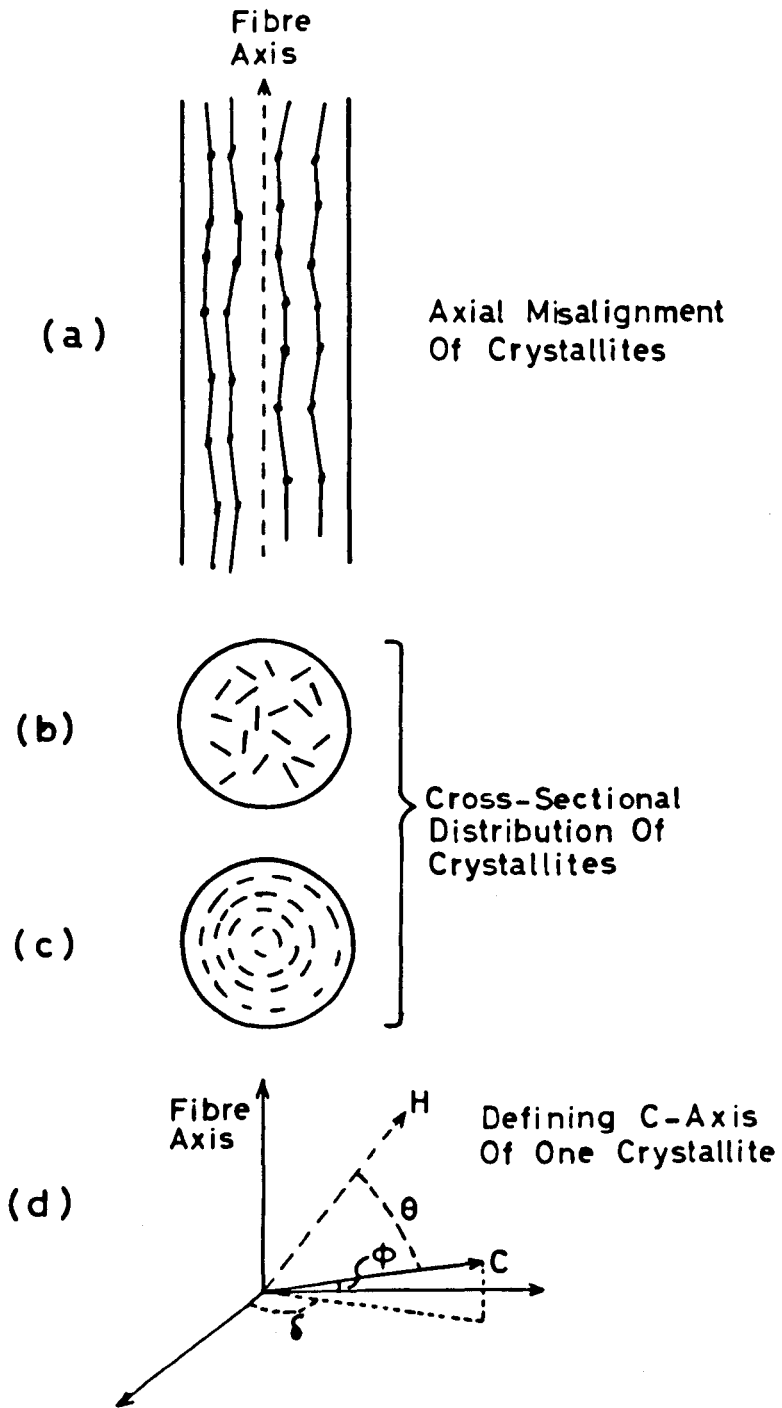


FIGURE 5.4.

above 1750°C, parallels the growth and perfection of the crystallites within the fibre and indeed would seem to be a good measure of their degree of development. This conclusion has been the subject of a short communication⁽⁷⁵⁾. The absence of g-anisotropy below 1750°C will be given due consideration in later sections.

5.6 Effect of Crystallite Misorientation on g-Anisotropy

All that is known about the structure of carbon fibres (see section 3.3.2) in addition to the g-anisotropy in these materials (see section 5.3), indicates that the crystallites in carbon fibres are highly oriented with their basal planes arranged approximately parallel to the fibre axis. The relative degree of orientation can be defined by an angle Z (in degrees) which is evaluated from flat plate transmission photographs by measuring, on an automatic rotating stage microdensitometer, the angular half width of the density profile round the (002) diffraction arc at half peak density⁽⁷⁶⁾; small Z values thus imply a high degree of alignment along the fibre axis.

The situation is described schematically in Fig. 5.4a. The angle ϕ between the basal planes of a crystallite and the fibre axis will represent the misalignment of that crystallite. In addition to crystallite misalignments relative to the fibre axis, their c-axes are symmetrically distributed in a plane orthogonal to the axis. This is clearly shown by a wealth of X-ray and electron diffraction studies^(63,76).

Although the exact pattern of this distribution is unknown (Fig. 5.4b and c are but two possibilities), this is responsible for halving the observed anisotropy. That is to say, when the static magnetic field is perpendicular to the fibre axis, g_{\perp} will result from crystallites presenting a variety of angles with the direction of the field (Fig. 5.4b and c). This leads to the result that

$$\Delta g = g_{\perp} - g_{\parallel} = \frac{g_3 - g_1}{2} = \frac{A}{2} \quad (5.1)$$

The effect of the crystallite misorientation with respect to the fibre axis on the overall g-value can be estimated simply by considering the g-value contributed by one crystallite at an angle ϕ to the fibre axis. The g_{\parallel} -value of such a crystallite can be written as:

$$g_{\parallel}(\phi) = g_1 + (g_3 - g_1)\text{Cos}^2(90 - \phi) = g_1 + A \text{Sin}^2\phi$$

By averaging this result over all values of ϕ one obtains

$$g_{\parallel} = g_1 + A \overline{\text{sin}^2\phi} \quad (5.2)$$

where $\overline{\text{sin}^2\phi}$ is the average of all $\text{sin}^2\phi$ values.

In a similar way when the static magnetic field is perpendicular to the fibre axis and bearing in mind equation 5.1, g_{\perp} may be written as

$$g_{\perp}(\phi) = g_1 + \frac{g_3 - g_1}{2} \text{Cos}^2\phi = g_1 + \frac{A}{2} (1 - \text{Sin}^2\phi)$$

Averaging this becomes

$$g_{\perp} = g_1 + \frac{A}{2} - \frac{A}{2} \overline{\text{sin}^2\phi} \quad (5.3)$$

The results expressed by equations 5.2 and 5.3 can be derived in a more formal manner by expressing the g-value of one crystallite in any direction θ measured relative to a plane perpendicular to the fibre axis. In polar coordinates $(90 - \phi)$ and δ completely specify in space the direction of the c-axis relative to the fibre axis (see Fig. 5.4d). The g-value can then be written as:

$$g(\theta) = g_1 + A \left[\cos \theta \cos \phi \sin \delta + \sin \phi \sin \theta \right]^2 \quad (5.4)$$

The values $g_{||} (\theta = \pi/2)$ and $g_{\perp} (\theta = 0)$ can then be obtained by averaging over all possible orientations, as follows:

$$g_{||} = \frac{\int_0^{\phi} \{g_1 + A \sin^2 \phi\} d\phi}{\int_0^{\phi} d\phi} = g_1 + A \overline{\sin^2 \phi} \quad (5.2^*)$$

and

$$\begin{aligned} g_{\perp} &= \frac{\int_0^{2\pi} \int_0^{\phi} \{g_1 + A \cos^2 \phi \sin^2 \delta\} d\delta \cdot d\phi}{\int_0^{2\pi} \int_0^{\phi} d\delta \cdot d\phi} \\ &= g_1 + \frac{A}{2} \overline{\cos^2 \phi} = g_1 + \frac{A}{2} - \frac{A}{2} \overline{\sin^2 \phi} \end{aligned} \quad (5.3^*)$$

Clearly the equations 5.2 and 5.3 show that the effect of crystallite misorientation is to decrease g_{\perp} and increase $g_{||}$ with a net decrease of Δg_{expt} which is given by

$$\begin{aligned} \Delta g_{\text{expt}} &= g_{\perp} - g_{||} = \frac{A}{2} - \frac{3}{2} A \overline{\sin^2 \phi} \\ \Delta g_{\text{expt}} / \Delta g_{\text{true}} &= \Delta g_{\text{expt}} / (\frac{1}{2}A) = 1 - 3 \overline{\sin^2 \phi} \end{aligned} \quad (5.5)$$

EFFECT OF CRYSTALLITE MISALIGNMENT
UPON Δg

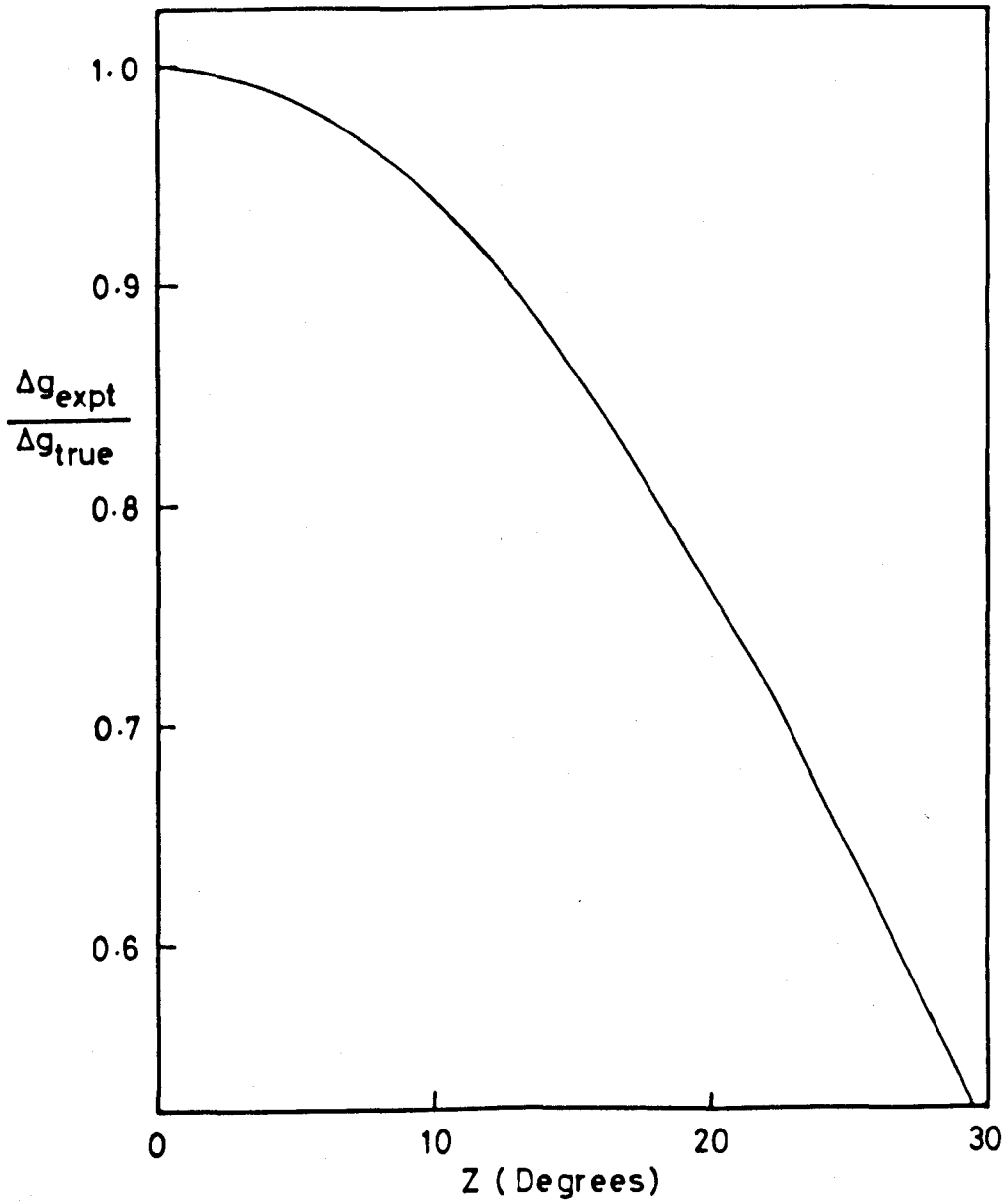


FIGURE 5.5.

Putting $\phi = 10^\circ$, which in terms of crystallite misalignment is a large value (see section 3.3.2), in equation 5.5 one gets

$$\Delta g_{\text{expt}}/\Delta g_{\text{true}} \sim 0.9$$

which in fact shows that crystallite misalignments of this order of magnitude do not appreciably affect the observed Δg . E.G. Cooper (this department, private communication), assuming a Gaussian distribution of crystallites, calculated the expectation value of g_{\perp} , for various misalignments (see Fig. 5.5). Typical Z values of $\sim 10^\circ$ (N.B. $Z = \phi$) produce a correction factor ~ 0.94 . Thus the g-anisotropy is insensitive to small misalignments of crystallites and its increase with HTT must be regarded as being linked with increased crystallite growth and perfection, rather than increased alignment. Further support for this view is the fact that g_{\parallel} is invariably close to 2.0026 (see Table 5.1) that is to say, the g_{\perp} value for crystallites. This would not have been the case if Δg was sensitive to crystallite misalignment.

5.7 Variation of ' Δg ' with Ambient Temperature

The variation of Δg with temperature (as described in section 4.1.2) is shown in Fig. 5.6a for a fibre heat treated at $2,700^\circ\text{C}$. As the temperature is decreased below room temperature, Δg at first increases, goes through a flat maximum and then decreases. This reversal in the g-anisotropy variation with temperature is well understood in terms of Mrozowski's analysis of the ESR in carbonaceous materials, who also reported a similar g-value behaviour in neutron irradiated carbon blacks (51).

REVERSAL OF g-ANISOTROPY WITH TEMPERATURE

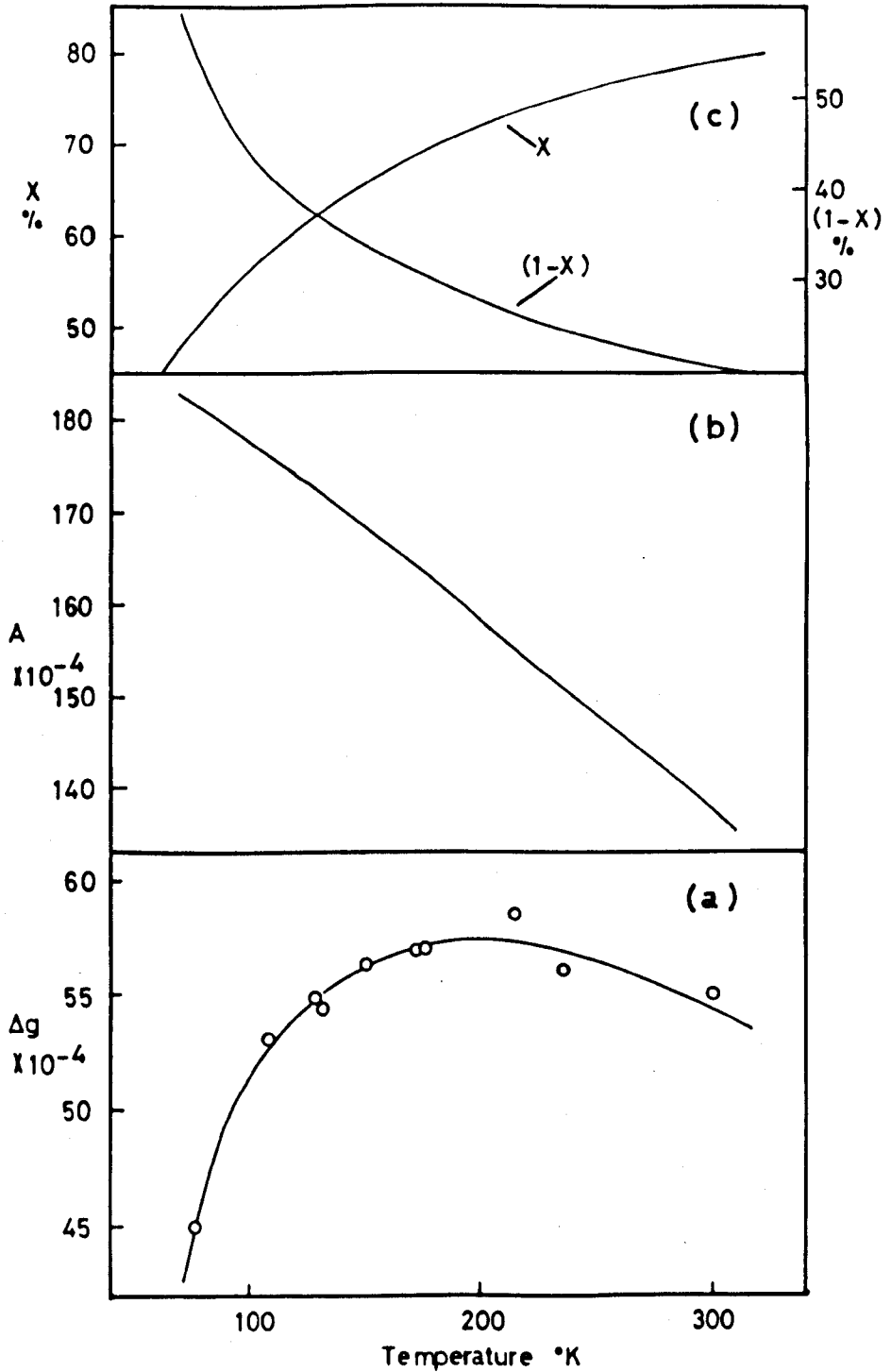


FIGURE 5.6.

According to Mrozowski the g-value of the resonance results from a simple mixing of localized and conduction electrons, each spin centre contributing an amount proportional to its absorption intensity. If X_T is the fraction of conduction electrons present at a temperature T, then the anisotropy purely for the conduction part can be written using equation 5.1a as

$$A_{(T)} = 2 \frac{\Delta g_{(T)}}{X_{(T)}} \quad (5.5)$$

The quantity $X_{(T)}$ can be obtained by carefully measuring the resonance intensity (section 4.6) at two temperatures and using equation 3.2 (section 3.2.2). The two temperatures usually chosen are room temperature and liquid nitrogen which yields $X_{300^{\circ}\text{K}}$ from which X at any temperature can be easily computed. The variation of X and (1 - X) with temperature for the sample at HTT 2700°C are shown in Fig. 5.6c. As the temperature decreases the localized contribution (1 - X), which follows Curie's law, increases and the contribution of conduction carriers, X, decreases correspondingly. The value of X can then be used to compute a 'crystallite' anisotropy A by means of equation 5.5 at various temperatures from the values of Δg obtained from Fig. 5.6a. The resulting temperature variation of A (Fig. 5.6b) is seen to increase with decreasing temperature as indeed is expected for graphitic crystallites. That the value of A is much lower than that for single crystal graphite⁽³¹⁾ merely indicates the lack of perfection and small size of these crystallites.

The reversal in the g-anisotropy can now be seen to result from the influence of two competing factors. The first factor tends to

VARIATION OF CRYSTALLITE ANISOTROPY WITH HTT

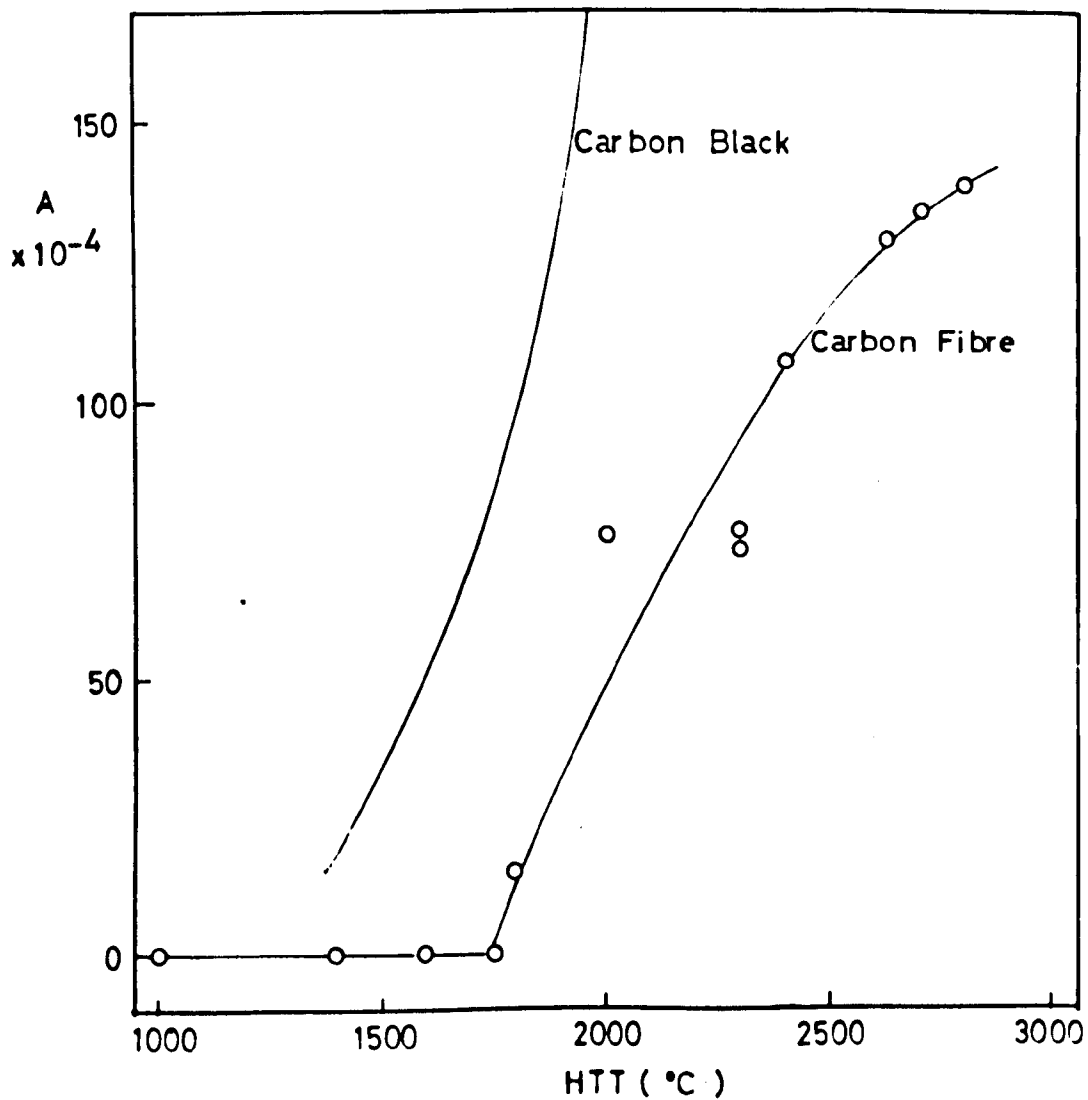


FIGURE 5.7.

increase Δg as the temperature decreases and arises from the temperature dependence of A; and the second factor tends to decrease Δg as the temperature is lowered and arises from the increased effect of localized centres (decrease in X) which tends to pull the g-value towards the free electron g-value of 2.0023.

The observation that Δg at 77°K is lower than Δg at 300°K (Fig. 5.3, section 5.5) is thus explained as being due to this reversal in the Δg vs T curve.

5.8 Variation of 'A' with HTT

The crystallite anisotropy at room temperature $A_{300^\circ\text{K}}$ is plotted against HTT in Fig. 5.7. The crystallite anisotropy for a soft carbon⁽⁵⁵⁾ is plotted in the same figure for comparison.

The crystallite anisotropy for carbon fibres sets in at a HTT of about 1750°C and increases with increasing HTT, remaining however well below the curve for soft carbons which begins to appear at a somewhat lower HTT (~1300°C). The crystallite anisotropy at higher HTT is still rising rapidly for the soft carbons but appears to be levelling off for the carbon fibres, suggesting that crystallite growth in these materials is somehow arrested. This point will be pursued in greater detail in section 5.11.

5.9 Variation of ESR Intensity with HTT

The measurements of spin susceptibility in carbon fibres were performed as outlined in section 4.4, and these are plotted in Fig. 5.8a

VARIATION OF ESR INTENSITY WITH HTT

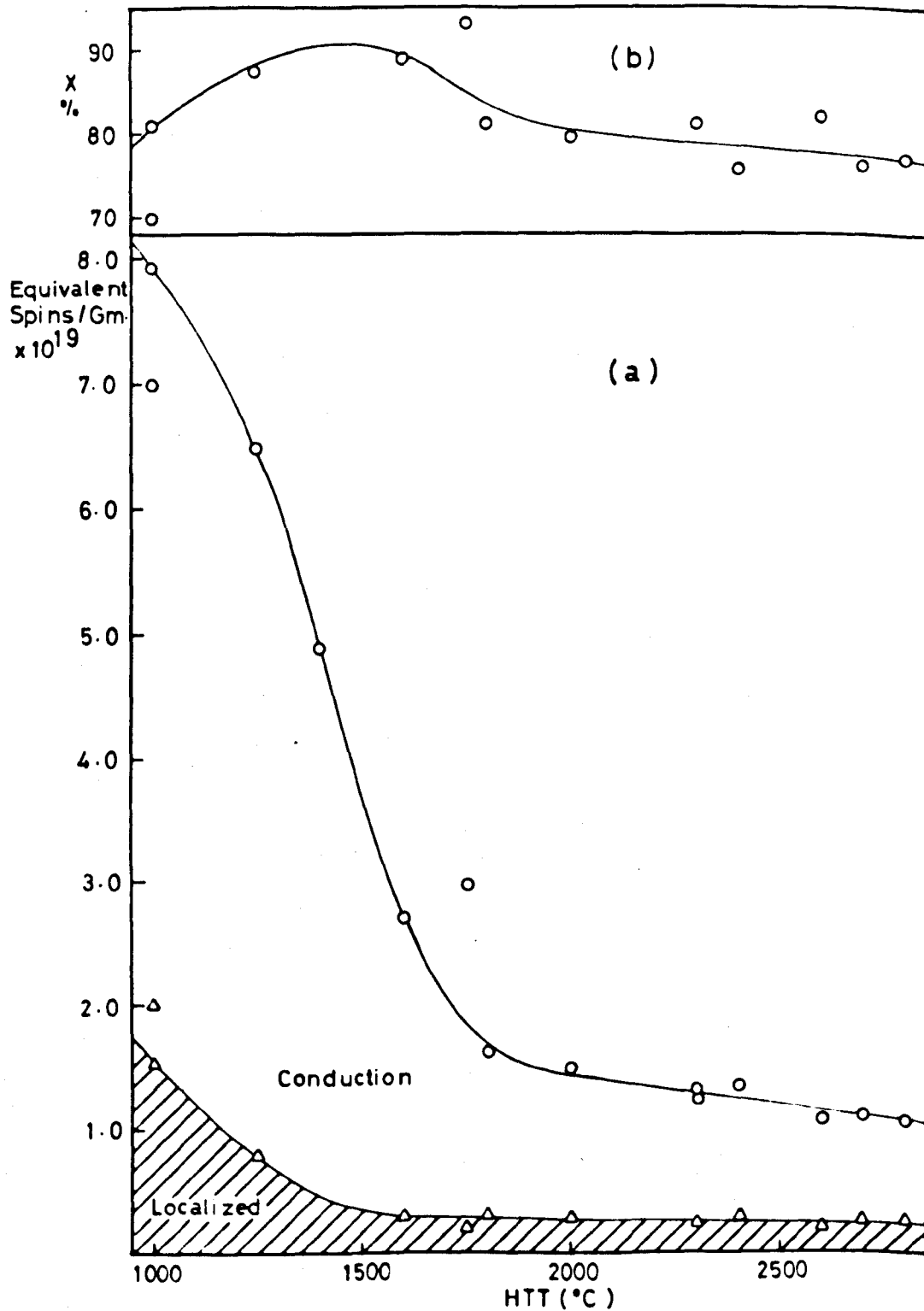


FIGURE 5.8.

against HTT. When the spin concentrations for the fibres are compared with values obtained for carbon blacks⁽⁵⁵⁾, remarkable agreement is observed, which in fact could be fortuitous in view of the relative uncertainty associated with the determination of absolute spin concentrations. The ESR intensity is a measure of the density of states at the Fermi level and such a close agreement between the spin concentrations in two materials as different as carbon blacks which are graphitizing and carbon fibres which are nominally non-graphitizing is indeed somewhat surprising.

The ESR intensity falls sharply at first but decreases much less rapidly above HTT 1700°C. The intensity is made up of two parts, a conduction part and a localized part (shaded in Fig. 5.8a), the proportion being determined by the ratio X, which is plotted in Fig. 5.8b. The proportion of conduction carriers X is fairly large (~80 - 90%) throughout the HTT range and appears to go through a maximum at HTT ~1500°C.

The rapid fall in ESR intensity below HTT ~1700°C seems to be significant structurally and is taken to mean that the number of available holes for conduction (i.e. dangling σ bonds) is falling rapidly in this region as the HTT is increased (see section 3.2.1). This is in line with the knowledge that these bonds are being taken up to form carbon hexagon rings. In terms of the band structure for these materials, the suggestion that the Fermi level is rising from deep inside the valence band towards the band edge (section 3.2.1), seems to receive confirmation from these results. It should be emphasized, however, that the shape of

the density of state curve for these materials is not known nor is it known whether this shape varies with HTT and if so to what extent, so that caution should be exercised when relating the position of the Fermi level with the density of states as observed by the ESR resonance.

5.10 The Line Width

The data obtained for the line width is summarized in Table 5.2. The line width both at room temperature and liquid nitrogen is very scattered. This apparently random variation appears to be present in all types of carbon fibres and at times can be distressing as very broad lines can prevent the accurate measurement of the other ESR parameters. The line width exhibits very little angular dependence, on average the line width is 2% broader with the magnetic field perpendicular to the fibre axis and this increase lies within the experimental uncertainty. It can therefore be concluded that the ESR resonance, in these samples, is to a first approximation, symmetrical about the fibre axis. If this were not the case, with the magnetic field perpendicular to the fibre axis, one would observe a superposition of lines varying between g_1 and g_3 giving rise to a broader line than that observed with the magnetic field parallel to the fibre axis, where the fibre would have a value of g_1 .

It seems that the line width of carbons is the least understood of all ESR parameters, even for the well studied graphitizing blacks. It is interesting to note that Mrozowski and co-workers⁽⁵⁵⁾ observed that the line width seemed to be very susceptible to conditions prevailing during heat treatment, and hence the scattering of values. They suggest

Table 5.2

HTT (°C)	Line Width ΔH at 300°K	$\Delta H_{\perp} / \Delta H_{\parallel}$ at 300°C	$\Delta H_{77^{\circ}\text{K}} / \Delta H_{300^{\circ}\text{K}}$
1000	50	1.00	0.84
1250	143	-	0.84
1400	133	-	0.35
1600	11	1.07	0.87
1750	18	1.01	1.45
1800	21	1.00	1.03
2300	23	1.02	1.22
2300	24	1.00	1.18
2400	19	1.06	0.83
2670	77	1.00	0.60
2700	36	1.05	0.77
2800	63	1.04	0.76

Uncertainty $\pm 5\%$ for all data

that relative changes in width with temperature are more regular. The ratio of the line widths at 77°K and 300°K for carbon fibres, is given in Table 5.2, and the values are again somewhat scattered. At higher HTT (>2400°C) the line appears to narrow on cooling, whereas between 1750°C and 2300°C the line broadens.

The line width of polycrystalline graphite broadens with decreasing temperature, showing an approximate T^{-1} ⁽⁴⁰⁾ dependence while carbon blacks have a width which is independent of temperature when heat treated below -1600°C and tends towards $T^{-\frac{1}{2}}$ ⁽⁵⁵⁾ dependence with increasing degree of graphitization. In general agreement with those results the width of single crystal graphite also broadens with decreasing temperature⁽³¹⁾ and furthermore this latter result is confirmed by the author's experience with Pyrographite. The temperature dependence of carbon fibres particularly at high HTT is thus exactly the reverse of that observed in graphitic materials and must be assumed to result from some more complicated process or altogether from another mechanism (such as impurities).

It should be noted in this context that for carbon blacks the width at room temperature seemed to depend on the amount of material heat treated and upon its state (powdered or solid), the larger amount and more condensed state leading to a sharper line. These observations would tend to support the idea of the line being controlled by impurities present during heat treatments. However the width also seemed to be very sensitive to the sample residence time in the region of 1000 - 1500°C where nearly all graphitic materials apparently experience a line broadening (the so-called Hennig-Smaller Effect⁽⁸⁰⁾).

5.11 Discussion of ESR Results

In the preparation of graphitic carbons from high polymers, fusion must occur during the early stages of carbonization so that the decomposing material can undergo a preliminary orientation⁽⁷⁷⁾.

Polyacrylonitrile (PAN) undergoes pyrolysis without fusing and forms a non-graphitizing carbon⁽⁷⁸⁾. This fact is borne out by a great variety of data which goes to show that although the graphitic crystallites formed within the fibres are highly oriented with their basal planes parallel to the fibre axis, they do not attain the degree of perfection and size observed in graphitizing carbons.

The ESR data (sections 5.5, 5.8) are consistent with the generally accepted view of very limited graphitic crystallite development within carbon fibres. The g-anisotropy values Δg and more significantly, the crystallite anisotropy A do not, even at the highest HTT, approach that of single crystal graphite. The interesting question of what causes one polymer to give rise to a graphitizing carbon while another gives rise to a non-graphitizing carbon remains somewhat obscure. Franklin⁽⁵⁷⁾ who first dealt with the problem, suggested that in non-graphitizing carbons the structure is stabilized at an early stage by criss-cross bonding between the carbon layers. Such interlayer bonding is believed to prohibit the formation of intercalation compounds which would cause the separation of the layers (s-effect) in order to accommodate the foreign atom. Nevertheless the intercalation of potassium and caesium in carbon fibres has been reported by Ruland and co-workers⁽⁶⁵⁾, who cite this as evidence that no such cross-linking exists⁽⁶¹⁾.

The favourable mechanical properties of carbon fibres, however, are difficult to explain in the absence of cross-linking but can be ascribed to some extent on fibrillar branching (see section 3.3.2). Furthermore in the absence of cross-linking, the causes that prevent graphitization remain to be explained. In fact because of their small size, intercalation of the potassium and caesium atoms possibly provides inconclusive evidence as to the lack of cross-linking in these materials. Bromine, which is a somewhat larger molecule, is known to readily intercalate in graphitized materials and in view of this an attempt was made to intercalate this molecule in carbon fibres. The ESR signal of these materials, which is extremely sensitive to bromine intercalation (72), remained unchanged after prolonged exposure of the fibres to bromine, indicating the absence of intercalation. This evidence somewhat weakens the arguments against the existence of cross-linking, but the question still remains unanswered.

The applicability of ESR techniques to the study of carbon fibres can now be assessed in the light of the information presented in the previous sections of this chapter.

In section 5.6 it was demonstrated that the anisotropy Δg is insensitive to slight crystallite misalignments with respect to the fibre axis. This stems basically from the $\cos^2\theta$ variation of the anisotropy which is not pronounced in the vicinity of $\theta = 0$ and $\theta = \pi/2$. This insensitivity of Δg to slight misalignments of the crystallites makes ESR techniques unsuitable for the study of this parameter. On the other hand had this not been the case, far greater experimental

precision would have been required in mounting the fibres with all their axes perfectly parallel. In this case it would have been necessary for the parallelism to be better than 4° , which is the order of misalignment of crystallites in high quality carbon fibres. To achieve this for the several hundred fibres necessary to produce a measurable ESR signal, would have involved considerable experimental difficulties and the simple mounting techniques described in section 4.2, would have been quite inadequate.

It was hoped that the value of $g_{||}$ might be used to extract information on crystallite misalignment. The argument was based on the fact that in single crystal graphite g_1 is temperature independent while g_3 increases strongly with decrease in temperature so that the anisotropy A becomes fairly large. If this were also true for fibre crystallites the equation 5.2 shows that $g_{||}$ will increase in the presence of a misalignment ϕ by an amount $A \overline{\sin^2\phi}$ from the value g_1 which it would take in the absence of misalignment. Although the quantity $\overline{\sin^2\phi}$ is small, the quantity A , it was thought, could have been made large enough by cooling to liquid nitrogen temperatures to produce a noticeable change in $g_{||}$ from which the misalignment could be estimated.

However when the value of A for fibre crystallites was obtained it was found to be very much smaller than that for single crystal graphite and the increase in A on going from 300°K to 77°K was in no way comparable to that observed for single crystal graphite (see section 5.5). Furthermore the greatly increased contribution of the localized centres to the ESR at low temperatures considerably reduces the effect of the

X-RAY PARAMETERS AND THE g-SHIFT

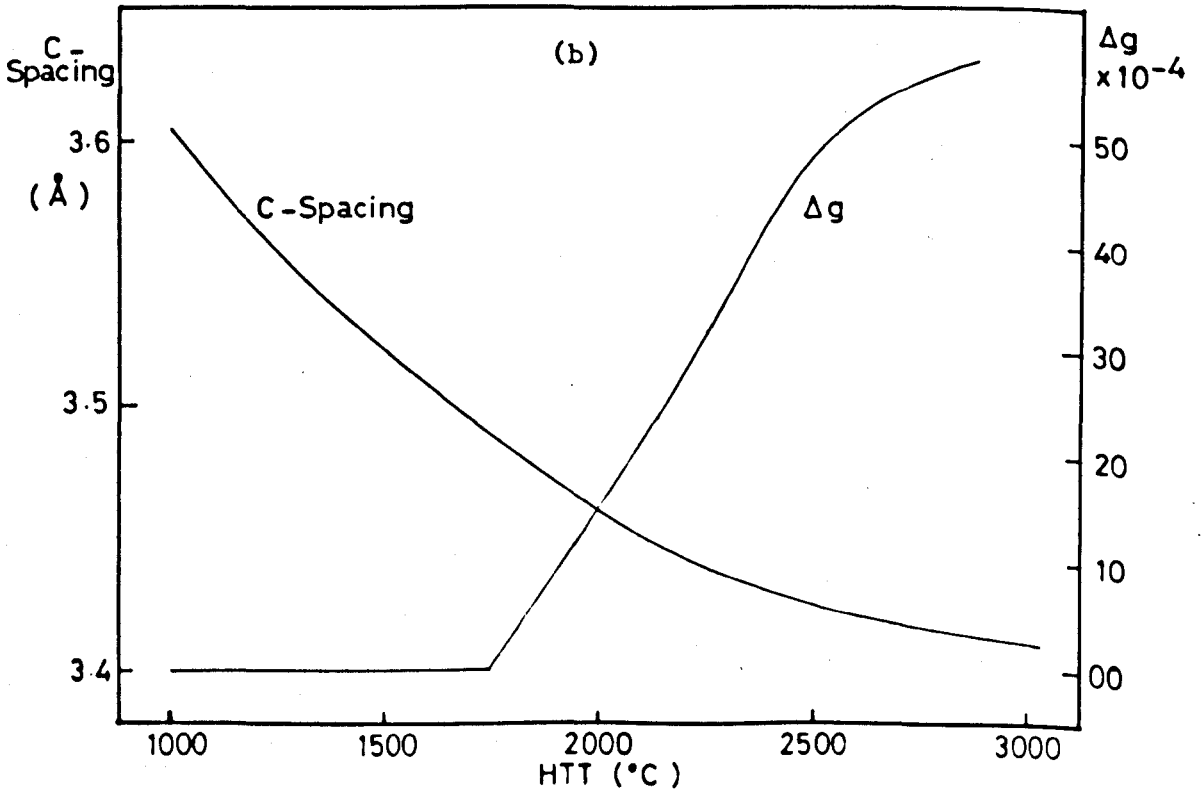
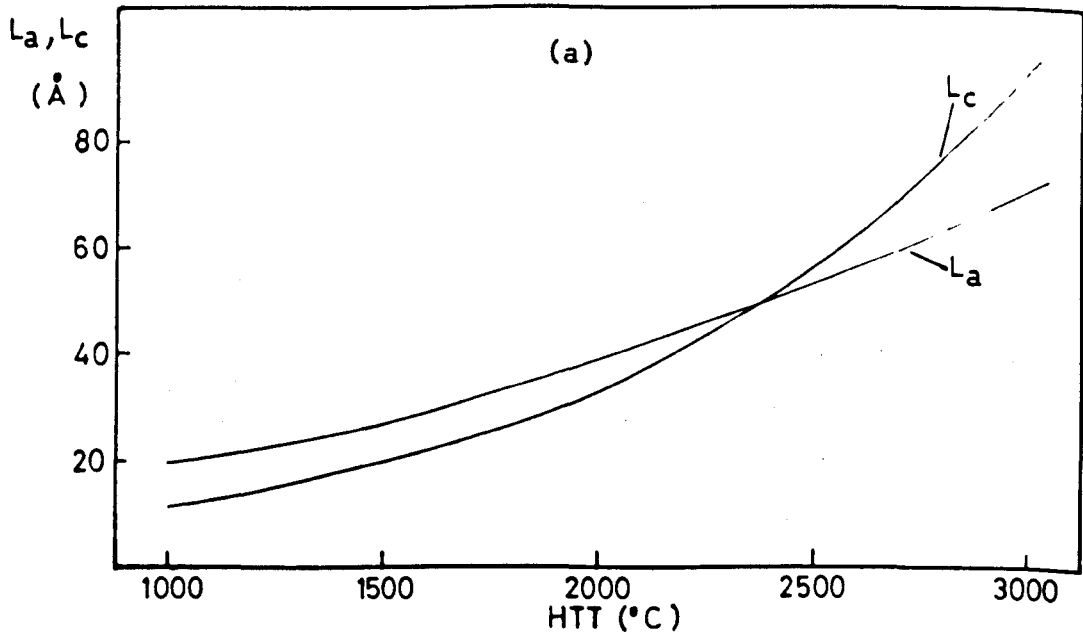


FIGURE 5.9.

quantity A, as is demonstrated by the reversal of Δg with decreasing temperature (see section 5.5).

In the light of these arguments it can therefore be safely concluded that measurement of the g-value of the ESR resonance does not provide information as to the degree of misalignment of the graphitic crystallites in carbon fibres.

On the other hand the g-anisotropy definitely increases, after its appearance at HHT ~ 1750°C, with increasing heat treatment. This suggests that the g-anisotropy is somehow related to the growth of crystallites within the fibres. The development of these crystallites can be followed by X-ray techniques, which yields the crystallite size in terms of its dimensions L_a (in the basal planes) and L_c (along the c-axis) together with the interlayer or c-spacing. Typical variations of these parameters with HTT for carbon fibres are shown in Fig. 5.9a and b*. In Fig. 5.9b the Δg variation with HTT is included for comparison.

It is immediately apparent from Figs. 5.9 a and b that there exists a basic difference between the X-ray parameters and the behaviour of the g-anisotropy. The values of L_c , L_a , and c-spacing vary continuously as the heat treatment increases, whereas Δg remains undetected up to a HTT of about 1750°C after which it increases with increasing heat treatment. Structurally, there appears to be no reason to believe that the turbostratic graphitic crystallites present in fibres heat treated below 1750°C should be any different from those occurring at higher heat

* Data kindly provided by Marjoram, R. Rolls-Royce Ltd., Research Establishment at Old Hall, Derby.

CRYSTALLITE ANISOTROPY vs C-SPACING

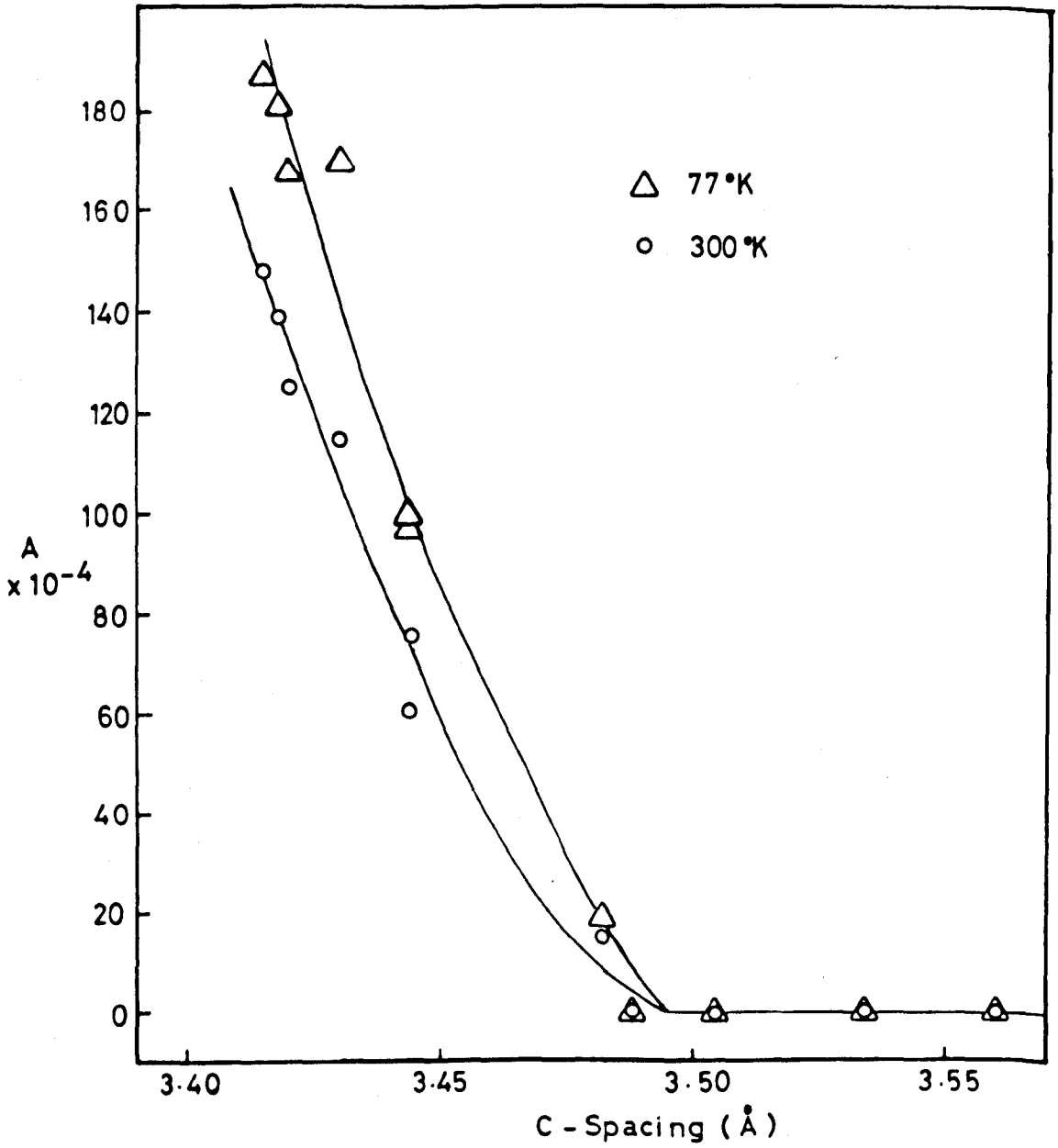


FIGURE 5-10.

treatments. The sudden appearance of the g-anisotropy at about 1750°C therefore poses some interesting questions. The interest in the processes occurring at a HTT of 1750°C gains in importance when it is realized that this is the approximate temperature at which the thermal energy of the carbon atoms becomes strong enough to break the carbon-carbon bonds, enabling them to take up more ordered and less strained positions. Indeed it is only above heat treatments of 1750°C that hot stretching of fibres (section 3.3.1) is feasible without fibre breakage.

Bearing in mind that interlayer interactions are responsible for the marked g-anisotropy present in graphite (see section 3.3.1), it would seem reasonable to suppose that the predominant factor responsible for the appearance of the g-shift in carbon fibres would be the interlayer or c-spacing of the graphitic crystallites present in the fibres. Indeed it would be difficult to see an increase in the L_a and L_c values of about 10A between the HTT of 1500 and 2000°C producing such a marked effect. Using Mrozowski's M-effect the crystallite anisotropy A was calculated for room temperature and liquid nitrogen temperature and was plotted against the c-spacing obtained from X-ray diffraction as shown in Fig. 5.10. As would be expected for grossly turbostratic crystallites the magnitude of A at room temperature is well below that of single crystal graphite ($A = 0.0461$) and rises fairly steeply with decreasing c-spacing. Furthermore the change of the anisotropy A as the temperature is lowered to liquid nitrogen temperatures is far below that of single crystal graphite (which increases from 0.0461 to 0.1244).

The large anisotropy A and its dependence on temperature in single crystal graphite appears to be due to the degeneracy of the energy bands of graphite at the zone edge (see section 3.1.1) and the sensitivity of the g -value to the position of the Fermi level relative to the band edge⁽⁷⁹⁾.

The increase in A for carbon blacks with decreasing c -spacing has been discussed by Arnold⁽⁵⁴⁾ in similar terms. The increasing crystallite anisotropy is attributed to two effects; one is the result of the upward motion of the Fermi level into a region of larger spin-orbit interaction (F -effect) and the other is an increase in the spin-orbit interaction as a result of the change of the overall band structure from turbostratic (touching bands or even with an energy gap) to graphite (band overlap). From figure 4 of Arnold's paper (which is a similar plot to Fig. 5.10), the crystallite anisotropy for carbon blacks is seen to appear at a value of c -spacing almost exactly equal to $3.49A$ which is the value at which A sets in for carbon fibres. That this should be so for two materials as widely different as the graphitizing carbon blacks and the non-graphitizing carbon fibres (Δg for the two materials in fact appears at different HTT, see Fig. 5.7) is indeed remarkable and would seem to suggest that the value of $3.49A$ is the c -spacing at which the g -shift first makes its appearance, and that this spacing is critical in terms of interlayer interactions independently of the type of carbon under consideration.

One would be tempted at this point to suggest that, although the c -spacing varies gradually, it is only at the critical interlayer

separation of 3.49A that interlayer interactions become strong enough to introduce a g-shift.

If this explanation is accepted the question of what role to assign to the Fermi level, to which the g-shift is known to be very sensitive, is bound to arise. Indeed the behaviour of the ESR intensity immediately prior to the appearance of the g-shift could be taken to indicate a rapidly rising Fermi level. The appearance of the g-anisotropy at 1750°C could then be viewed as the entrance of the Fermi level into the region of greater spin-orbit coupling which exists at the top of the band.

Which of the two factors, critical interlayer separation or position of Fermi level, is preponderant in appearance of the g-shift, or whether a combination of the two is the determining factor, cannot on the available ESR information be answered. Correlation with other electronic properties (with which Chapter 6 is concerned) is thought to be of interest in this context.

Before this discussion is brought to a close, there remains one aspect of the problem which requires attention. This is concerned with the existence of a perfectly graphitized phase in carbonaceous materials. This third phase (the other two being the amorphous carbon structure and the turbostratic crystallites) was first reported by Franklin⁽⁵⁷⁾ in various non-graphitic carbons. In carbon fibres the existence of small amounts of more perfect three dimensional graphite was reported by Johnson and Tyson⁽⁶⁷⁾ and Fourdeux et al.⁽⁸¹⁾.
By observing the X-ray diffraction profiles under specified conditions

it was apparently discovered that high modulus fibres can have a considerable degree (~40%) of the graphitized phase, which remains under normal conditions undetected because the preferred orientation peculiar to these fibres makes the identification of this phase difficult⁽⁸²⁾.

The question here is whether the g-anisotropy in carbon fibres is in fact due entirely to this perfectly graphitic phase. The fact that the crystallite anisotropy is much lower than that for single crystal graphite could be attributed to some mixing effect with the surrounding turbostratic and amorphous phases. If such is the case then, although the magnitude of A is expected to be relatively small, its temperature dependence must be the same as that for single crystal graphite, provided, and there appears to be no reason to doubt this, the mixing effect does not change with temperature. In fact this is not found to be so. The g-anisotropy between room temperature and liquid nitrogen temperature for single crystal graphite varies by a factor of ~2.65 whereas for carbon fibres the factor does not exceed ~1.6. Upon this particular piece of experimental evidence the idea that the g-anisotropy arises from a small proportion of perfectly graphitized material does not appear to be well founded. However, should a closer correlation between the appearance of the graphite phase and the g-shift be established, then this idea would warrant further examination. Unfortunately detailed X-ray and electron diffraction data are not at present available.

CHAPTER 6

ELECTRONIC PROPERTIES OF CARBON FIBRES

6.1 Introduction

Transport phenomena have been widely used to study the electronic structure of carbons and graphites. The band structure proposed by Mrozowski (outlined in section 3.2.1) has been able, qualitatively, to describe a large mass of data and the model has not been, so far, challenged by subsequent workers. It appears however that a quantitative treatment of transport phenomena is hampered by a number of considerable difficulties. These arise from the large degree of Fermi degeneracy in these materials where the Fermi level is believed to be inside the valence band and the inapplicability of conventional metal or semi-conductor models. This is because the amorphous structure of many carbons does not allow assumptions to be made as to the relationship between the energy of the electron and its momentum vector i.e. the shape of the E vs \underline{k} surfaces. In crystalline materials these surfaces are approximately parabolic. However in amorphous materials the lack of knowledge as to the shape of these E vs \underline{k} surfaces prohibits the prediction of the density of state curve and consequently the exact calculation of the density of states at the Fermi level, a parameter which is necessary for the computation of such transport phenomena as the Hall effect and the TEP.

From the experimental point of view, the situation is further complicated by the fact that most studies dealing with the electronic

properties of carbons have been performed on compressed powders or baked rods which possess the disadvantage of either numerous interparticle contacts or of mixed composition. In this respect it was felt that carbon fibres, as small single wire-like strands, which can be comparatively easily mounted and studied, would be an ideal experimental material. Furthermore the detailed correlation between the electronic properties and the ESR data of the same sample, something not previously attempted, was felt to be of interest in providing a deeper understanding of the underlying electronic phenomena and in clarifying the ESR data presented in Chapter 5.

To this end the electrical resistivity and its temperature dependence, the Seebeck thermoelectric effect and the magneto resistance is investigated in this chapter.

6.2 The Electrical Resistance

The electrical resistance of carbon and its temperature dependence varies greatly according to the degree of carbonization and graphitization of the material. For single crystal graphite the resistivity in the c-direction is much greater than in the direction of layer planes (see section 3.1.2), along which the current preferentially flows. This feature is common to all carbonaceous materials where the low resistance path will always be along the carbon hexagon rings. It is fairly evident that in amorphous carbons the predominant part of the resistivity will be taken up by the scattering of carriers at the discontinuities arising at the crystallite edges. The thermal lattice

scattering which can become predominant in the basal plane conductivity of very large graphitic crystallites can be safely disregarded when dealing with amorphous carbons. The resistance in these materials has been suggested by Mrozowski⁽³⁶⁾ to be made up of two contributions, namely, scattering of crystallite boundaries 'B' and intercrystalline contacts 'C', both of which increase greatly in effect with diminishing crystallite size.

The increase in basal plane resistivity with temperature in single crystal graphite is clearly due to the predominance of thermal lattice scattering which must be proportional to the temperature. It is difficult to see, on the other hand, how effects 'B' and 'C' can account for the negative temperature variation observed in carbons.

(Mrozowski in fact suggested that 'C' might be some decreasing function of temperature, but offered no justification for this assumption

The factor 'B' of course must be temperature independent.) Klein suggested that the negative resistivity variations with temperature in the polycrystalline graphites he investigated, resulted primarily from carrier-density variations. This suggestion will be examined further when the results of the resistivity of carbon fibres are discussed.

6.2.1 Measurement of longitudinal resistivity

A single carbon fibre was stretched under light tension on a microscope slide. By means of a colloidal silver preparation (Polaron Instruments) four contacts were painted on the fibre and extended to the edges of the slide where electrical leads could easily

be clipped on. The resistance of fibre between the two central contacts was then measured by means of a standard four probe technique employing a sensitive potentiometer (Tinsley & Co. Ltd., Type 1384D). The advantage of this method of resistance measurement lies in the elimination of contact resistances at the silver-fibre junction. The current flowing through the fibre could be varied to enable verification of Ohm's Law and the absence of Joule heating.

The fibre dimensions were then measured by means of a travelling microscope with a calibrated eyepiece. The diameter of the fibre was measured at several points along the length of the fibre and an average value used to calculate the resistivity (ρ).

The uncertainties in the resistivities obtained in this way are of the order of 10% which is almost exclusively derived from the uncertainty in estimating fibre diameters. The diameters, in fact, varied from fibre to fibre even in one particular batch, within a range of 7 to 10 microns; however resistivity values for one batch reproducible to within $\pm 10\%$ were always obtained.

To determine the resistivity at 77°K the fibre was immersed in liquid nitrogen. The ratio $\rho_{77^{\circ}\text{K}}/\rho_{300^{\circ}\text{K}}$, not being subject to diameter measurements, is reproducible to within 1%.

Variation of resistivity with temperature could also be followed from liquid nitrogen up to some 200°C by means of simple experimental arrangement. This consisted of a quartz tube well insulated by means of asbestos. The tube and asbestos lagging were made

LONGITUDINAL RESISTIVITY vs HTT

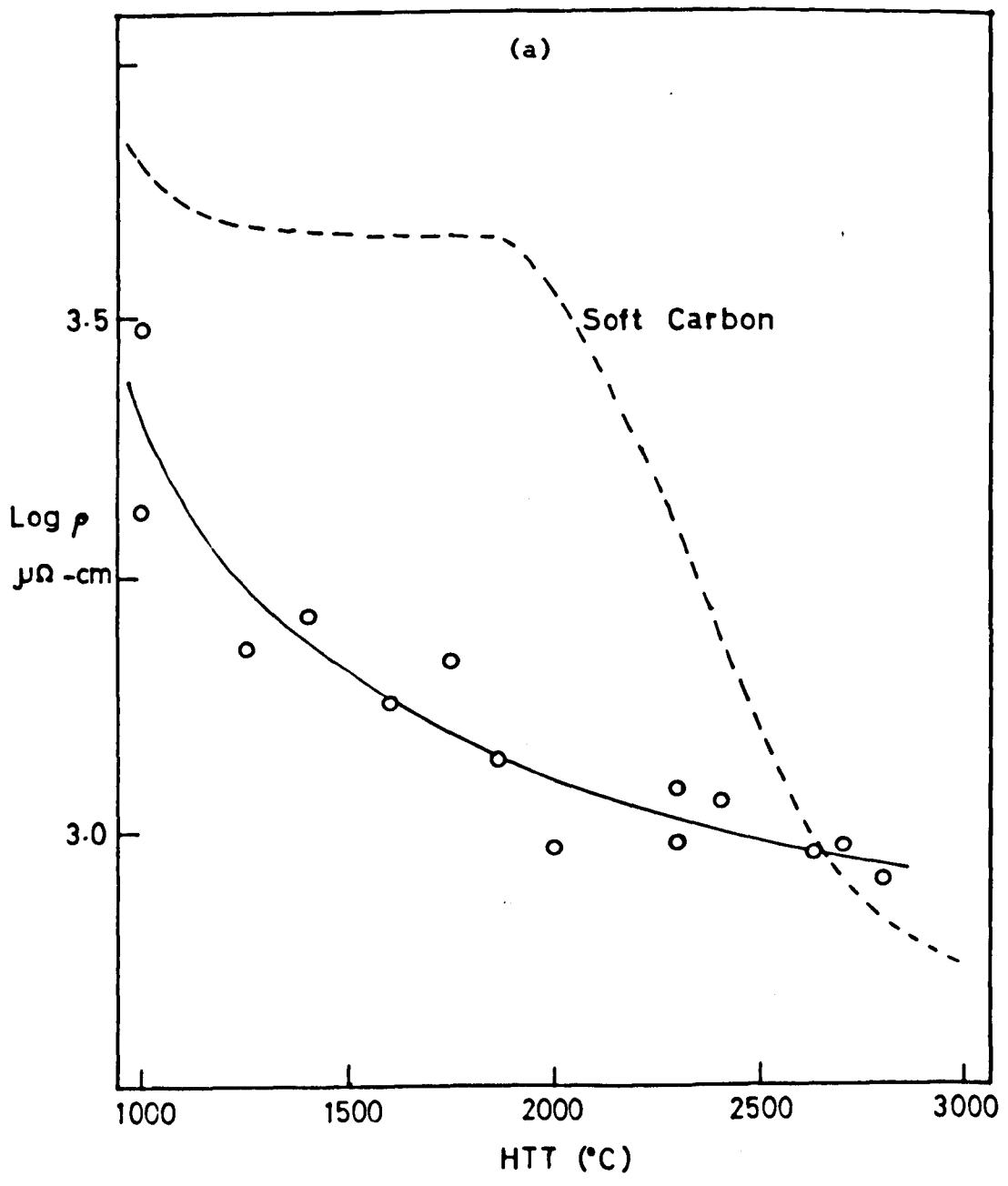


FIGURE 6.1.

to fit into a double quartz dewar. The sample mounted in a similar fashion to that described above was then inserted into the quartz tube at the end of a long asbestos plug. The whole arrangement could then be cooled to liquid nitrogen temperatures and left to slowly rise to room temperature, above which the temperature could be further raised by using heating coils wound around the quartz tube. The temperature, which was monitored by means of a copper-constantan thermocouple, varied sufficiently slowly to enable accurate measurements of resistance to be made.

6.2.2 Room temperature resistivity results

Fig. 6.1a shows the variation of the electrical resistivity with HTT. The resistivity of the carbon fibres is lower than that for soft carbons (included in the figure for comparison) at moderate HTT and very similar in magnitude to the results reported by Shindo⁽⁵⁹⁾ and Yamaguchi⁽⁸³⁾ who performed resistivity measurements on PAN based carbon fibres. The lower resistivity of carbon fibres compared to soft carbons, which for the same HTT are far more graphitized, can only be ascribed to the preferential alignment of the graphitic crystallites along the fibre axis. Basal plane conductivity will provide a lower resistance path along the fibre axis. Furthermore the crystallites being stacked end to end, so to speak, probably offer lower intercrystalline contact resistances than the corresponding polycrystalline materials. At higher HTT however the crystallites in the soft carbons become larger and larger until excitation of electrons across the greatly reduced band gap causes the resistivity for these materials to decrease rapidly

(above HTT ~ 2000°C) and to fall below that of carbon fibres, the crystallite growth of which is known to be somewhat arrested.

It is interesting to note that although a fair amount of scatter exists in the experimental points there appears to be no sign of the resistivity plateau, which occurs for the soft carbon and to some extent is also present in hard carbons⁽³⁷⁾. The presence of the plateau was ascribed to two counterbalancing effects, namely the growth of crystallites and the decrease in the number of excess carriers⁽³⁶⁾. One possibility for the absence of the plateau in carbon fibres could be that, because of the preferred orientation, crystallite growth although limited would cause intercrystalline resistances to fall more rapidly than they otherwise would in polycrystalline materials. The decrease in carrier concentration which is about the same for soft and hard carbons, as is indicated by the similarity of their spin susceptibility (see section 5.9), would not then be sufficient to provide the compensation necessary for the formation of the plateau.

6.2.3 Variation of resistance with temperature

Fig. 6.1b shows the variation of resistance ρ_T with temperature, expressed as a ratio ρ_T/ρ_{LN} for four fibres, treated at low (810°C), moderate (1000°C) and high (2500°C) temperatures. A highly graphitized fibre hot stretched at 2600°C to 24% of its length is also included for comparison. A near linear decrease of the resistivity is observed for the fibres above 1000°C. The low temperature fibre (810°C) is in fact an exception in this respect. Its temperature dependence, which is very

TEMPERATURE VARIATION OF RESISTANCE

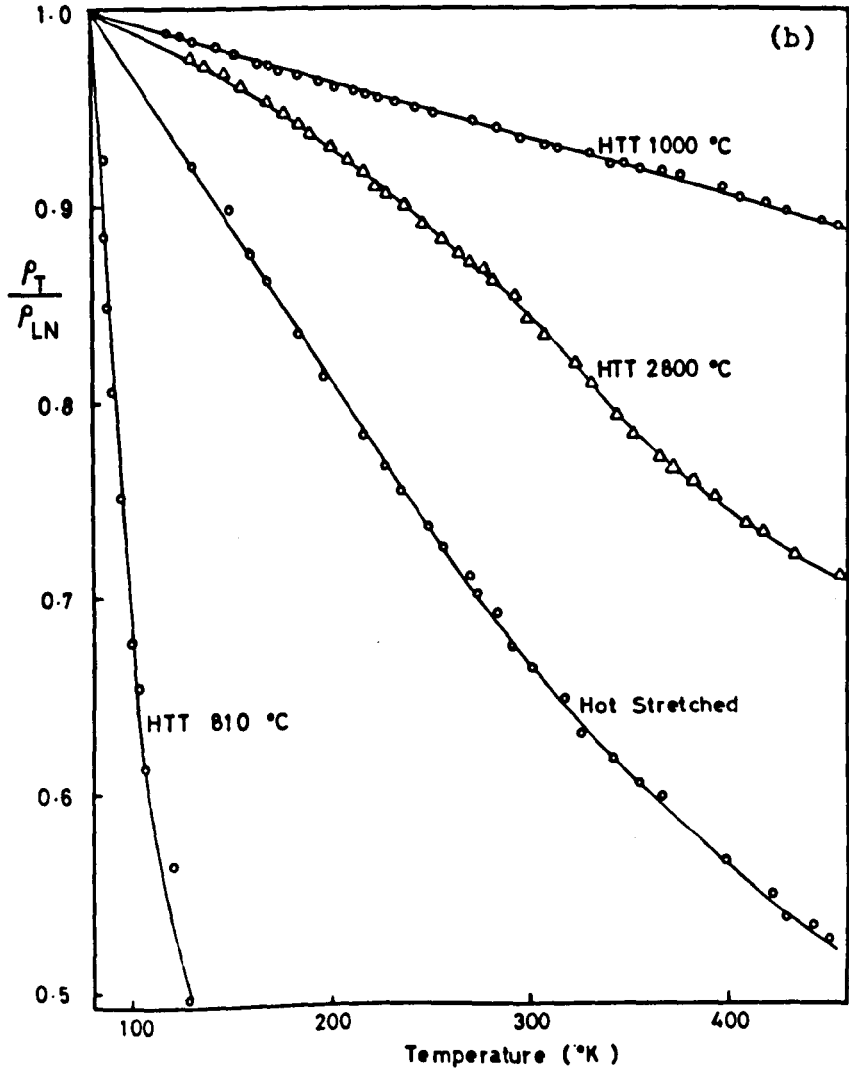
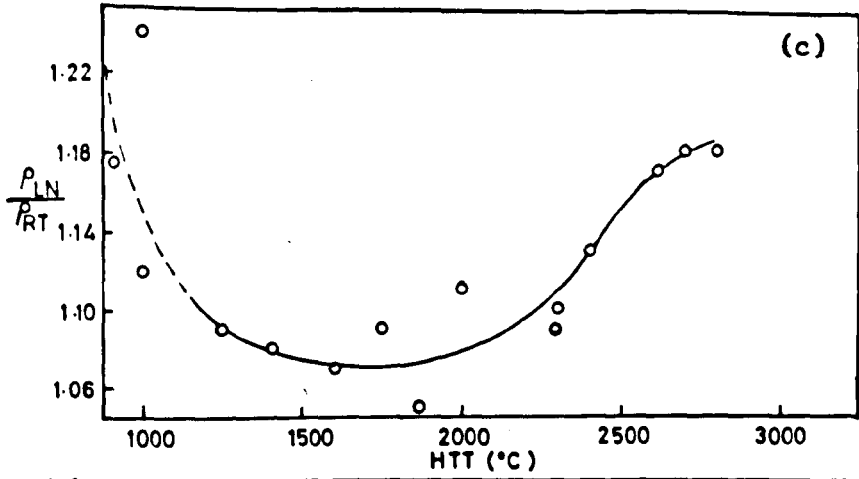


FIGURE 6.1.

large and nearly exponentially falls with increasing temperature, suggests that this sample is still in the region where the conductivity is governed by thermally excited carriers as in the case of conventional semi-conductors (see section 3.2.1).

Leaving this sample aside for the time being, examination of Fig. 6.1b immediately reveals that the slope of resistivity vs temperature curves become more pronounced with increasing graphitization, suggesting a relationship between these two parameters. Because of the near linearity of the resistivity variation with temperature, the ratio for ρ_{LN}/ρ_{RT} will be a fair approximation of the temperature dependence of these materials. This ratio is plotted against HTT in Fig. 6.1c. As one goes to lower HTT this ratio increases because the resistivity becomes more and more dependent on thermally activated carriers. The increase in the ratio ρ_{LN}/ρ_{RT} for higher HTT after metallic behaviour sets in, is indeed very peculiar and can only be viewed as somehow associated with increased graphitization. The minimum in the curve results from these two opposing tendencies.

Examining the situation for high HTT (i.e. $>1000^{\circ}\text{C}$) fibres, the two questions requiring attention are firstly the decrease of resistivity with temperature and secondly the increase in the magnitude of this decrease with increasing graphitization.

It has been suggested that the first of these effects might be linked with increased scattering at lower temperatures⁽³⁶⁾. It has also been suggested that the increase in resistance observed in polycrystalline graphites when the temperature is lowered is due to a

decrease in an effective number of carriers, the decrease being determined by the number of excess holes present⁽³⁸⁾. Klein⁽⁸⁴⁾ treated transport processes in the layer planes of pyrolytic graphites theoretically and was able to show that when the temperature is lowered, the resistance of a polycrystalline graphite sample increases owing to the decreasing carrier concentration and not to enhanced scattering. The temperature dependence of the resistivity in a material such as carbon fibres tends to be insensitive to macroscopic factors such as porosity and therefore processes along the fibre axis, in view of the high degree of crystallite orientation, might well behave in the same way as those occurring in the layer planes of pyrolytic graphites.

Klein has observed similar increases in the magnitude of the temperature dependence with increased graphitization in those pyrographites. This he attributed to be caused by shifts in the Fermi level. This seems to be supported by neutron bombardment⁽⁸⁵⁾ and bromination⁽⁸⁶⁾ studies which show that depressing the Fermi level decreases the magnitude of the temperature dependence of the resistivity. In carbon fibres evidence exists to the effect that Fermi level from about HTT 1500°C is slowly rising with increasing graphitization towards the band edge. Such an explanation could therefore account for the increase in the ρ_{LN}/ρ_{RT} ratio with graphitization.

6.3 Thermoelectric Power (TEP)

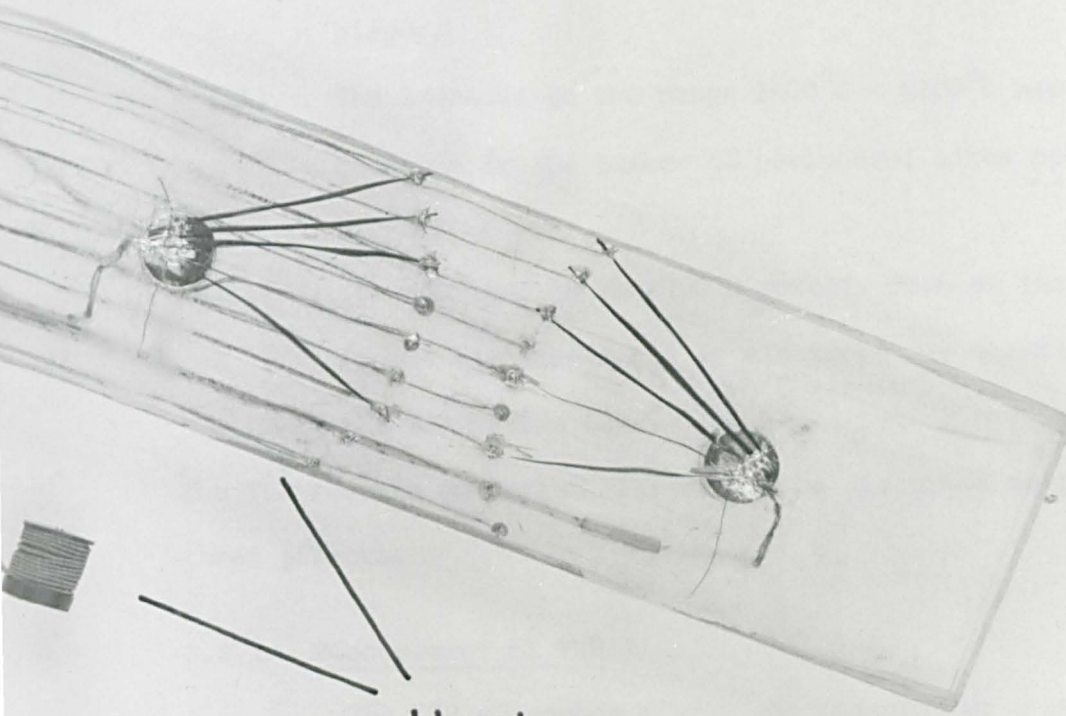
The most straightforward way of obtaining information on the processes of conduction in materials is by studying the Hall effect.

The magnitude of the Hall constant R for a single carrier type process is inversely related to the effective number of carriers and coupled with conductivity measurements will also yield their mobility. The sign of R will in addition be indicative of the type of conduction present.

Because of obvious experimental reasons, Hall measurements cannot be conducted on carbon fibres. The Seebeck effect on the other hand is easily measured, and although its relation to the number of carriers is not as straightforward as that of the Hall coefficient, it provides essentially the same information. Basically the effect arises when the two contacts to a conducting material are maintained at different temperatures. The carriers at the hot junction diffuse towards the cold junction so that a potential having the same sign as the diffusing majority carrier is developed. In defining this effect it is necessary to separate the contributions of the two materials so that the TEP of the reference material needs to be known. The TEP depends on the location of the Fermi level and can therefore be expressed in terms of the density of states, and thus a close relationship exists between the thermoelectric power and the Hall effect.

The TEP of soft and hard carbons has been studied in detail by Loebner⁽³⁷⁾. (For an account of the historical background for TEP measurements in carbons, the reader is referred to the introduction of his paper.) When his results are compared with the Hall effect studies conducted by Mrozowski and Chabersky⁽³⁸⁾, it becomes clear that the two parameters are closely related and largely substantiate the qualitative band model proposed by Mrozowski, discussed in detail in section 3.2.1.

FIBRES MOUNTED FOR TEP



Heater

FIGURE 6.2.

According to the model proposed by Mrozowski and his associates, the dependence of the TEP and Hall coefficient on HTT is explained by three effects:

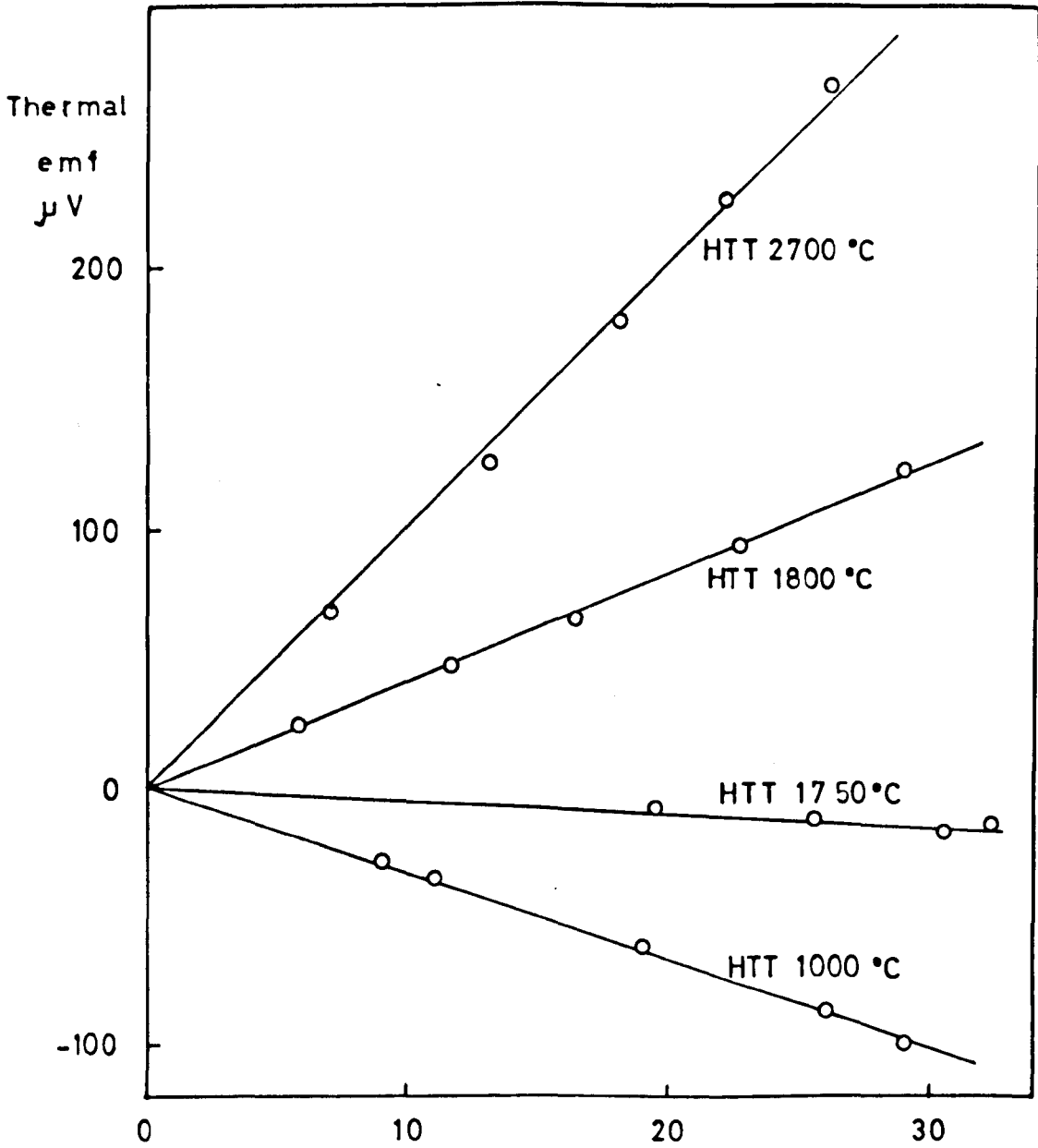
- (i) The initial drop at low HTT results from an increasing number of excess holes which are created by π -electrons being trapped in the free valence σ -orbitals on the periphery of crystalline planes.
- (ii) The increase in the range $1400^{\circ}\text{C} - 2000^{\circ}\text{C}$ results from a decrease in the number of peripheral sites occurring with crystal growth.
- (iii) The decrease above 2600°C results from an increase of carriers (holes and electrons) as electrons are thermally excited into the conduction band.

The TEP results on carbon fibres will be discussed on the basis of these three effects.

6.3.1 Measurement of TEP

The TEP of carbon fibres was measured by a thermocouple type of arrangement composed of a bundle of carbon fibres and a gold wire reference, junctions being made with the aid of colloidal silver paint. The cold junction was painted onto the flat surface of a small brass solid cylinder which acted as a heat sink and remained at room temperature, while the hot junction was painted on a similar brass cylinder around which an electric heater was wound. The temperature of the cold and hot junctions could be monitored by means of two calibrated copper-constantan thermocouples soldered onto the surfaces of the two brass

THERMAL EMF vs TEMPERATURE



ΔT Temperature Difference

FIGURE 6.3.

cylinders. This arrangement was mounted into a flat perspex base so that the fibre bundles could be conveniently stretched across the two junctions. The thermal e.m.f. was measured across a circuit break in the fibre bundle rather than in the gold wire since this enabled several fibre-gold thermocouples to be set up using the same gold wire, and measurements on all of them to be made during one run (see Fig. 6.2). The linearity of the effect was checked by plotting the thermal e.m.f. against the temperature difference between the cold junction (kept at room temperature) and the hot junction (which was raised from RT to not more than 40°C). A number of representative plots of thermal e.m.f. against ΔT are shown in Fig. 6.3*. The TEP relative gold is then given by the slope of the straight lines, and this is easily converted to the absolute scale by adding the value of 1.95 $\mu\text{V}/^\circ\text{C}$ which is quoted by Cusack and Kendall⁽⁸⁷⁾ as being the absolute TEP for gold, a value which agrees closely with the more recent value given by Huebener⁽⁸⁸⁾. This quantity was further checked by the author against that of thermocouple grade copper wire.

6.3.2 TEP results

The variation of TEP for a series of fibres heat treated from 910°C to 2800°C is shown in Fig. 6.4. The curve for a soft carbon⁽³⁷⁾ is also included for comparison. At low HTT the TEP is positive but rapidly decreases because of the large increases in the number of holes occurring in this region. The fact that the TEP actually becomes

* The sign of the thermal e.m.f. is taken as positive when the current tends to flow from the carbon fibre to the gold wire at the cold junction

TEP vs HTT

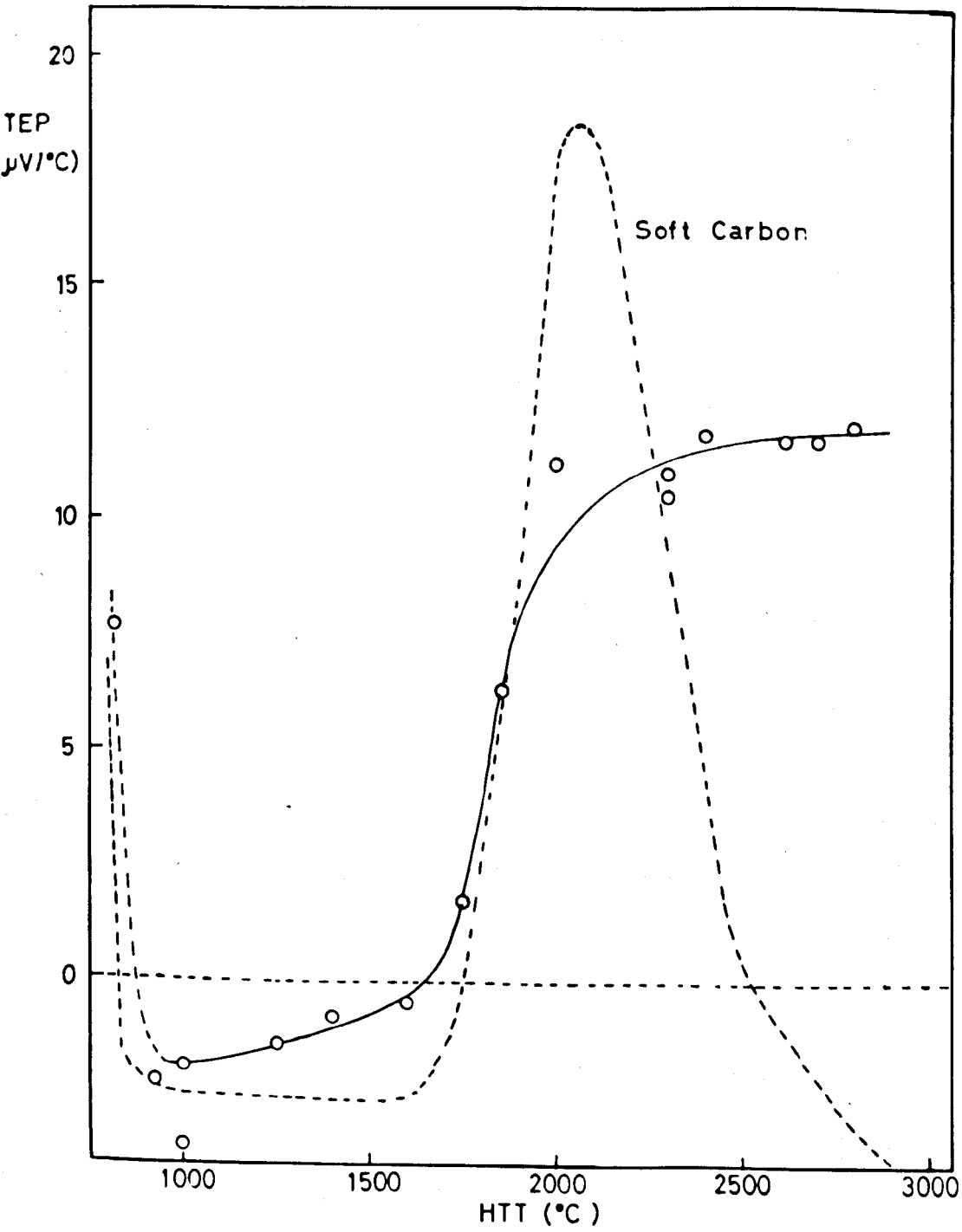


FIGURE 6.4.

negative in the range of HTT from 900°C to 1500°C is somewhat baffling since one is almost certainly in the presence of an excess hole process of conduction. Loebner's explanation, which he admits to be somewhat unorthodox, is that the Fermi level is in fact depressed so low into the valence band that it crosses the E vs k inflection point, so that the effective masses of carriers changes sign. The number of excess holes subsequently decreases with HTT as crystallite growth sets in ($\text{HTT} > 1000^{\circ}\text{C}$) causing a rise in the Fermi level, which again crosses the inflection point, at a HTT 1700°C , where the TEP becomes positive.

When it is recalled that the appearance of the g -shift occurs between $1700 - 1750^{\circ}\text{C}$ (see section 5.5), it becomes increasingly evident that this HTT is likely to be associated with a fundamental change of electronic structure in these materials.

The TEP for these carbon fibres continued to increase with increasing HTT but appears to level off at $12.0 \mu\text{V}/^{\circ}\text{C}$. This behaviour contrasts with that of soft carbons who reach a maximum of $18.5 \mu\text{V}/^{\circ}\text{C}$ and then decrease due to the excitation of electrons from the valence to the conduction band (see section 3.2.1).

The fact that the TEP for carbon fibres does not become as large as that for soft carbons could be taken to indicate that the removal of holes during crystallite growth does not go beyond a certain limit which is lower than that for soft carbons. The absence of the decrease in TEP at higher HTT suggests that there still exists a considerable energy gap between the valence and conduction bands preventing the creation of carriers by thermal excitation across the band.

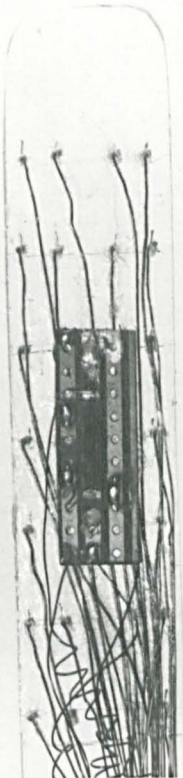
6.4 The Magneto-Resistance

When a magnetic field is applied transversely to a conductor carrying current, the trajectories of electrons between collisions will acquire a curvature. This means that the component of motion in the direction of the applied electric field will be reduced by the presence of the magnetic field, and therefore the resistance will be higher. The change in the resistance due to the application of a magnetic field (usually expressed as $\Delta\rho/\rho_0$ in %) is known as the magneto-resistance, and will therefore be expected to be positive and to disappear when the magnetic field is applied longitudinally, i.e. in the direction of the velocity of electrons. However the longitudinal magneto-resistance is often found to be of the same order of magnitude as the transverse magneto-resistance. In fact, in crystalline materials, the magneto-resistance reflects the anisotropy of the energy bands occupied by the electrons. Single crystal graphite is a good example of this. The transverse magneto-resistance for a basal plane current, varies with the angle between the magnetic field H and the c -axis, rising to large positive values when H is parallel to the c -axis and going to zero when H is perpendicular to the c -axis⁽⁸⁹⁾. The effect becomes increasingly large at low temperatures and at high magnetic fields exhibits de Haas van Alphen periodicities⁽²⁵⁾.

Bearing in mind the positive magneto-resistance of single crystal graphite and indeed of all conducting pure single crystals, the negative magneto-resistance, discovered by Mrozowski and Chaberski⁽³⁸⁾ in 1956 in polycrystalline graphite, is a striking galvanomagnetic

effect. Negative magneto-resistance has subsequently been observed in a wide range of carbons and under a variety of experimental conditions. Since carbons which exhibit negative magneto-resistance are composed of crystallites of size 300A or less, it can be safely inferred that the origin of the effect lies in the particular characteristics of its polycrystalline state. Although other electronic properties of carbons can be understood in a qualitative manner on the basis of Mrozowski's band model, the origin of the negative magneto-resistance remains a puzzling problem.

Tentative suggestions that the negative magneto-resistance was associated with hole conduction because it was observed with materials exhibiting positive Hall coefficients, have been made⁽³⁸⁾, but this has not been supported by more recent work^(90,91). Fujita⁽³⁹⁾ has shown that the diffuse scattering at crystallite boundaries can be influenced to such an extent that it could be the cause of a negative magneto-resistance of the observed order of magnitude. Toyoda and Mrozowski⁽⁹²⁾ suggest that the magneto-resistance is composed of two parts which appear to be additive. The regular positive magneto-resistance present in graphitized materials, decreases when the graphitic layers are spread apart and when the Fermi level moves out from the overlap region. The negative part appears only when the crystallites become sufficiently small, and is independent of the position of the Fermi level or c-spacing, and is found to become increasingly large in magnitude with decreasing temperature and increasing magnetic fields. At very high magnetic fields the magneto-resistance goes through a maximum negative value after



(b)



(a)

FIBRES MOUNTED FOR MAGNETORESISTANCE

FIGURE 6.5

which it tends towards positive values. This has been taken to indicate that while the positive component increases strongly with magnetic field, the negative part saturates at higher fields, so that the former eventually predominates⁽⁹²⁾. The origin of the negative component has also been ascribed to imperfections of the atomic arrangements in the graphitic crystals⁽⁹³⁾.

It appears that at the present time a thorough understanding is generally accepted to be lacking. The magneto-resistance of carbon fibres for which several other electronic properties are available was therefore thought to be of interest.

6.4.1 Measurement of magneto-resistance

The four-probe method of measuring the resistance described in section 6.2.1 was used throughout to measure the magneto-resistance. Measurements were carried out on single fibres as well as bundles. The results for the same batch were always reproducible and for systematic studies bundles of fibres were usually used because of the greater care with which these could be handled and mounted. The fibres were positioned inside a cryostat which was placed between the poles of a large electromagnet (maximum field about 13 KG) which could rotate in the horizontal plane. The fibre axes were also horizontal so that rotating the magnet enabled the variation of the magneto-resistance with the angle θ between the magnetic field H and the fibre axis (which is also the direction of flow of current) to be investigated. The cryostat could then be filled with liquid nitrogen or liquid helium. It was found impractical to measure one fibre at a time and in view of the large

ANGULAR VARIATION OF TRANSVERSE
MAGNETORESISTANCE FOR A
PYROGRAPHITE

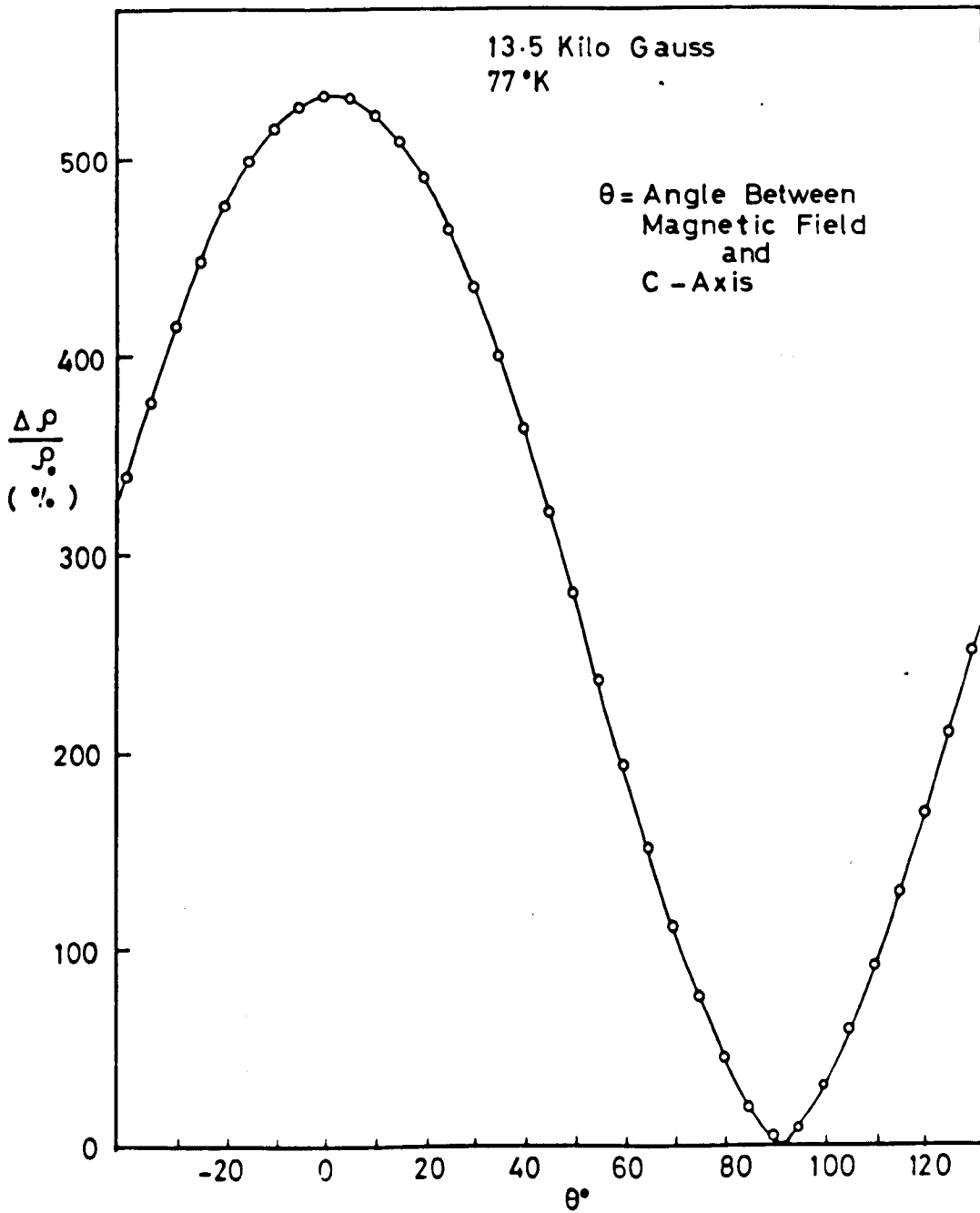


FIGURE 6.6.

FIELD DEPENDENCE OF TRANSVERSE MAGNETORESISTANCE

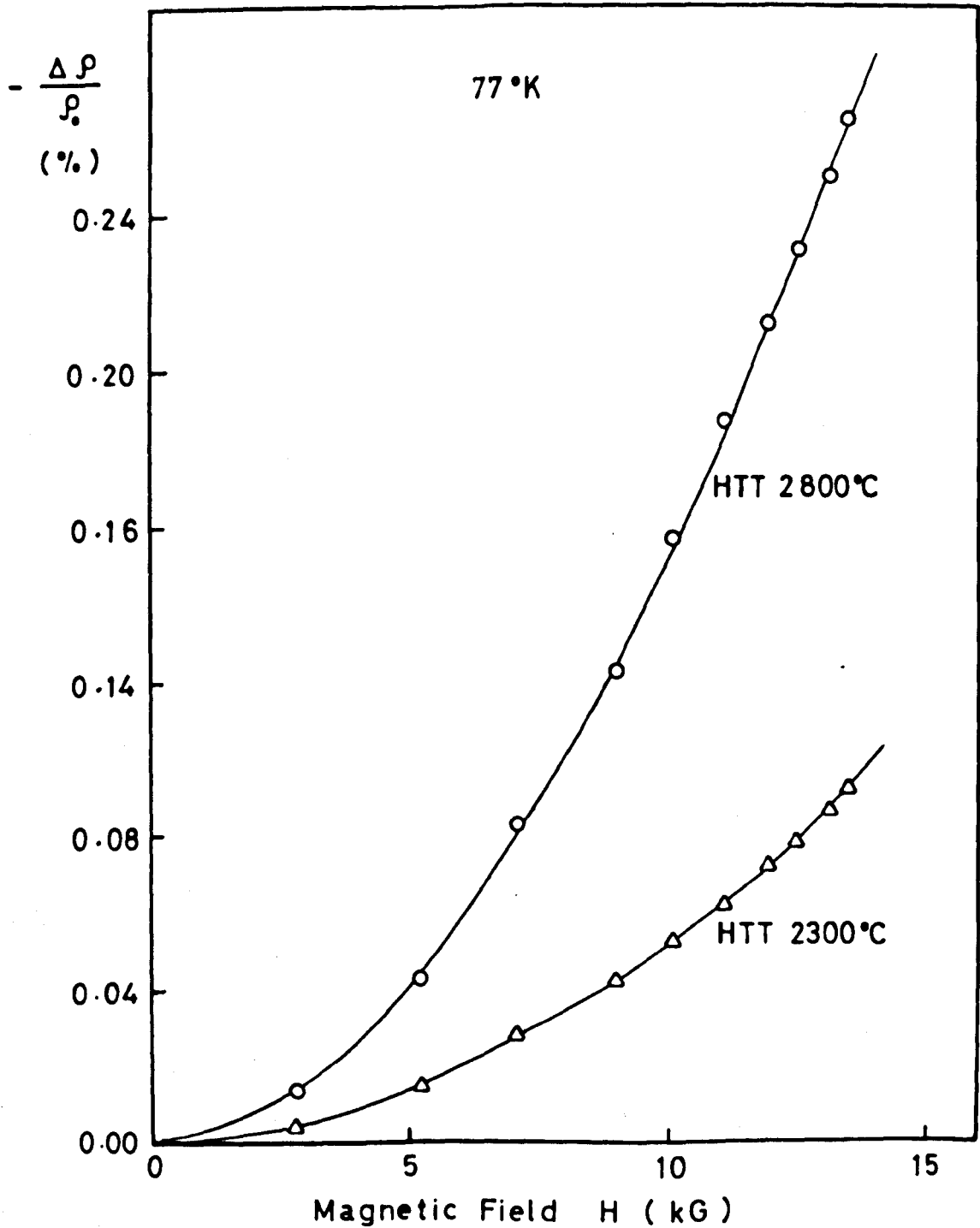


FIGURE 6.7.

number of fibres investigated a sample holder enabling seven fibres to be mounted and investigated in one run was constructed (see Fig. 6.5).

On the back face of the sample holder a specimen of pyrographite is fixed (shown in Fig. 6.5b) and was used to orientate the fibres in the magnetic field when a full angular rotation for fibres was not desired. This made use of the strong angular variation of the magneto-resistance of pyrographite, as can be seen from Fig. 6.6.

6.4.2 Results

The field dependence of the transverse magneto-resistance was investigated for the fibres at three fixed temperatures namely 4.2°K, 77°K and 300°K. Fig. 6.7 shows a typical $\Delta\rho/\rho_0$ vs H curves for two fibres heat treated at 2300°C and 2800°C measured at 77°K. By suitable log-log plots (see Fig. 6.8) it can be shown that the magneto-resistance follows a relationship $\Delta\rho/\rho_0 \propto H^X$, the exponent X being determined by the slope of this graph. This relationship was obeyed at all field values and temperatures investigated, however the exponent X varied with temperature and also depended upon the size of the magneto-resistance. For negative magneto-resistance (HTT > -1750°C) the exponent X was 1.2 at 4.2°K, 1.8 at 77°K and 2.0 at 300°K. In the region of positive magneto-resistance (only detected at 4.2°K) the exponent appeared to be greater than these values.

The variation of the magneto-resistance with HTT for the three temperatures 4.2°K, 77°K and 300°K is shown in Fig. 6.9. At low HTT (below about 1750°C) $\Delta\rho/\rho_0$ is positive for the curve at 4.2°K and becomes negative at about 1750°C, after which it increases in magnitude

FIELD DEPENDENCE OF TRANSVERSE MAGNETORESISTANCE (Log-Log)

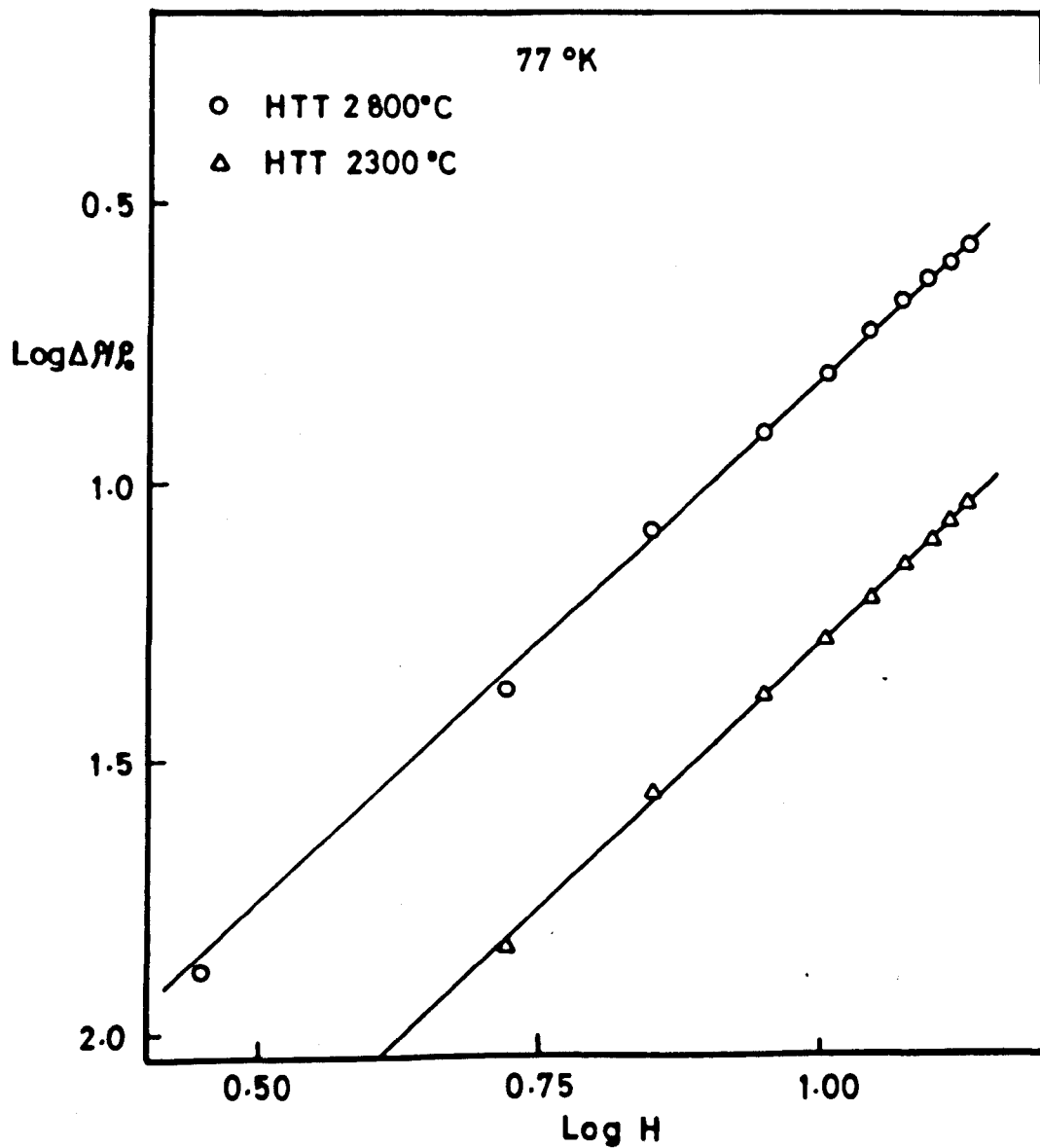


FIGURE 6.8.

TRANSVERSE MAGNETORESISTANCE vs HTT

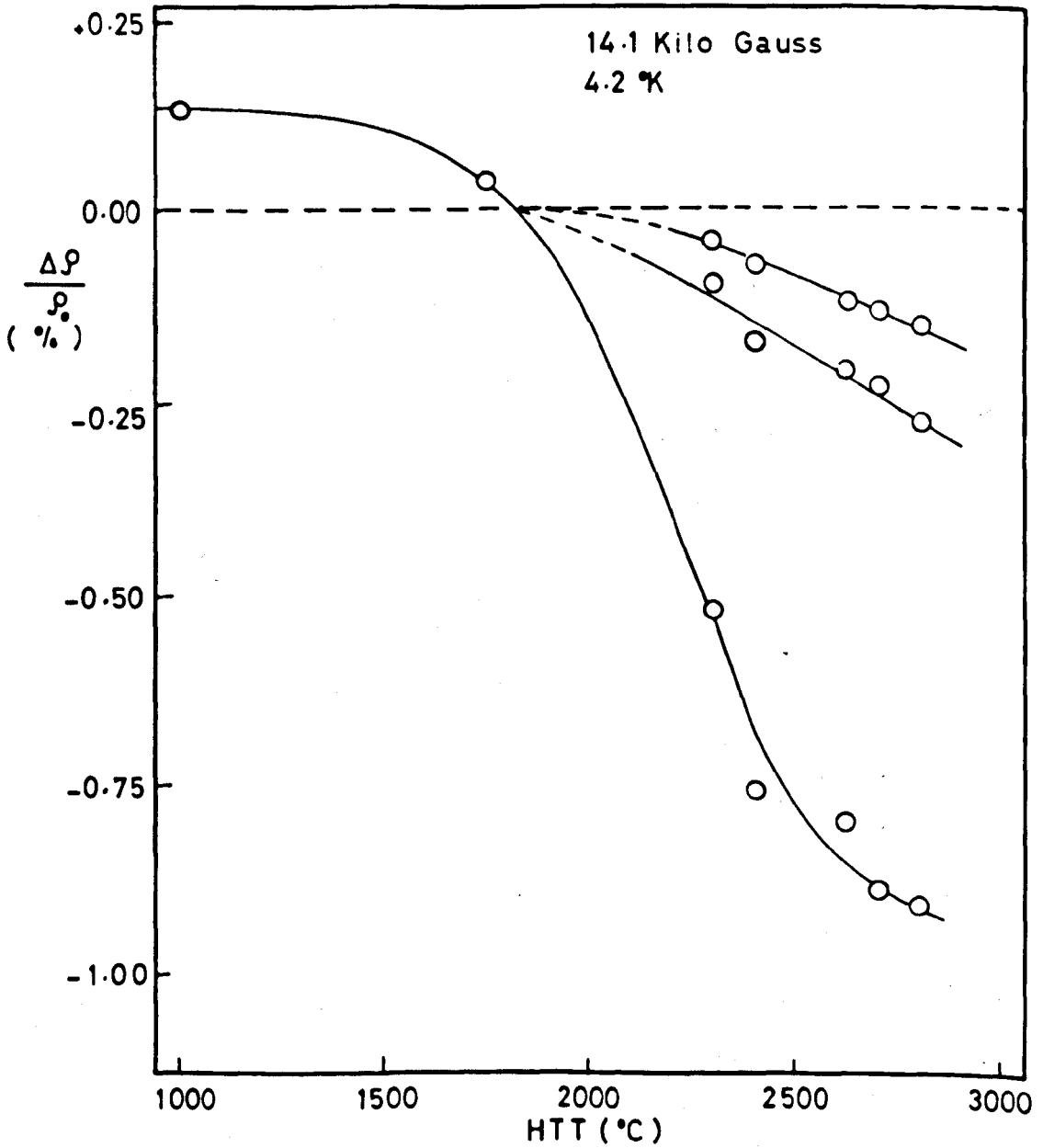


FIGURE 6.9.

with increasing HTT. The effect is greatly reduced as one goes to higher ambient temperatures. Although at 77°K and 300°K $\Delta\rho/\rho_0$ is too small to be measured, at heat treatment temperatures lower than 1750°C it is believed that the effect of raising the ambient temperature merely decreases the magnitude of the magneto-resistance without altering its sign, so that all three curves would cross over into the negative region at 1750°C. The impression gained, from the g-anisotropy and the TEP studies, that the HTT in the vicinity of 1750°C is associated with a major electronic change is thus further reinforced.

The observation of negative magneto-resistance above a HTT of 1750°C poses an interesting problem. Of the available explanations for the effect^(38,90), Fujita's diffuse scattering at crystallite boundaries⁽³⁹⁾ appears to be the most attractive. In view of the use made of Fujita's ideas in the arguments developed in the next section, the essence of his ideas will now be considered.

The zero-field resistivity is given approximately by

$$\rho \propto M^* \langle v \rangle / (n |e| \ell)$$

where e , M^* , $n \langle v \rangle$ and ℓ are respectively, charge, effective mass density, average speed, and mean free path of carriers. Except for ℓ these parameters are unlikely to change appreciably when a weak magnetic field is applied. The change in mean free path ℓ should then roughly determine the behaviour of the magneto-resistance at low fields.

If, as is the case for most conducting materials, the carriers are diffusely scattered at the crystallite boundaries (i.e. electrons

arriving at the crystallite boundary may leave the surface in all possible directions within the crystallite with equal probability), then for small crystallites, Fujita shows that the application of a magnetic field will tend to lengthen the mean free path and hence cause negative magneto-resistance. This can be seen from Fig. 6.10 (Figure 1, reference 39).

Consider an electron starting from the point A on the crystallite boundary, proceeding on a straight line AC (inside the crystallite), in the absence of a magnetic field and hitting the wall at C. The length EC may be defined as the free path of the electrons with respect to the charge transport in the upward direction. The application of the magnetic field B will induce a curvature in AC so that the free path is shortened to EC'. By symmetry an electron starting at A' will have its free path lengthened from FD to FD'. It is clear from the diagram that $DD' > CC'$ so that a net increase in the free path occurs on the application of B. These arguments hold quite generally and Fujita's computations have shown that the resulting magneto-resistance is negative, increases with crystallite size so long as boundary scattering is predominant, and is of the correct magnitude.

The negative magneto-resistance for carbon fibres increases with increasing HTT in agreement with Fujita's arguments. However, it is worth noting that the field dependence of the negative magneto-resistance shows no sign of saturating with increasing magnetic field up to 14 Kg. Clearly this is because the high degree of crystallite development

responsible for the positive component* is absent in these fibres. This is in line with all previous results.

At the other extreme (HTT < 1750°C), the appearance of the positive magneto-resistance is surprising in view of the fact that X-ray data indicates the presence of small crystallites in the fibres. A likely explanation for this could be that boundary scattering ceases to predominate. This point is examined further in the next section.

6.5 General Discussion

In Chapter 5 it was shown that the g -anisotropy for carbon fibres sets in at a HTT of 1750°C. Confronting this with the remarkable change of sign of both the TEP and magneto-resistance at precisely that HTT, it becomes evident that these changes cannot be merely the result of some coincidence and must be ascribed to a fundamental change in the electronic structure of these materials. The conclusions reached on the basis of the ESR data (section 5.11), that the appearance of the g -shift is associated with two factors, namely a critical layer separation at which interlayer interactions occur or the entrance of the Fermi

* The positive component, for large graphite crystallites, clearly arises when, extending Fujita's arguments, the diameter of the electron orbits become smaller than the crystallite size. The result will be that scattering at the boundaries will no longer be the predominant factor and conventional mechanisms will then be responsible for positive magneto-resistance.

level into a region of greater spin-orbit coupling must be reappraised in the light of the information obtained from the other electronic properties. The procedure which it is proposed to adopt in this discussion is to begin by examining the changes occurring at a HTT of 1750°C on the basis of the available band model for carbons which was put forward mainly by Mrozowski's School. It will then emerge from this analysis that the model adequately accounts for a number of observations but is unable to explain the change of sign of the magneto-resistance which occurs at 1750°C and generally breaks down below that HTT. Finally on the basis of the available information it is suggested that although the band model proposed by Mrozowski is probably valid above a HTT of 1750°C the processes occurring below that HTT are dominated by the stresses and defects created in the material during the heat treatment process. The removal of these stresses at 1750°C due to the ability of the carbon-carbon bond to be thermally broken at this temperature is shown to play a more significant role than hitherto suspected in the properties of these materials.

6.5.1 Band overlap model

Generally speaking, the ESR intensity is the most direct way of obtaining the density of states $n(E_F)$ at the Fermi level and must therefore reflect the shape of the $n(E)$ vs E curve. Now the presence of a minimum in the ESR intensity at high heat treatments has been ascribed to the existence of band overlap^(94,55). The minimum in the ESR intensity can then be ascribed to the Fermi level traversing the region of overlap at high heat treatments. This apparent overlap has been suggested to occur

BAND OVERLAP MODEL

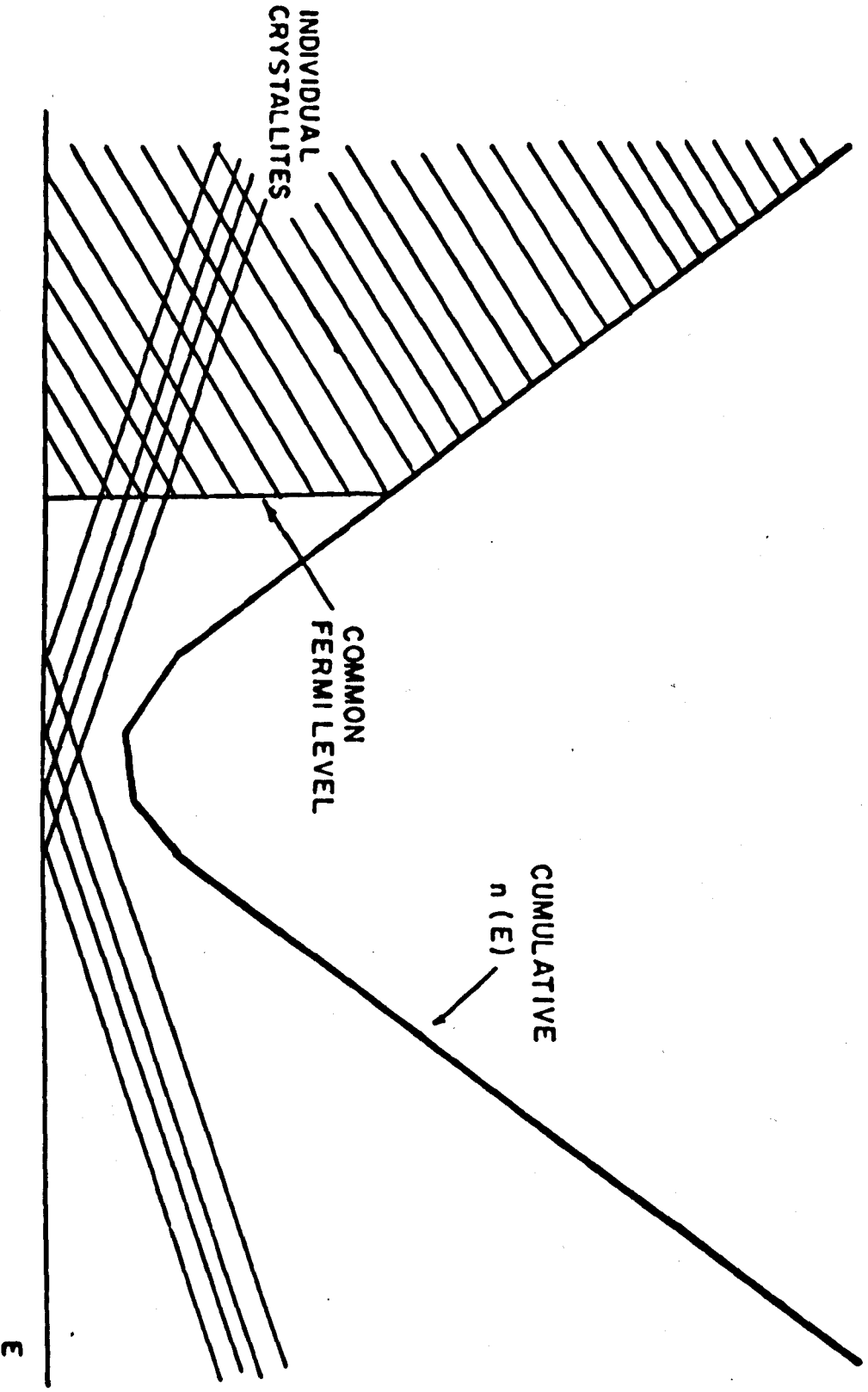


FIGURE 6.11

even in the case of a model with a gap in an "average band structure", as a result of the statistical fluctuations in the distribution of traps between crystallites in conjunction with the requirement of matching the Fermi level of all crystallites⁽⁵⁶⁾. This is shown schematically in Fig. 6.11 (Figure 9, reference 56).

Evidence for such a band picture is available from several sources. With the aid of ESR intensity measurements, this model has been generally substantiated, by following the movement of the Fermi level upon doping partially graphitized carbon black with sodium and potassium⁽⁵⁶⁾. Furthermore examination of the temperature variation of the Hall effect at various positions of the Fermi level in similar doping experiments yields interesting results⁽⁹²⁾. The Hall coefficient which is temperature independent in both single carrier regions (above and below the overlap), decreases linearly at the top of the overlap and increases linearly at the bottom of the overlap with decreasing temperature. These different behaviours can be induced in soft carbons by suitable doping down to a HTT of about 1600°C. However it should be emphasized that no temperature dependence is observed irrespective of the amount of doping for a carbon black heat treated at and below 1600°C. Clearly the band model described in Fig. 6.11 does not apply at this HTT.

6.5.2 The ESR intensity

Whether a model with overlapping bands or with an energy gap is assumed to exist at lower heat treatment temperatures a decrease in the ESR intensity can be taken to be associated with a rising Fermi level. The decrease in the ESR intensity proceeds rapidly at low HTTs, but

this decrease is less pronounced at high HTTs (see Fig. 5.8).

This could be taken to indicate that above about 1800°C the Fermi level is near the top of the valence band (or if overlapping bands are considered near the density minimum). Clearly the highest heat treatments (2800°C) do not produce a subsequent increase in the ESR intensity showing that the Fermi level does not traverse this density minimum as indeed is expected for these nominally non-graphitizing carbons.

It is noted in passing that both the localized and the delocalized components of the intensity also decrease with HTT. The latter part, being proportional to the number of carriers taking part in the conduction process, indicates, when coupled with the decreasing resistivity (see Fig. 6.1a) that the mobility must be increasing with increasing HTT. This is consistent with the diminishing intercrystalline contacts associated with crystal growth as discussed in section 6.2.2.

6.5.3 The TEP

The TEP above 1750°C rises with increasing heat treatment. This is consistent with the decrease in the number of carriers occurring in this region as indeed can also be inferred from the decreasing ESR intensity. The maximum in the TEP observed for soft carbons is not passed in these fibres, suggesting that the Fermi level, which is already close to the density minimum from about 1800°C (as is inferred for the ESR intensity) does not even at the highest heat treatments enter the band overlap region, and the carriers retain their positive hole character. It will be seen in the next chapter that hot stretching can

cause sufficient graphitization for the Fermi level to become placed in the overlap region so that some n-type character is introduced in the conduction process, causing the TEP to go through the maximum.

Clearly the change of sign of the TEP at a HTT of 1750°C is significant. This has been suggested to be associated with the Fermi level crossing the E vs k inflection point. If this explanation is accepted, it now appears that this inflection point must be present fairly near the top of the valence band. This conclusion was also reached by Toyoda and Mrozowski⁽⁹²⁾ who elegantly estimated the amount of sodium needed to raise the Fermi level from the inflection point (monitored by change of sign of the Hall effect) to the centre of the band overlap (monitored by the minimum in the ESR intensity). This of course should not be taken as confirming the existence of such an inflection point but merely as indicating that whatever is the cause for the change of sign, this occurs fairly near the top of the band edge. It should be emphasized, however, that doping material heat treated below 1700°C behaved in an exceptional manner causing these authors to wonder if such materials possessed an inflection point at all.

6.5.4 The magneto-resistance

The implications of the change of sign of the magneto-resistance precisely at a HTT of 1750°C will now be considered. Although a complete theoretical explanation for negative magneto-resistance is yet to be formulated, there seems to be general agreement that the effect is observed only in the presence of small crystallites and that it is independent of Fermi level variations. There is also evidence to the

effect that a positive magneto-resistance appears when graphitic order is established and increases in absolute value with increase in the degree of graphitization, i.e. decrease in layer spacing. This positive component which is sensitive to the position of the Fermi level, is identified with the conventional positive magneto-resistance of single crystal graphite. The positive and negative components appear to be additive.

The X-ray data clearly indicates the presence of small crystallites in the region below 1750°C so that the positive magneto-resistance observed in this region presents a problem which cannot be resolved on the current models. Careful consideration of the available data suggests that the behaviour can be explained on one simple assumption, namely that the boundary scattering only becomes predominant at a HTT of 1750°C and above. This is believed to be due to the crystallites finding themselves in a situation of considerable stress so that the crystallite boundary fields, responsible for the scattering giving rise to the negative magneto-resistance, are swamped by the random fields created by the presence of the stress and defects. This in effect leads to random scattering as that prevailing in amorphous materials and leads to positive magneto-resistance. The stresses are believed to be removed at a HTT of 1750°C where the negative magneto-resistance makes its appearance. Evidence for this contention will now be discussed.

6.5.5 Origin of stresses

In soft carbons the HTT of approximately 1750°C is associated with a major structural change which can be clearly followed by X-ray techniques. It is only above that HTT that distinct evidence of three dimensional order appears as well as a distinct change in the interlayer spacing and a marked increase in the rate of the growth of crystallites. This occurs because 1750°C is the approximate temperature at which the thermal energy of the atoms becomes strong enough to break the carbon-carbon bonds, with the result that the carbon atoms can now take up more ordered and less strained positions⁽⁵⁸⁾.

In contrast, for non-graphitizing carbons, these changes are less evident. This of course is because graphitization is hindered in these materials. Nevertheless the fact remains that the HTT of approximately 1750°C corresponds to the temperature at which the carbon-carbon bonds can be broken. In fact Johnson and Tyson⁽⁹⁵⁾ have recently reported marked discontinuities in the changes of the low-angle X-ray diffraction parameters in the vicinity of 1800°C . These discontinuities are attributed to increased perfection of the crystallites. It is significant to recall in this context that hot stretching carbon fibres is only possible without fibre breakage above 1750°C . Furthermore it is also interesting to note that diamond transforms rapidly into graphite at about 1750°C (reference 21, p.62). Thus strong evidence exists to the effect that rearrangement of carbon atoms can only occur above this HTT.

It is contended that prior to the HTT of 1750°C the stresses created in the material by the heat treatment are not able to anneal. The presence of these stresses cause the normal electric fields associated with the boundaries of crystallites to become insignificant when compared to stress fields which predominate the structure. This is taken to be responsible for the positive magneto-resistance. Above 1750°C the stresses are annealed so that the crystallite boundary fields become the predominant scattering mechanism and negative magneto-resistance makes its appearance.

It is believed that these arguments in no way interfere with the interpretation of the ESR intensity and TEP data presented in the previous sections; their effect on the appearance of the g-anisotropy at the HTT of 1750°C will now be examined.

6.5.6 The g-anisotropy

The appearance of the g-anisotropy is associated with the reversal of sign for the TEP and magneto-resistance. The TEP is known to be strongly dependent on the position of the Fermi level and the change of sign of the magneto-resistance is believed to be closely related to the removal of stresses in the material. It is therefore tempting to suggest that the appearance of the g-shift is critically related to these two parameters. Bearing in mind that the band overlap proposed by Mrozowski occurs for additive contributions to the density of state by individual crystallites (section 6.5.1, Fig. 6.11) and that the minimum in the density of states occurs in the region of the band overlap of individual crystallites, one could argue that in the presence of stresses

(below 1750°C) the crystallite contributions are absent because of deformation of their fields. Or alternatively that the band overlap for the crystallites does not exist. Both these suppositions would presumably result in a model where the valence and conduction bands are separated by an energy gap. Such a model would have the virtue of explaining the behaviour of carbon blacks heat treated below about 1750°C, a behaviour which was shown by doping experiments not to conform to that of carbons heat treated at higher temperatures. Clearly in such a band model no g-shift can be expected.

Immediately on attaining the HTT of 1750°C the stresses in the material are annealed and the model as proposed by Mrozowski is created. The g-shift then appears as a result of the presence of the Fermi level near the density minimum and the region of crystallite overlap.

It must be recalled at this point that in section 5.11 it was demonstrated that although for soft carbons the g-shift appears at a somewhat lower HTT (~1,250°C) than for the nominally non-graphitizing carbons, the shift occurs at an identical layer separation (of 3.49A) for both these materials. According to the arguments developed above, this can only be explained if the model as proposed by Mrozowski appears in soft carbons far earlier than in hard carbons. That is to say that the stresses created during heat treatment are more readily annealed in the case of soft carbons. This leads to the conclusion that these stresses in hard carbons are likely to be associated with interlayer cross linking, the removal of which necessitates temperatures in excess of 1750°C, at which thermal breakage of the carbon-carbon bond can occur.

There remains a discrepancy which requires attention; this is concerned with the change of sign of the TEP which occurs for both soft and hard carbons at 1750°C. That this should be so is not in itself taken to be extraordinary, but the implication is that at ~1250°C for soft carbon the Fermi level would be located below the inflection point and somewhat removed from the band overlap region. The appearance of the g-shift in such a situation can only be explained if the interlayer interactions (i.e. the c-spacing) by far outweighs any variation in the position of the Fermi level (a conclusion also reached by Mrozowski⁽⁵¹⁾) or alternatively that the interpretation of the negative TEP as being the result of a Fermi level being depressed below the inflection point is erroneous.

In view of the great sensitivity of single crystal graphite to the position of the Fermi level, it is felt that even below the inflection point, if such exists, the Fermi level must still be in the vicinity of the band overlap and that the c-spacing must indeed be the dominant factor via the interlayer interactions mainly responsible for the appearance of the g-shift.

Finally the conclusions arrived at from the available information can be summarized as follows:

(a) The ESR of carbon fibres does not differ in any basic way from the ESR of carbons and graphites and is amenable to analysis by methods developed for these materials.

(b) The HTT of 1750°C appears to be associated with an important structural change as is indicated by the changes which occur in all the major properties investigated for these materials.

(c) The appearance of the g-shift is believed to occur at a critical interlayer or c-spacing of 3.49A, where the interlayer interactions abruptly become large enough to produce the g-anisotropy. The position of the Fermi level is thought to be fairly close to the top of the valence band and is not believed to play an overriding role in the appearance of the g-anisotropy.

(d) It is believed that the negative magneto-resistance only appears above a HTT of 1750°C because of the distortion in the crystallite fields caused by the stresses present in the material prior to that HTT.

(e) The band model proposed by Mrozowski clearly fails below heat treatment temperatures of about 1750°C.

(f) The change of sign of the TEP at a HTT of about 1750°C is ascribed, in the absence of any other explanation, to the Fermi level crossing the E vs k inflection point.

CHAPTER 7

EFFECT OF HOT STRETCHING

7.1 Introduction

The series of fibres considered in Chapters 5 and 6 (henceforth referred to as series I) do not exhibit the outstanding mechanical properties which characterise the very best carbon fibres at present available. In general the strength of carbon fibres is thought to be controlled by cross-linking present in the polycrystalline material. Young's modulus on the other hand has been shown to be governed by the orientation of the basal planes of the graphitic crystallites relative to the fibre axis⁽⁶⁰⁾. The greater the degree of preferred basal plane orientation along this axis, the greater the value of Young's modulus for the fibre. Consequently, from a technological point of view, techniques which enhance crystallite alignment are of primary importance.

It will be recalled (section 3.3.1) that two methods of producing high modulus carbon fibres are available. The first of these consists in restraining the natural shrinkage of the fibre during the initial carbonization stage and the second, known as hot stretching, involves stretching the fibres at high enough temperatures for plastic flow to take place^(96,97). Both techniques result in improved crystallite alignment. The first method presumably involves the preservation of the original polymer array, whereas the second is associated with some form of stress recrystallization. Clearly the importance of hot stretching in the manufacture of carbon fibres cannot be overestimated.

In this chapter the effect of hot stretching on the electronic and ESR properties of carbon fibres are investigated. The samples used for this purpose (referred to as series II) consisted of pairs of fibre batches with each pair possessing an identical thermal history. One fibre in each pair was subjected to hot stretching while the other remained unstretched and was used for control purposes. Because of the restriction imposed by the inability to hot stretch carbon fibres below a HTT of about 1750°C , all the specimens of series II were treated above that HTT.

Generally the effect of hot stretching on the properties of these fibres is similar to the increase in graphitization produced on raising the HTT. However it will be seen that the properties of the fibres of series II do not correlate well with each other or with the properties of the fibres of series I, when these are expressed in terms of the HTT. However all the data fall nicely in line when related to a parameter associated with the degree of graphitization, which will be referred to as the 'graphitic order'. The relatively high graphitic order obtained on hot stretching allows observations previously made on fibres of series I to be supplemented and confirmed.

The various theoretical considerations and experimental techniques associated with the parameters with which this chapter is concerned, have been given considerable attention in previous sections of this thesis. In this chapter, therefore, the emphasis is placed on presenting the experimental results, and suggesting practical applications where these might be of value.

EFFECT OF HOT STRETCHING UPON THE g -ANISOTROPY

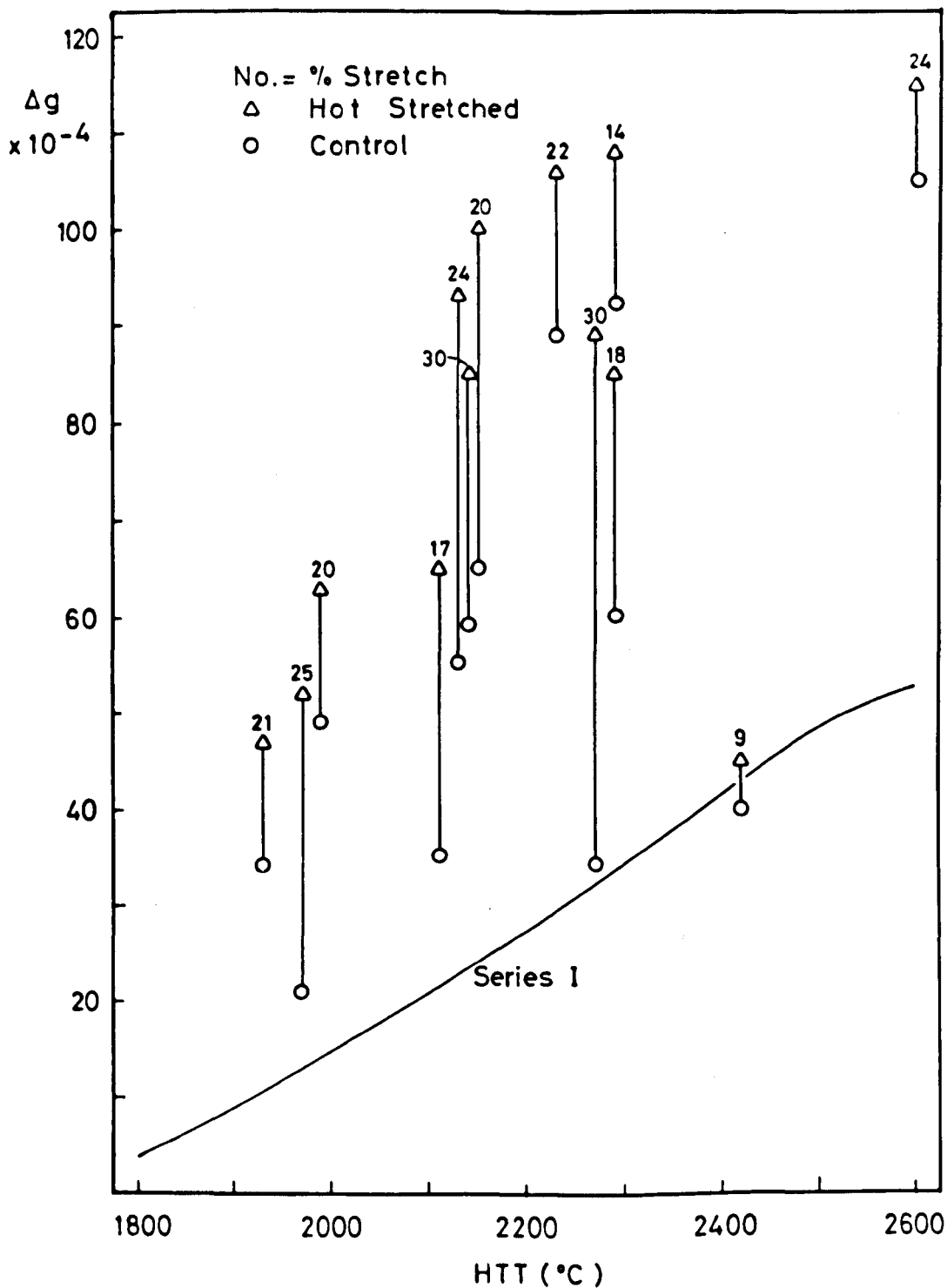


FIGURE 7.1.

7.2 The g-Anisotropy

The effect of hot stretching upon the g-anisotropy is shown in Fig. 7.1. The g-anisotropy for the fibres of series I is also included for comparison. It is immediately apparent that the control fibres of series II, not only do not fall on the g-anisotropy vs HTT curve of the first series but also they do not even form a continuous line amongst themselves. In general the control fibres of series II have a higher anisotropy than the fibres of series I for a given HTT. While the reasons for these anomalies are not fully understood, they are presumably due to variations in the detailed thermal history of the samples and also perhaps to differences in the structure of the original organic fibre precursor. These results clearly indicate that the HTT alone cannot be taken as a criterion for the degree of graphitization in these fibres, unless great care is taken in controlling the conditions under which the fibres are manufactured. This was the case for the fibres of series I. However in the absence of X-ray data, the need for a parameter, generally representative of the 'graphitic order', is felt.

Hot stretching carbon fibres invariably produces an increase in the g-anisotropy (Fig. 7.1). The increase in Young's modulus associated with hot stretching, has been ascribed to increased alignment of the graphitic crystallites⁽⁶⁰⁾. However it has been shown that the g-anisotropy is little affected by small changes in misalignment (section 5.6). In fact the Z-values available for these fibres were smaller than 10^0 and the changes in this parameter upon hot stretching clearly could not account for the observed increase in g-anisotropy.

REVERSAL OF g-ANISOTROPY WITH TEMPERATURE

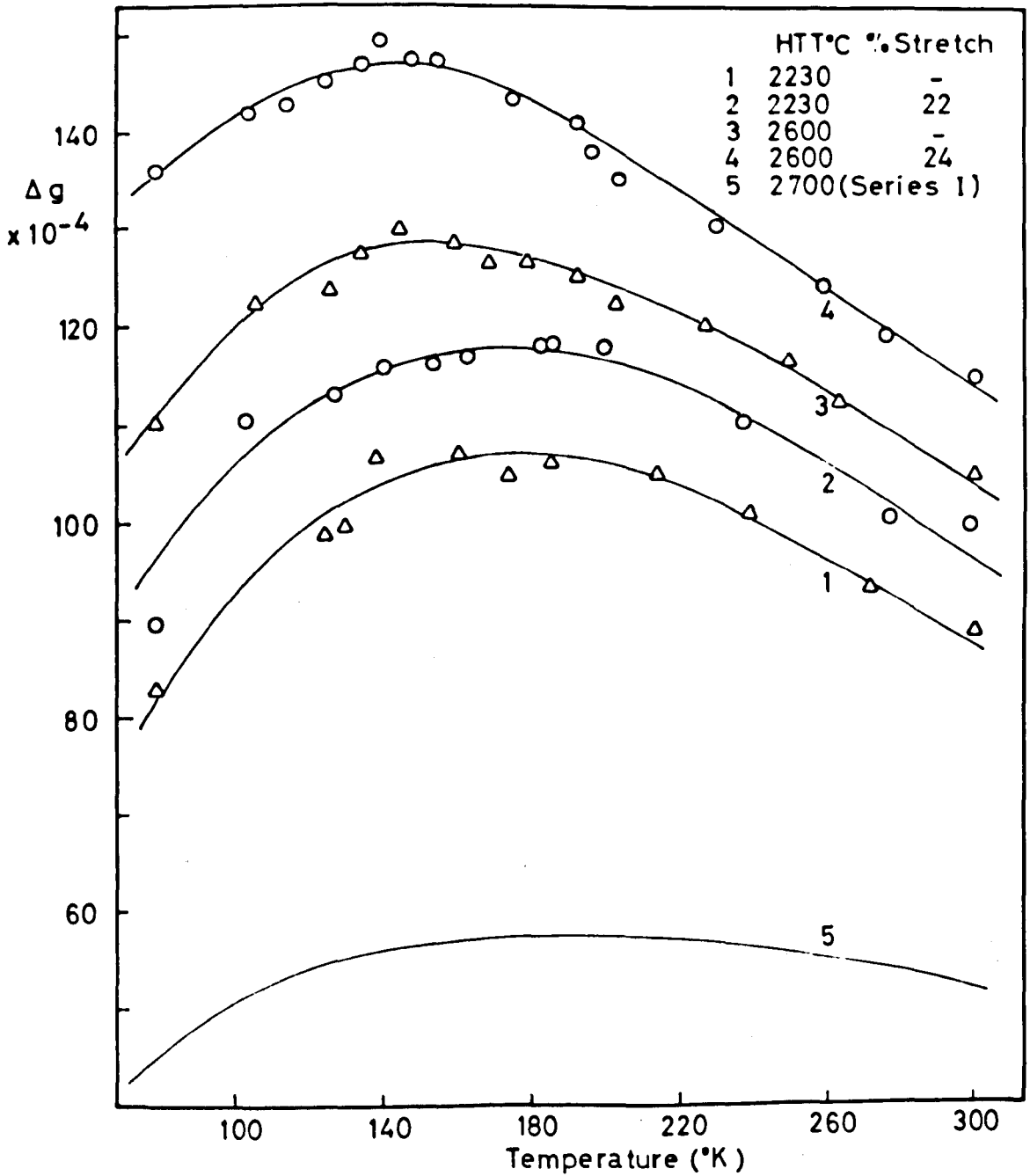


FIGURE 7.2.

The conclusion can therefore be drawn, that hot stretching must be accompanied not only by increased alignment of crystallites but also by an improvement in their perfection; that is to say, a decrease in the interlayer or c-spacing to which it is believed the g-shift is particularly sensitive (section 6.6).

Unfortunately the samples available, in addition to differences in thermal histories, had not been stretched by equal amounts, so that a quantitative discussion of the effect of hot stretching could not be attempted. It is felt, however, that for an equal percentage stretch a small change in Δg is produced at lower and higher heat treatments than is produced at moderate heat treatments. This could well arise from graphitization being hindered at lower heat treatments by diminished ease of plastic flow. At higher heat treatments the material, being already highly 'graphitized', does not on hot stretching produce a marked increase in g-anisotropy.

The increased graphitization of series II enables the reversal of the g-anisotropy with temperature, discussed in section 5.7, to be followed with greater ease. Fig. 7.2 shows this reversal of the g-shift for two pairs of fibres from series II together with the fibre heat treated at 2700°C of series I (Fig. 5.6a) which is included for comparison.

The crystallite anisotropy for the fibre with the greatest degree of graphitization, i.e. largest g-anisotropy, was computed for various temperatures and this is shown in Fig. 7.3. The figure also includes the variation of the g-anisotropy with temperature determined

g-ANISOTROPY FOR FIBRE CRYSTALLITE AND SINGLE CRYSTAL GRAPHITE vs TEMPERATURE

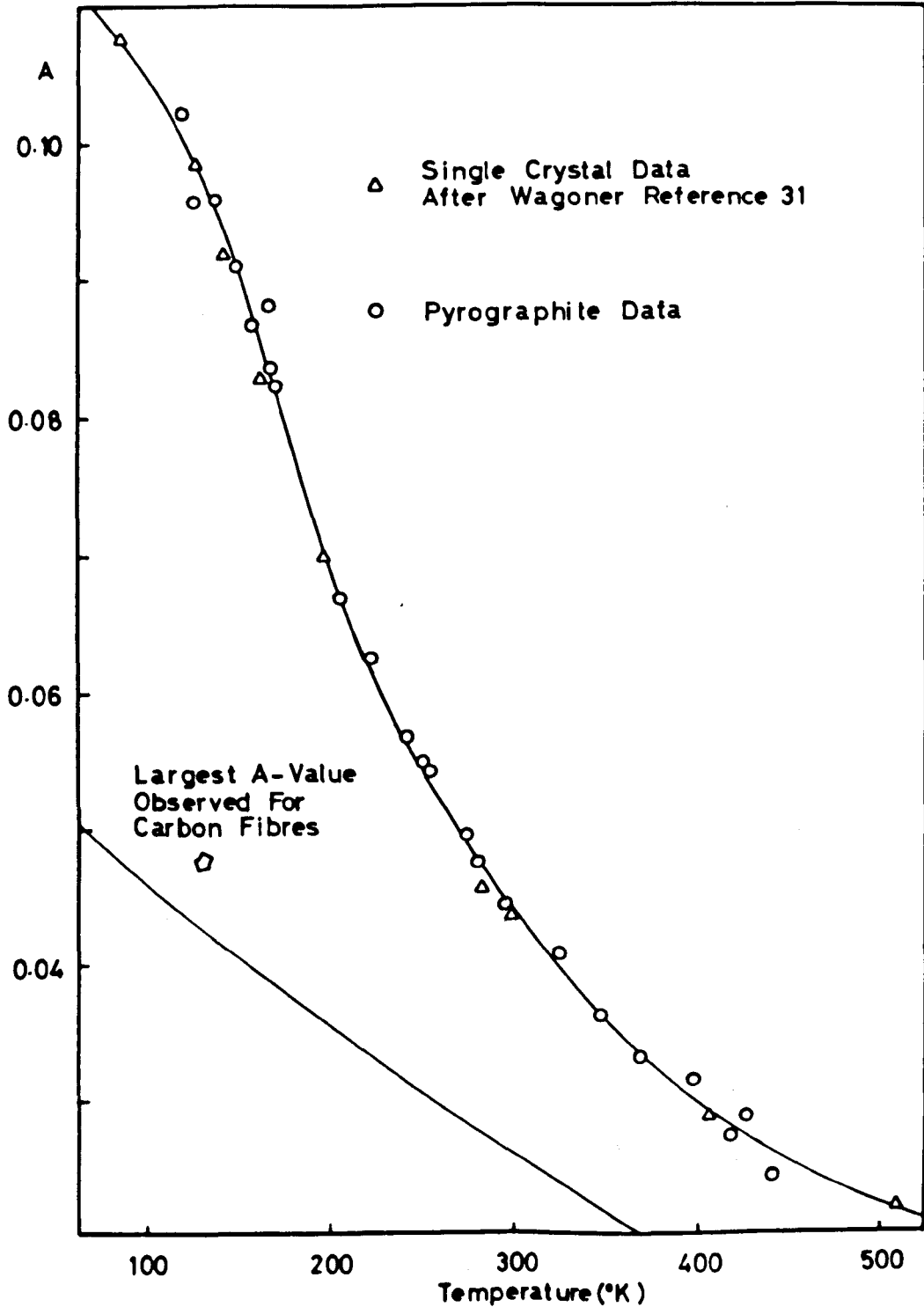


FIGURE 7.3.

Table 7.1

Line Width Ratio $\Delta H_{\perp} / \Delta H_{\parallel}$

IDENTIFICATION		CONTROL		STRETCHED	
HTT °C	% Stretch	300°K	77°K	300°K	77°K
2290	14	1.15	1.18	1.29	1.30
2140	30	1.02	1.07	1.07	1.14
2600	24	1.10	1.36	1.18	1.44
2150	20	1.03	1.08	1.13	1.16
SERIES I AVERAGE		1.02± 03	1.03±.03		

experimentally for a sample of pyrographite. The observed anisotropy for the pyrographite agrees well with Wagoner's data obtained for single crystal graphite⁽³¹⁾. Clearly the crystallite anisotropy even in very highly 'graphitized' carbon fibres remains inferior to that of single crystal graphite, indicating that the crystallites in carbon fibres never attain the perfection of single crystal graphite.

7.3 Line Width Anisotropy

The line width, it will be remembered, was very scattered and showed no correlation with the HTT or g-anisotropy (section 5.10). This again was found to be true for the fibres of series II. In Table 5.2 it was seen that the line width with the magnetic field perpendicular to the fibre axis ΔH_{\perp} was on the average 2% broader than the line width with the magnetic field parallel to the fibre axis ΔH_{\parallel} . Since this was within the experimental uncertainty of the measurement, no conclusions were drawn from this observation. However in the highly graphitized fibres of series II, it becomes clear that the line width shows a definite anisotropy. Investigation of this anisotropy, in a parameter which is difficult to measure with a high degree of precision, required the line width to be computed from the slope of a line shape analysis (section 4.3). The resulting angular variation of the line width is shown in Fig. 7.4a*.

* The choice of the sample for this angular variation was dictated by the necessity for a narrow line width, to enable greater precision of measurement. Furthermore the measurements were carried out at 77°K as the anisotropy is generally enhanced at lower temperatures.

LINE WIDTH ANISOTROPY

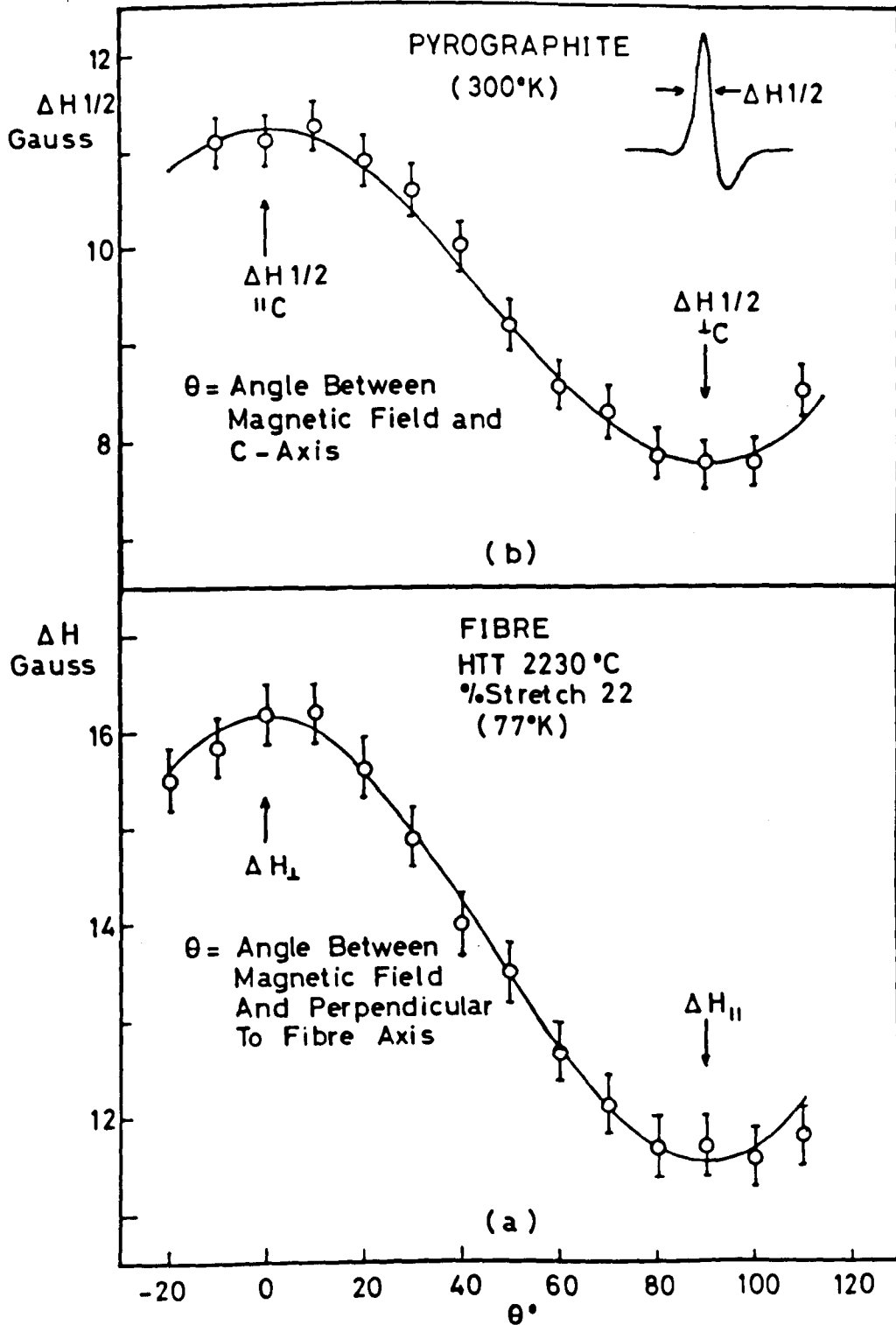


FIGURE 7.4.

The variation of the line width with the direction of the magnetic field could be fairly well fitted by a \cos^2 function which was a maximum for the magnetic field perpendicular to the fibre axis. The line width for a pyrographite sample $\Delta H_{\frac{1}{2}}$, was also examined for comparison and a similar variation was observed with the width going through a maximum when the magnetic field is parallel to the c-axis. This observation confirms data previously reported by Delhaes and Marchand⁽⁷⁴⁾, who showed that the results were consistent with an anisotropy in the spin-spin relaxation time T_2 arising from the band structure of these materials⁽⁹⁸⁾.

Bearing in mind that the crystallites in carbon fibres are aligned with their c-axis symmetrically distributed in a plane perpendicular to the fibre axis (section 5.6) and that the ESR line in these materials is a result of motional averaging (section 3.2.2), it seems reasonable to suggest that the observed line width anisotropy results from the inherent anisotropy in the graphitic crystallites within the fibres. Clearly when the magnetic field is perpendicular to fibre axis a broader line width is contributed by the crystallites to the overall line width than when the field is pointing along the fibre, that is to say, along the crystallite basal planes. It should be emphasized however that the contribution of the crystallites to the line width represents only a fraction of the total line width, the remaining part of which has so far eluded all attempts made to explain its origin. This part is believed to be responsible for the lack of correlation of the line width with any of the parameters associated with carbon fibres.

EFFECT OF HOT STRETCHING UPON THE ELECTRICAL RESISTANCE

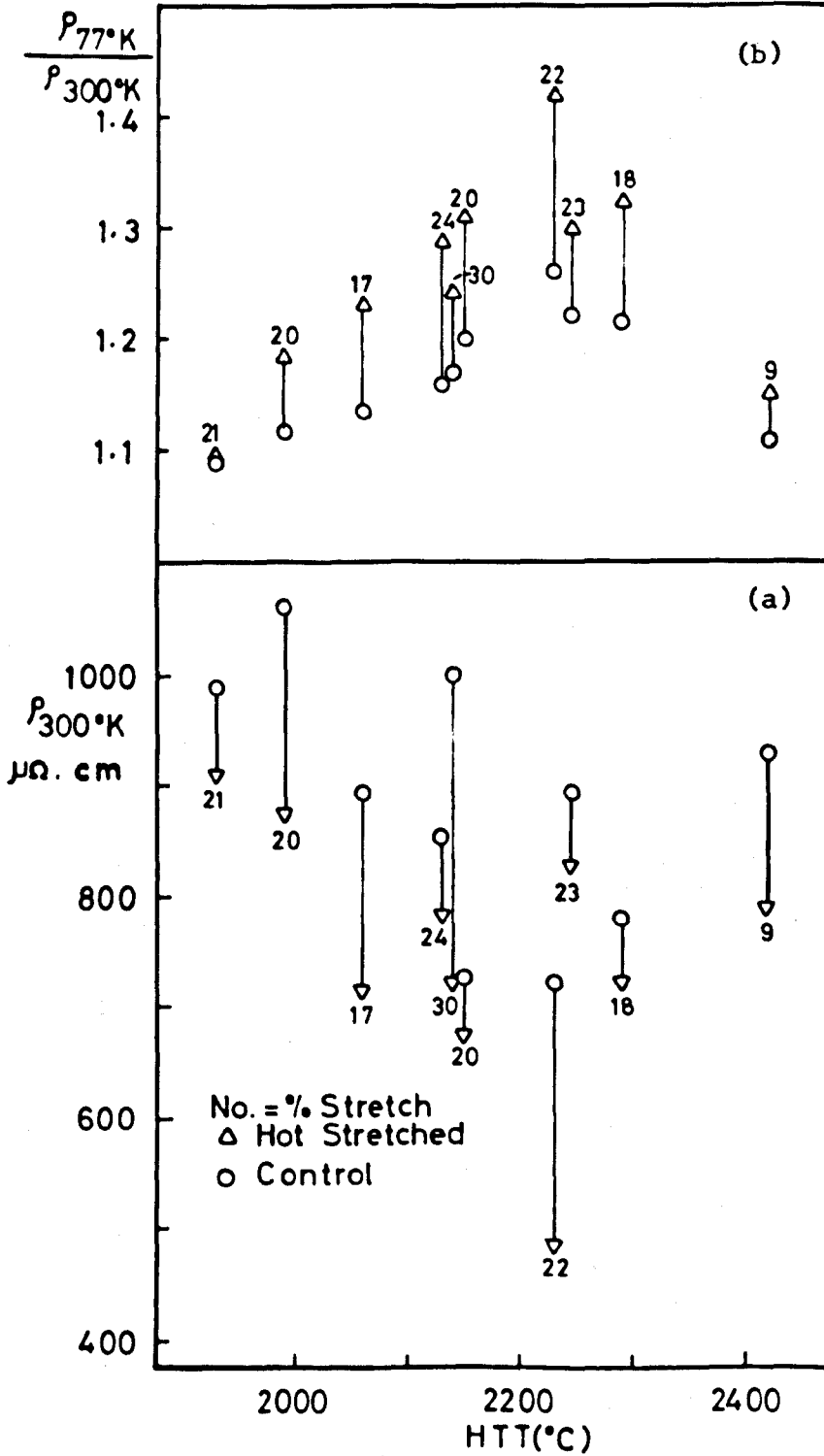


FIGURE 7.5.

Table 7.1 gives the ratio of $\Delta H_{\perp} / \Delta H_{\parallel}$ for a number of fibres both at 77 and 300°K. The table shows that this ratio is always greater than unity and increases both with decreasing temperature and on hot stretching. This is not unexpected since $\Delta H_{\perp} / \Delta H_{\parallel}$ for the pyrographite sample was seen to increase with decreasing temperature and that hot stretching would clearly enhance graphitization and hence the line width anisotropy.

7.4 The Electrical Resistivity

The effect of hot stretching on the electrical resistivity of carbon fibres is summarized in Fig. 7.5. The room temperature resistivity (Fig. 7.5a) invariably decreased on hot stretching, which indeed is not unexpected as on hot stretching both crystalline growth and increased crystallite alignment is bound to enhance basal plane conductivity and reduce intercrystallite contact resistances.

The temperature variation of the resistance, expressed as the ratio $\rho_{770\text{K}} / \rho_{300\text{K}}$ (Fig. 7.5b), on the other hand, increases with hot stretching and when it is recalled that this ratio was found to increase with increasing HTT (section 6.2.3), this result falls in line with the increased graphitization expected upon hot stretching.

7.5 The TEP

The effect of hot stretching upon the TEP of carbon fibres differs from the behaviour observed with the other properties of these materials. On hot stretching the g-anisotropy, the resistivity, the

EFFECT OF HOT STRETCHING ON TEP

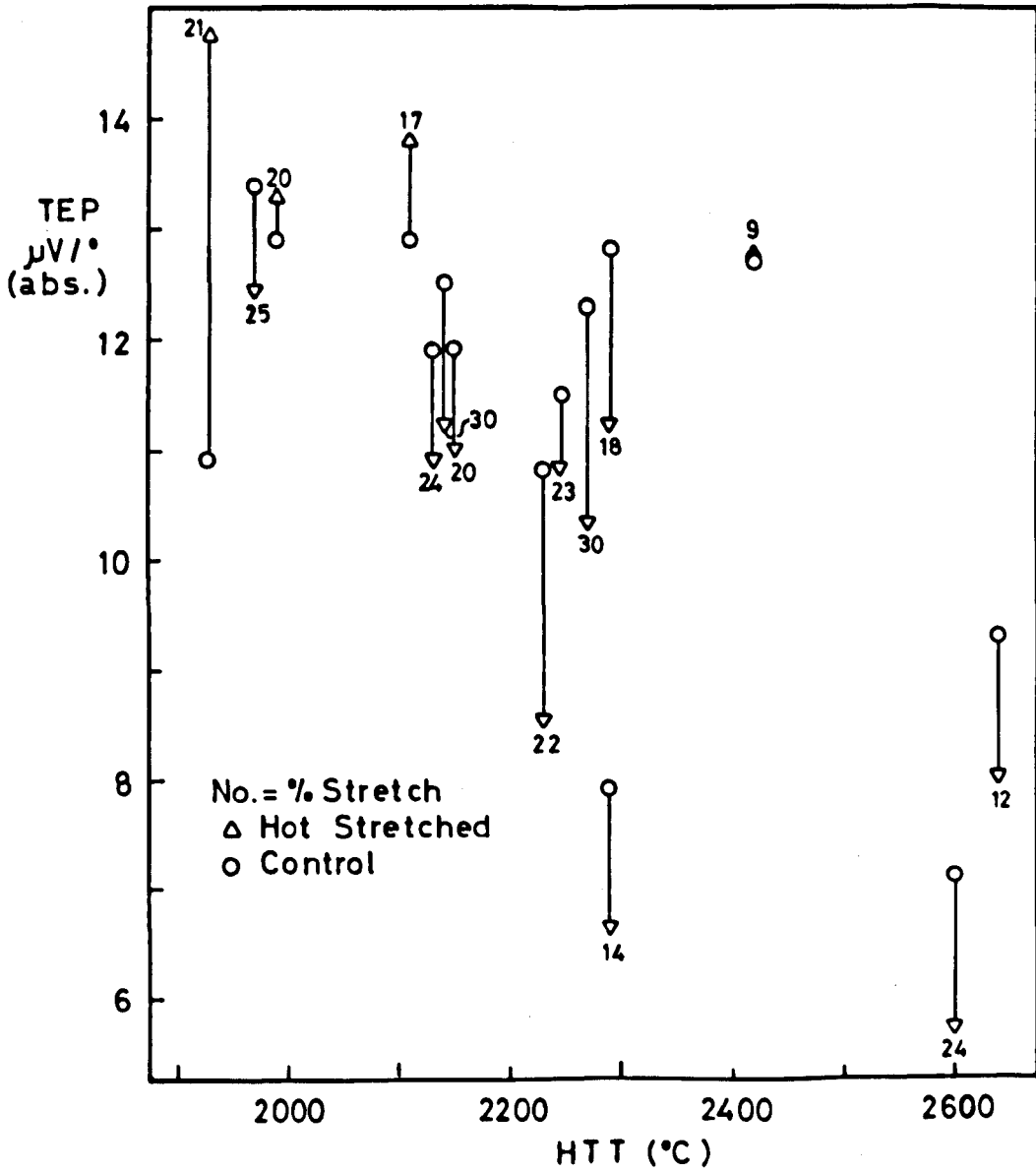


FIGURE 7.6.

EFFECT OF HOT STRETCHING ON MAGNETORESISTANCE

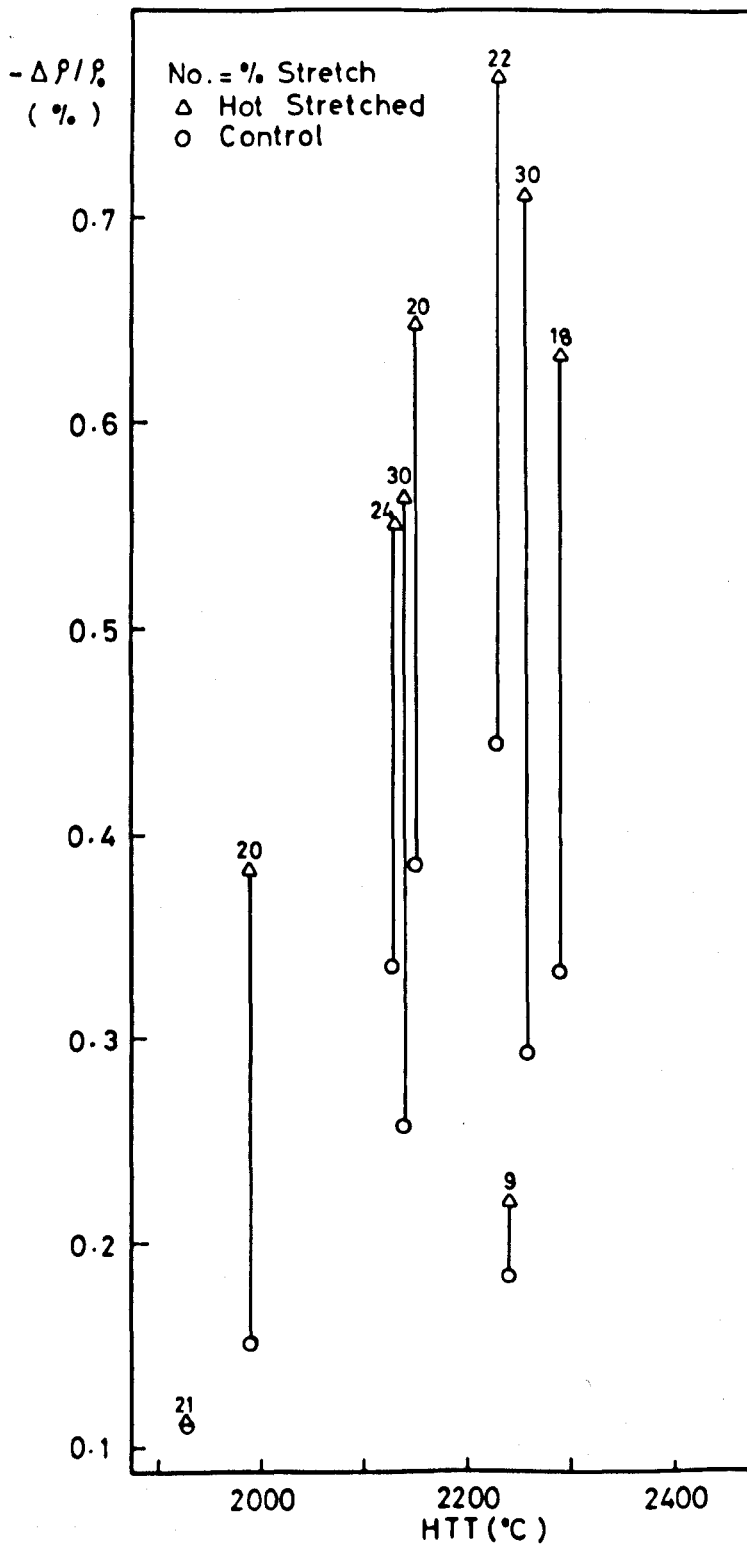


FIGURE 7.7.

resistivity ratio $\rho_{770\text{K}}/\rho_{300\text{K}}$ and the magneto-resistance (section 7.6) each changes in one direction. The TEP, on the other hand, exhibits (Fig. 7.6) two types of behaviour, showing in some instances an increase in magnitude and in others a decrease on hot stretching. This behaviour seemed at first to be somewhat extraordinary; however it was noticed that the fibres whose TEP tended to increase with hot stretching appeared to lie in the lower region of the HTT range, while those whose TEP decreased were in the higher HTT range. It will be recalled that the TEP for soft carbons goes through a maximum with increasing HTT, i.e. graphitization. Clearly then, if the control sample is situated past the TEP maximum, further graphitization on hot stretching will produce a decrease in TEP. If, on the other hand, the control is present before the maximum, then either an increase or a decrease in the TEP will be observed according to whether the increase in graphitization places the stretched fibre before or after the TEP maximum. That this is indeed the explanation for the observed behaviour of the TEP upon hot stretching will be clearly demonstrated in section 7.7.

7.6 The Magneto-resistance

The magneto-resistance, which is always negative, increases in magnitude in all cases upon hot stretching (Fig. 7.7). This result agrees well with Fujita's⁽³⁹⁾ mechanism which predicts an increase in the magnitude of $\Delta\rho/\rho_0$ with increasing crystallite size as long as boundary scattering remains predominant.

ANGULAR VARIATION OF MAGNETORESISTANCE

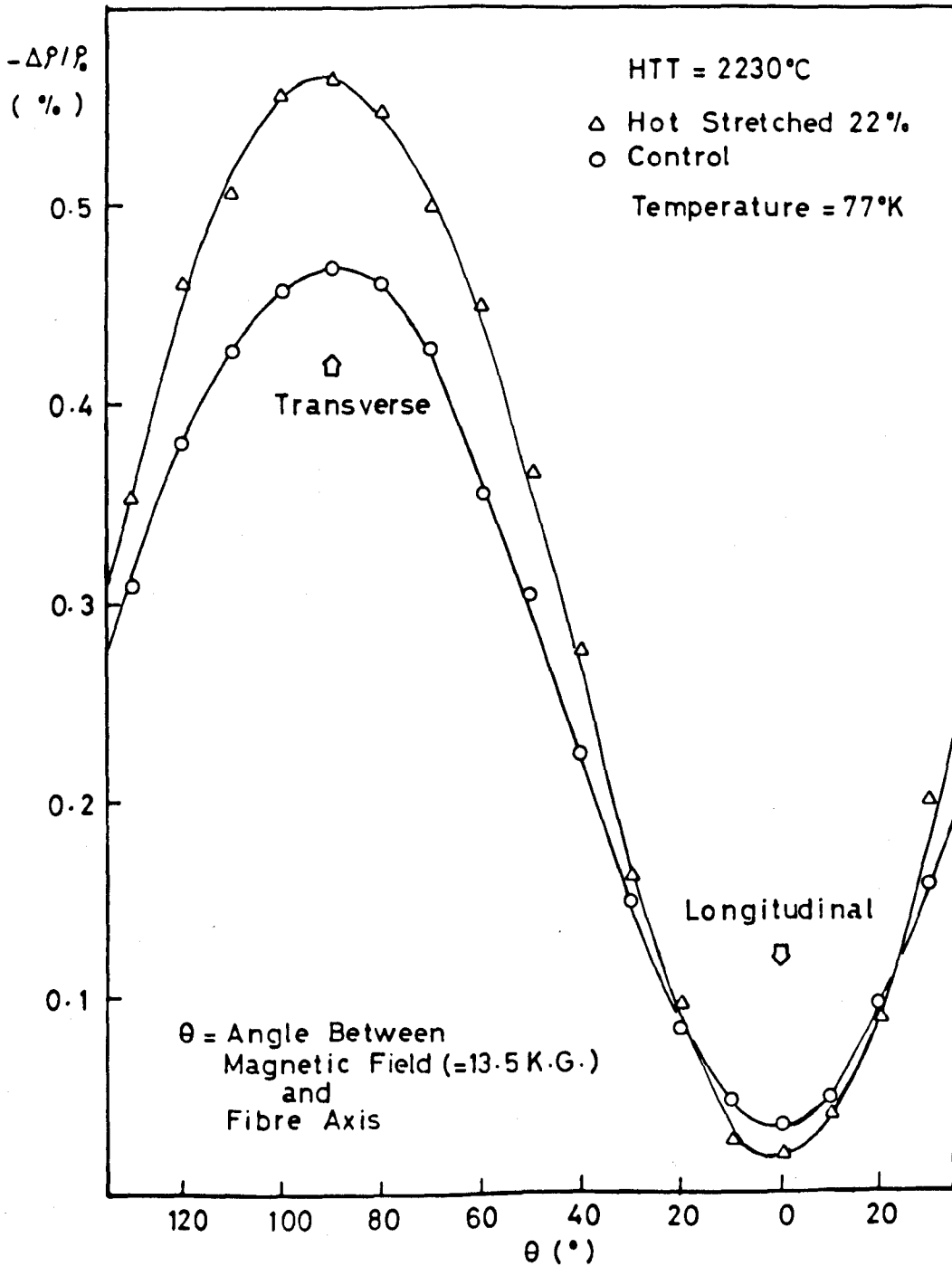


FIGURE 7.8.

Table 7.2

Ratio of Longitudinal to Transverse Magneto-Resistance

$$\frac{(\Delta\rho/\rho_0)_L}{(\Delta\rho/\rho_0)_T}$$

IDENTIFICATION		CONTROL	STRETCHED
HTT	% Stretch		
2420	9	13.5	9.0
1990	20	14.0	7.0
2140	30	10.6	6.4
2230	22	5.9	5.2
2800	-	8.0	-
2700	-	8.7	-
2670	-	9.7	-
2300	-	13.1	-

Consideration of the angular variation of the magneto-resistance for these highly 'graphitized' fibres leads to an interesting result. A typical angular variation plot for a pair of fibres of series II is shown in Fig. 7.8. Clearly on hot stretching the transverse magneto-resistance increased, but surprisingly the longitudinal magneto-resistance does not vanish for either fibre. Furthermore, although the transverse magneto-resistance for the stretched fibre is greater than that of the control, its longitudinal magneto-resistance falls below that of the control. Since hot stretching increases both the crystallite size and crystallite orientation, this result suggests that whereas the increase in the transverse magneto-resistance is due to the increase in crystallite size, the decrease in the longitudinal magneto-resistance on hot stretching is due to the increased preferential alignment of crystallites. It follows that if the crystallites are all perfectly aligned along the fibre axis, the longitudinal effect would vanish as indeed occurs in the case of perfect graphite (Fig. 6.6). Consequently it appears that the departure of the longitudinal magneto-resistance from zero could afford an alternate method, to the usual X-ray techniques, of obtaining the degree of misalignment of graphitic crystallites in carbon fibres provided however that a suitable mathematical treatment is developed.

It is encouraging to note that the ratio of the longitudinal magneto-resistance to the transverse magneto-resistance $(\Delta\rho/\rho_o)_L/(\Delta\rho/\rho_o)_T$ decreases on hot stretching for four pairs of fibres investigated, indicating an increase in preferred orientation upon hot stretching as

GENERAL CORRELATION OF THE ELECTRONIC PROPERTIES WITH g -ANISOTROPY

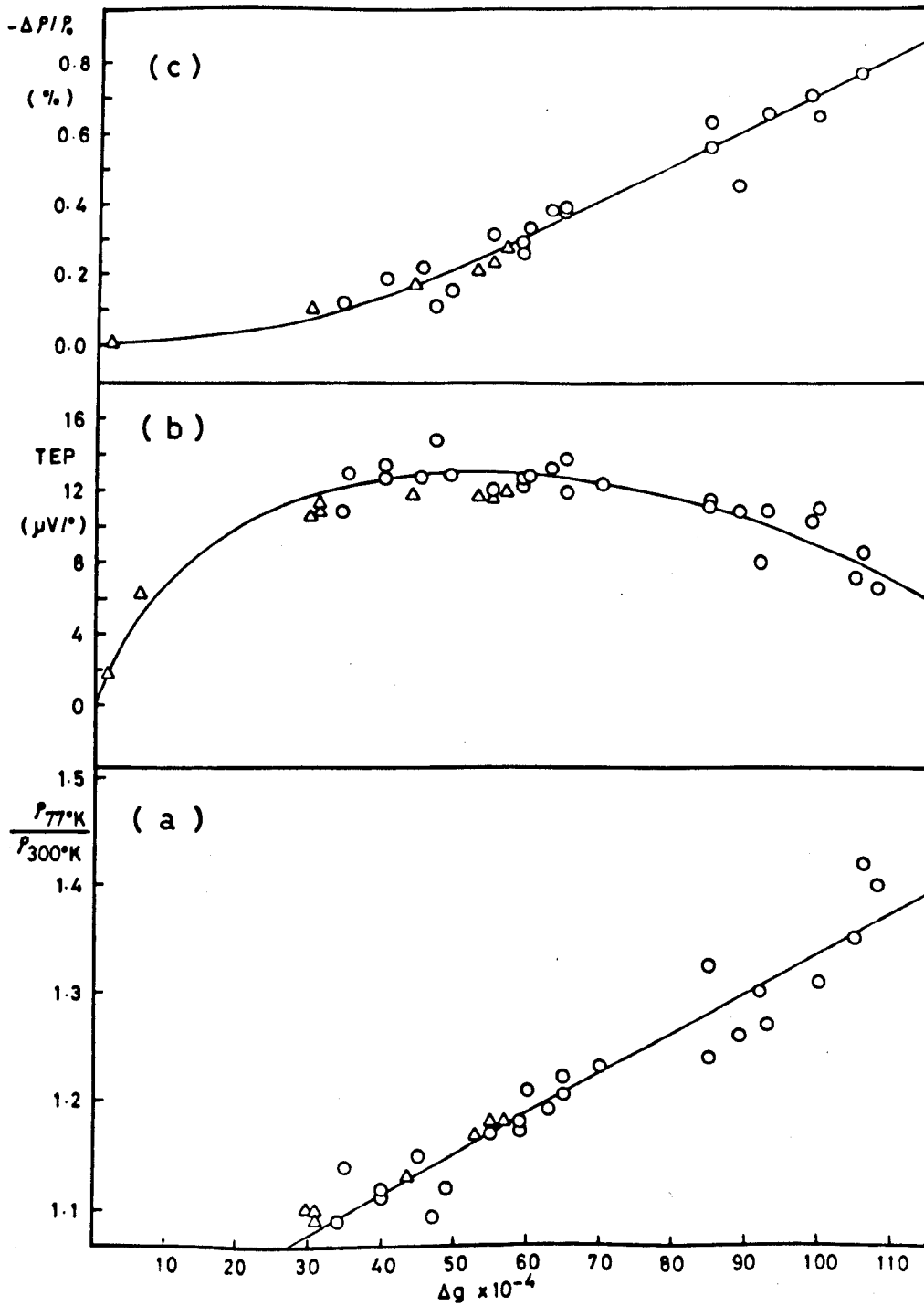


FIGURE 7.9.

indeed is confirmed by X-ray data⁽⁹⁹⁾ (Table 7.2). Increased heat treatment on the basis of this parameter also appears to favour increased crystallite alignment.

7.7 Conclusion

All the parameters directly associated with the degree of graphitization of carbon fibres, namely the g-anisotropy, the $\rho_{77^{\circ}\text{K}}/\rho_{300^{\circ}\text{K}}$ ratio, the electrical resistivity, and the magneto-resistance unambiguously change on hot stretching in a direction indicating increased graphitization. It is believed that the absence of correlation between the control fibres of series II with each other and with the fibres of series I is due to differences in thermal history or other factors, which in effect invalidates the use of the HTT as a parameter to which the degree of graphitization can be referred. The need for such a parameter becomes particularly felt when hot stretching is applied, as the degree of graphitization is then also dependent on the amount of stretch. It is felt that the g-anisotropy which is so critically dependent on crystallite perfection could well play the role of just such a parameter. To test the validity of the g-anisotropy as a monitor of the 'graphitic order' cross plots of all the available data for the fibres of both series I and II were performed and this is shown in Fig. 7.9.

The TEP (Fig. 7.5b) definitely appears to go through a maximum value with increasing graphitic order, thus confirming the explanation put forward in section 7.5 for the observed changes in this parameter upon hot stretching.

Both the magneto-resistance (Fig. 7.9c) and the $\rho_{77^{\circ}\text{K}}/\rho_{300^{\circ}\text{K}}$ ratio (Fig. 7.9a), appear to increase regularly with the g-anisotropy. It is therefore concluded that any of these three properties, namely $\Delta\rho/\rho_0$, $\rho_{77^{\circ}\text{K}}/\rho_{300^{\circ}\text{K}}$, and Δg can on a practical basis be used as a parameter to monitor the 'graphitic order' of carbon fibres as an alternative method to the usual X-ray techniques employed. The TEP however is not suitable for this purpose because of its passage through a maximum as the graphitic order is increased.

The fact that the experimental points from both series I and series II now fall into line with each other, greatly strengthens the idea that all these properties define a unique parameter, the graphitic order.

CHAPTER 8

CONCLUSIONS AND SUGGESTIONS FOR FUTURE WORK

Probably the most significant result that has emerged from this work is the discovery of the g-anisotropy in the ESR absorption line of the carbon fibres. The angular variation of this anisotropy clearly confirms that the graphitic crystallites, making up the structure of carbon fibres, are preferentially aligned with their basal planes parallel to the fibre axis. The g-anisotropy is intimately related to the degree of growth and perfection of the graphitic crystallites, to which carbon fibres owe their particular mechanical properties and their technological importance. Its magnitude provides, therefore, a practical alternative to the established X-ray diffraction, electron microscopy and electron diffraction techniques, for the study of the graphitization of carbon fibres.

Indeed the g-anisotropy is found to be a good measure of the stage of crystallite development or 'graphitic order' in these fibres. Thus the properties of widely different fibres fall into line when cross plotted against this parameter.

The fundamental features of the ESR spectra from carbon fibres do not differ in any basic way from the ESR of carbonaceous materials in general, and are therefore amenable to analysis by the techniques developed by Mrozowski and co-workers for carbon blacks. Such analysis enables the true crystallite g-value anisotropy, after allowance has been made for the depressing effect of the localized component, to be

made. This has revealed that even for the fibres with the greatest graphitization, the crystallite development is inferior to that of single crystal graphite. This result is in line with what is known of the non-graphitizing nature of these materials.

Unfortunately the g-anisotropy is inherently insensitive to small crystallite misalignments, but the longitudinal magneto-resistance, on the other hand, is believed to be a promising parameter in this respect. From the experimental point of view the magnitude of this latter effect could be greatly increased by going to lower temperatures and higher fields. Furthermore the accuracy of measurement could be improved by more sophisticated techniques than were used for this work. Should this be coupled with a suitable theoretical treatment, the problem could no doubt lead to the development of an interesting method of monitoring crystallite misalignments in carbon fibres.

It is noted in passing that hot stretching carbon fibres invariably produces in all of the properties investigated a change in the direction of increased graphitization.

It was also noted that the g-anisotropy in carbon fibres could only be observed at heat treatment temperatures above about 1750°C. This HTT also coincides with changes in the sign of two other important properties of these materials, the thermoelectric power (TEP) and the magneto-resistance, and furthermore is known to correspond to the temperature at which plastic flow can occur within the fibres through the thermal disruption of the carbon-carbon bond. Thus it becomes clear that the HTT of 1750°C is associated with a major change in the electronic structure of these materials.

It was noted that whereas for graphitizing carbon blacks changes in the sign of both the Hall effect and the TEP also occurred at this HTT (viz 1750°C), the g-anisotropy appeared earlier on in the heat treatment, thus making it unlikely that the abrupt appearance of the Fermi level in a region of greater spin-orbit coupling could be responsible for the sudden emergence of the anisotropy. However the anisotropy for both the carbon blacks and carbon fibres appeared at virtually an identical interlayer spacing (viz 3.49 Å), and this was taken as strong evidence to the effect that a critical interlayer spacing must exist above which the layer separation is too large to produce the interlayer interactions responsible for the g-anisotropy.

While the unique band structure of single crystal graphite has been given considerable theoretical considerations, no calculations, to the best of the author's knowledge, are available to indicate whether there exists a critical c-spacing at which interlayer interactions become sufficiently significant to start introducing the markedly anisotropic properties characteristic of single crystal graphite. It is therefore suggested that this point is worthy of future attention, mainly from a theoretical point of view.

This critical interlayer spacing occurs earlier in carbon blacks since these graphitize readily, whereas in carbon fibres sufficient crystallite order only occurs at 1750°C where cross-linking bonds hindering graphitization can be thermally broken. The rearrangement of carbon atoms which ensues also liberates the material from some of the stresses developed within it during the process of heat

treatment. The crystallite boundary fields, hitherto distorted by these stresses make their appearance thus giving rise to the negative magneto-resistance. That such a rearrangement of carbon atoms is indeed taking place at a HTT of 1750°C is supported by recent low angle X-ray diffraction data just published at the time of writing⁽⁹⁵⁾.

It is believed that the available evidence clearly suggests that the band overlap model, proposed by Mrozowski for these materials, breaks down below a HTT of about 1750°C .

It is fairly reasonable to suppose that a rearrangement of carbon atoms, such as is occurring at a HTT of 1750°C , be accompanied by a decrease in the number of 'dangling' σ -bonds, i.e. holes. This is believed to be associated with the change of sign of the TEP at that HTT. According to the available model this is caused by a rising Fermi level crossing the E vs k inflection point. This proposition, although somewhat tenuous, has so far been accepted in the absence of an alternative explanation.

During the final stages of this work, the author became aware of the existence of a model, originally developed for amorphous materials by N.F. Mott⁽¹⁰⁴⁾, which could possibly provide such an alternative explanation for the change of sign of the TEP and which indeed could possibly introduce an altogether new approach to the band structure of carbonaceous materials in general. It should be emphasised that an attempt to adapt this model to carbons is not actually carried out here. However it is felt that an outline of the model and its potentialities is of interest, if only to illustrate the attention which these ideas will deserve in future work.

MOTT'S BAND MODEL FOR AMORPHOUS MATERIALS

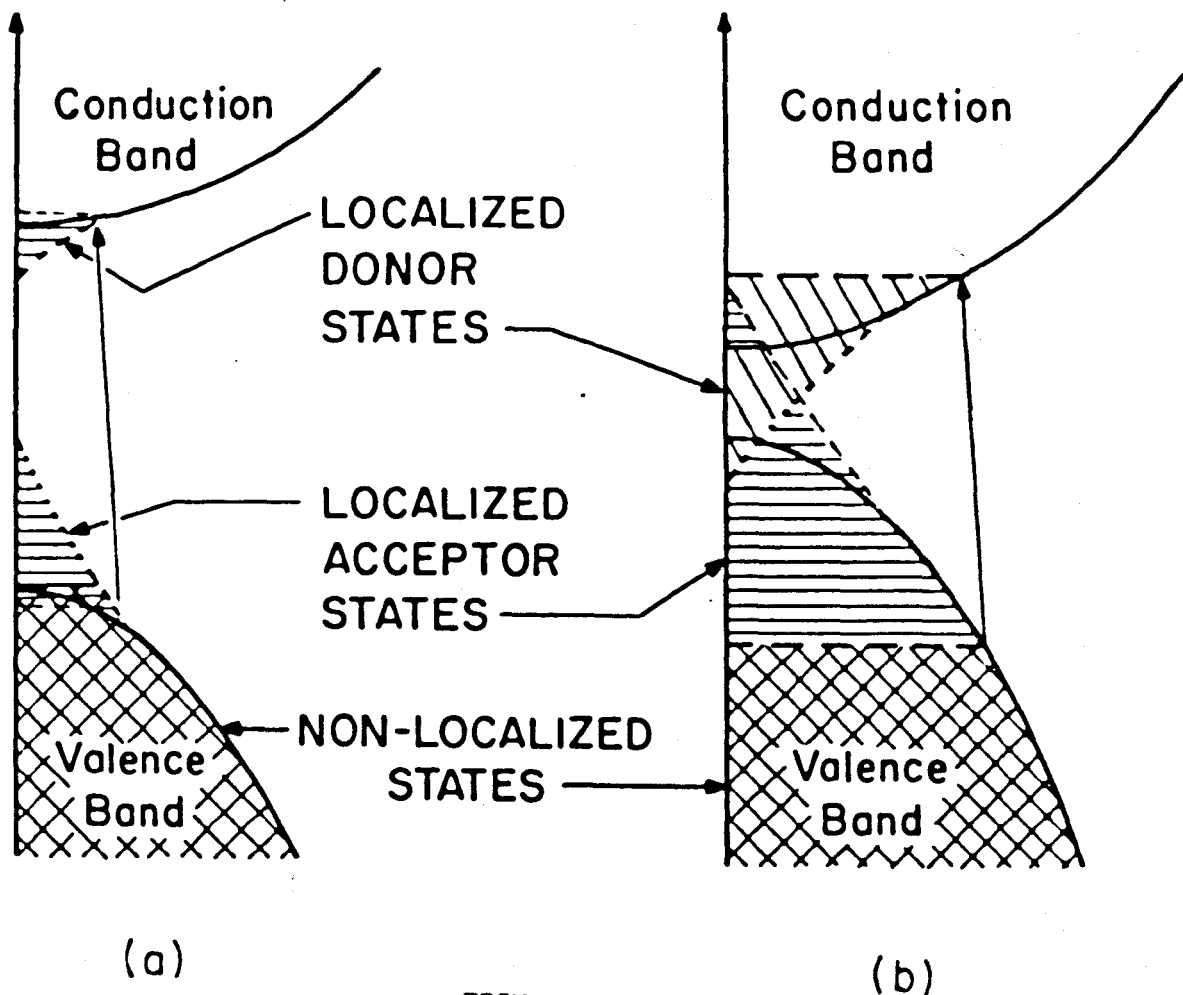


FIGURE 8.1

8.1 Electrons in Amorphous Materials

The band theory of solids has been developed on the basis of the existence of translational symmetry, i.e. long range order throughout a crystalline solid. The band structure of disordered lattices has however only been studied theoretically over the last few years, mainly by Mott⁽¹⁰⁴⁾. The theoretical concepts employed in these analyses apparently still contain some speculative features. However they form a good basis for a discussion of the transport properties of amorphous materials giving results which are not inconsistent with experimental data.

The theoretical analysis shows that as long as the short range order is maintained the essential features of the crystallite band structure are retained apart from several significant modifications. Due to fluctuations in the value of the distance between neighbouring atoms, the periodic potential shows fluctuations resulting in a tailing (smearing) of band edges (see Fig. 8.1). Some band states which are represented by wave functions extending throughout the lattice became localized in the disordered lattice. Localization is taken to indicate that the wave function has a probability amplitude decreasing exponentially with distance from the centre of localization. Conductivity is zero at $T = 0$ in localized states.

It is difficult to calculate the exact degree of tailing; however it appears that it may extend deep into the forbidden (Fig. 8.1a) zone and may even result in the overlapping of the conduction and valence bands (Fig. 8.1b).

Mott has discussed the criteria of localization and concluded that localized and non-localized states are separated by a critical electron energy at which the mean free path and the electron wavelength are comparable.

An electron in the localized state is effectively trapped and can move from one localized state to another only by hopping. This hopping process of conduction thus effectively produces an energy gap in a disordered lattice in which the mobility is negligible and the d.c. conductivity is zero at low temperatures. This leads to the description of the energy gap as a mobility gap in contrast with the conventional crystalline semiconductor band gap in which the density of states is zero.

At first glance it appears that the attractions of the application of such a model to carbons and graphites is threefold.

Firstly - The changes in the TEP of amorphous germanium, a situation in some respects very similar to that of carbons, can be explained purely in terms of changes in the population of the localized states⁽¹⁰⁰⁾, without resorting to the postulate of the Fermi level crossing the inflection point of the E vs k curve.

Secondly - Inherent in the theory is the association of localized states with amorphous structures. Clearly this could be linked with the localized component of the ESR observed in carbonaceous materials, the origin of which still remains somewhat uncertain.

Thirdly - The theory could perhaps be extended below the HTT of 1750°C where Mrozowski's band overlap model seems to fail. It is noted

in passing that the two models do in fact show some similarities with both postulating some degree of band overlap (Fig. 8.1b and Fig. 6.11). The extension of Mott's ideas all the way down to very low temperature materials seems, indeed, to follow quite naturally as conduction in these materials is believed to occur through hopping mechanisms^(101,102).

It should be fair to say that the idea of the application of Mott's model to vitreous carbons and pyrolytic graphites has previously been examined by Young⁽¹⁰³⁾. This author merely concludes that localized states are intrinsic in these materials but, however, does not proceed to examine the implication of these ideas on the interpretation of the various properties of carbonaceous materials.

It is believed that this area of study is of considerable interest.

REFERENCES

1. Slichter, C.P., "Principles of Magnetic Resonance" Harper and Row New York (1963).
2. Pake, G.E., "Paramagnetic Resonance" Benjamin, New York (1962).
3. Carrington, A. and McLachlan, A.D., "Introduction to Magnetic Resonance", Harper and Row, New York (1967).
4. Ingram, D.J.E., "Free Radicals as Studied by ESR" Butterworths, London (1958).
5. Ingram, D.J.E., "Spectroscopy at Radio and Microwave Frequencies" Butterworths, London (1967).
6. Poole, C.P., "Electron Spin Resonance" Interscience, New York (1967).
7. Ingram, D.J.E., "Encyclopedia of Physics" XVIII/I 94 (1968).
8. Assenheim, H.M. "Introduction to Electron Spin Resonance" Hilger & Watts Ltd., London (1966).
9. Kronig, R de L., Physica, 6, 33 (1939).
10. Van Vleck, J.H., Phys. Rev. 57, 426 (1940).
11. Bloch, F., Phys. Rev. 70, 460 (1946).
12. Abragam, A. "The Principles of Nuclear Magnetism", Clarendon Press, Oxford (1961).
13. Bloembergen, N., and Wang, S., Phys. Rev. 93, 72 (1954).
14. Kubo, R., and Tomita, K., Proc. Intern. Conf. Theoret. Phys., Kyoto and Tokyo, 779 (1953).

15. Kubo, R. and Tomita, K., J. Phys. Soc. Japan 9, 888 (1954).
16. Griffiths, R.B., Phys. Rev. 124 1023 (1961).
17. Van Vleck, J.H., Nuovo Cimento, 6 (Suppl.), 1081 (1957).
18. Gorter, C.J. and Van Vleck, J.H., Phys. Rev., 72, 1128 (1947).
19. Van Vleck, J.H., Phys. Rev. 74 1168 (1948).
20. Wilmshurst, T.H., Gambling, W.A. and Ingram, D.J.E., J. Electron. Control, 13 339 (1962).
21. Ubbelohde, A.R. and Lewis, F.A., "Graphite and its Crystal Compounds" Clarendon Press, Oxford (1960).
22. Wallace, P.R., Phys. Rev., 71 622 (1947).
23. Slonczewski, J.C. and Weiss, P.R., Phys. Rev. 109 272 (1958).
24. Haering, R.R., Canad. J. Phys. 36 352 (1958).
25. Soule, D.E., Phys. Rev. 112 698 708 (1958).
26. Ganguli, N. and Krishnan, K.S., Nature, 144, 667 (1939).
27. Primak, W. and Fuchs, L.H., Phys. Rev. 103 541, 544 (1956).
28. Galt, J.K., Yager, W.A. and Dail, H.W., Phys. Rev. 103, 1586 (1956)
29. Castle, J.G., Phys. Rev. 92, 1063 (1953).
30. Hennig, G.H. and Smaller, B. "Proc. 1st and 2nd Conf. on Carbon" Pergamon Press, London, 113 (1956).
31. Wagoner, G., Phys. Rev. 118, 647 (1960).
32. Dyson, F.J., Phys. Rev. 98, 349 (1955).
33. Feher, G. and Kip, A.F., Phys. Rev. 98 337 (1955).
34. McClure, J.W., Phys. Rev., 108, 612 (1957).

35. McClure, J.W. and Yafet, Y., Proc. Fifth Conf. on Carbon, Pergamon Press, London, 2, 22 (1963).
36. Mrozowski, S., Phys. Rev. 85, 609, 86, 1056 (1952).
37. Loebner, E.E., Phys. Rev. 102, 46 (1956).
38. Mrozowski, S. and Chaberski, A., Phys. Rev. 104, 74 (1956).
39. Fujita, S., Carbon 6, 746 (1968).
40. Singer, L.S., "Proc. Fifth Conf. on Carbon", Pergamon Press, London, 2, 37 (1963).
41. Singer, L.S. and Lewis, I.C., Carbon 2, 115 (1964).
42. Lewis, I.C. and Singer, L.S., Carbon, 5, 373 (1967).
43. Lewis, I.C. and Singer, L.S., Carbon, 7, 93 (1969).
44. Mrozowski, S. and Wobschall, D., J. Chem. Phys., 57, 915 (1960)
45. Mrozowski, S. and Andrew, J.F. "Proc. Fourth Conf. on Carbon", Pergamon Press, London, 207 (1960).
46. Austen, D.E.G., Ingram, D.J.E. and Tapley, J.C., Trans. Faraday Soc., 54, 400 (1958).
47. Austen, D.E.G., and Ingram, D.J.E., "Proc. Sheffield Conf. on Science in the Use of Coal", Institute of Fuel, London, A62 (1958).
48. Jacubowicz, Mme and Uebersfeld, J., J. Chim. Phys., 57, 926 (1960).
49. Lewis, I.C. and Singer, L.S., Carbon, 5, 373 (1967).
50. Singer, L.S. and Wagoner, G., J. Chem. Phys., 37, 1812 (1962).
51. Mrozowski, S., Carbon, 3 305 (1965).

52. Marchand, A. and Delhaes, P., Proc. XII Colloque Ampere, North Holland Publishing Co., Amsterdam, 135, (1963).
53. Mrozowski, S., Carbon, 4, 227 (1966).
54. Arnold, G.M., Carbon, 5, 33 (1967).
55. Arnold, G.M., and Mrozowski, S., Carbon, 6, 243 (1968).
56. Mrozowski, S., Carbon, 6, 841 (1968).
57. Franklin, R.E., Proc. Roy. Soc., A209, 196 (1951).
58. Badami, D.V., New Scientist, p.251, (5th February 1970).
59. Shindo, A., Report No. 317 (Government Industrial Research Institute - Osaka) (1961).
60. Watt, W., Phillips L.N. and Johnson W., Engineer, London (27th May 1966).
61. Fourdeux, A., Herinckx, C., Perret, R. and Ruland, W., C.R. Acad. Sc. Paris, 269C, 1597 (1969).
62. Johnson, W. and Watt, W., Nature, 215, 384 (1967).
63. Badami, D.V., Joiner, J.C. and Jones, G.A., Nature, 215, 386 (1967).
64. Ruland, W., Conf. on Fibres for Composites: Strength, Structure and Stability, University of Sussex, Brighton, 10 (1969).
65. Herinckx, C., Perret, R. and Ruland, W., Nature 220, 63 (1968).
66. Bacon, R. and Tang, M.M., Carbon 2, 221 (1964).
67. Johnson, D.J. and Tyson, C.N., Brit. J. Appl. Phys., 2, 787 (1969).
68. Jung, P., J. Sci. Inst. 37, 373 (1960).
69. Feher, G., Bell System Tech. 5 36, 449 (1957).

70. Ingram, D.J.E., Ref. 4, Chapter 3.
71. Wyard, S.J., J. Sci. Inst., 42, 769 (1965).
72. Robson, D., Ph.D. Thesis, University of Newcastle (1968).
73. Duffy, W., J. Chem. Phys. 36 490, (1962).
74. Delhaes, P. and Marchand A., Carbon, 6, 257 (1968).
75. Robson, D., Assabghy, F.Y.I. and Ingram, D.J.E., Nature, 221
51 (1969).
76. Jackson, P.W. and Marjoram, J.R., Nature 218, 83 (1968).
77. Kipling, J.J. and Shooter, P.V., 2nd Industrial Carbon and
Graphite Conference, Soc. Chem. Indst., London, 15 (1965).
78. Dollimore, D. and Heal, G.R., Carbon, 5, 65 (1967).
79. Elliot, R.J., Phys. Rev., 96, 266 (1954).
80. Mrozowski, S., and Kluth, E., Ninth Biennial Conf. on Carbon,
Boston, Summary of Papers, 50 (1969).
81. Fourdeux, A., Perret, R., and Ruland, W., Ninth Biennial Conf.
on Carbon, Boston, Summary of Papers, 159 (1969).
82. Ergun, S., Ninth Biennial Conf. on Carbon, Boston, Summary of
Papers, 157 (1969).
83. Yamaguchi, T., Carbon, 2 95 (1964).
84. Klein, C.A., Rev. Mod. Phys., 34, 56 (1962).
85. Smith, A.W. and Rasor, N.S., Phys. Rev. 104, 885 (1956).
86. Hennig, G.R., J. Chem. Phys., 19 922 (1951); 20, 1438 1443 (1952)
87. Cusack, N. and Kendall, P., Proc. Phys. Soc., 72, 898 (1958).

88. Huebener, R.P., Phys. Rev., 135, A1281 (1964).
89. Kinchin, G.H., Proc. Roy. Soc., A217, 9 (1953).
90. Yazawa, K., J. Phys. Soc. Japan, 26, 1407 (1969).
91. Komatsu, Y., Carbon, 7, 177 (1969).
92. Toyoda, S. and Mrozowski, S., Carbon, 7, 239 (1969).
93. Hishiyama, Y., Ninth Biennial Conf. on Carbon, Boston,
Summary of Papers, 42 (1969).
94. Castle, J.G. and Wobschall, D.C., Proc. Third Conf. on Carbon,
Pergamon Press, Oxford, 129 (1959).
95. Johnson, D.J. and Tyson, C.N., J. Phys. D.: Appl. Phys.,
3, 526 (1970).
96. Bacon, R. and Schalamon, W.A., Eighth Biennial Conf. on Carbon,
Buffalo, Abstracts (1967).
97. Johnson, W., Proceedings Third Industrial Carbon and Graphite
Conference, London (1970) SCI to be published.
98. Yafet, Y., Solid State Physics, 14, 70 (1963).
99. Johnson, J.W., Marjoram, J.R., and Rose, P.G., Nature, 221, 357
(1969).
100. Owen, A.E., Contemp. Phys., 11, 257 (1970).
101. Eley, D.D., Semiconductor Technology, Butterworths, London,
54, (1960).
102. Harker, H., Phil. Mag., 16, 1193 (1967).
103. Young, D.A., Carbon, 6, 135, (1968).
104. Mott, N.F., Adv. Phys. 16, 49, (1967).